“Secrets from a Deep Reef:

Structure, Biogeography and Palaeoclimate Reconstruction from Mingulay Reef Complex Sediment Cores”

Mélanie DOUARIN

M.Sc

Thesis submitted for the degree of Doctor of Philosophy

University of Edinburgh

2013

Declarations

I declare that this thesis is the result of my own investigations.

The work performed in laboratory and the data analysis were undertaken by me unless clearly mentioned in the relevant chapters.

I wrote the text, and other sources are acknowledged by footnotes giving explicit references. The figures were also composed by me except when clearly referenced in the captions. For the chapters constituting the main body of my thesis, which are presented in paper format, I acknowledge the precious contribution of my co-authors. However, being the lead author for all papers I have had a major intellectual input on the arguments presented.

This work has not been submitted for any other degree or professional qualification. This thesis is being submitted in partial fulfilment of the degree of PhD.

Mélanie Douarin

Edinburgh, May 2013

Abstract

A multi-disciplinary study of sediment core records from the Mingulay Reef Complex, a cold-water coral reefs system off western Scotland, highlights the potential of cold-water corals from which detailed centennial-scale palaeo-environmental reconstructions can be derived. This study provides a new insight on the mechanisms controlling *Lophelia pertusa* reef build-up, shifts in biodiversity, the physical/chemical/biological processes and the sedimentary regime. A detailed record of Mingulay Complex growth history shows unprecedented high average accumulation rates of 3 – 4 mm a^{-1}. Marine radiocarbon reconstruction derived from paired ^{14}C and U-series dated fossil corals revealed substantial abrupt oceanic shifts during the Holocene that have repetitively affected cold-water coral growth, eventually causing local disappearance. These periods of reduced accumulation rates are synchronous with other coral structures from the NE Atlantic illustrating basin wide events. Finally, trace/minor element ratios reproducibility within coral skeleton was investigated to test if palaeo-environmental reconstructions could be made from cold-water corals.

Acknowledgments

This work would not have been possible without the help and support of all the people that have accompanied me all along my PhD.

My first thanks go to my supervisor Mary Elliot, who has been caring from the beginning and always kept faith in me and my work. I have very much appreciated learning from her. Particular thanks need to be extended to Dan Sinclair with whom this project started and who remained involved despite the distance.

I am also very grateful to my co-supervisors: Murray Roberts and David Long, who always kept an eye on the smooth progress of my PhD; thanks again for your support and involvement. I would like to thank my co-authors for their extremely helpful contribution: Steve Noble, whose dedication from the beginning, has considerably contributed to the becoming of our investigation, Lea-Anne Henry for her keen enthusiasm and Steve Moreton for his constructive feedback.

Many thanks to the University of Edinburgh people for the stimulating discussions: Tom Crowley, Dick Kroon, Sandy Tudhope, Tom Russon, Kate Darling, Walter Geibert, Laetitia Pichevin, Magali Schweizer, Aleksey Sadekov… for making life easier: Colin Chilcott, Nicholas Olding, the "ion micro-prob" people but also "finance and IT" people and Alan and James... and for making the school of geosciences a great place to work, thanks to the PhD students and post-docs.

I also would like to thank my friends here and there that have always been of great support and especially Loïc. Last but not least I would not have enough words to thank the two best sisters I have been given and obviously my marvellous parents.

Thanks to you all for the work we have accomplished together! It was my pleasure working under you supervision, guidance, or just with you around.

Table of contents

List of figures

Chapter 2

Chapter 3

Chapter 4

Chapter 5

Chapter 6

Chapter 7

List of tables

Chapter 3

Chapter 4

Chapter 5

Chapter 7

List of abbreviation

AMOC	Atlantic Meridional Overturning Circulation
BP	Before Present (relative to AD 1950)
DIC	Dissolved Inorganic Carbon
EGC	East Greenland Current
ENAW	Eastern North Atlantic Water
ka	Thousands of years (age)
Kyr	Thousands of years (duration of time)
MOW	Mediterranean Outflow Water
NAC	North Atlantic Current
NACW	North Atlantic Central Water
NADW	North Atlantic Deep Water
SCC	Scottish Coastal Current
SPG	Sub-Polar Gyre
SSS	Sea Surface Salinity
SST	Sea Surface Temperature
STG	Sub-Tropical Gyre
THC	Thermohaline circulation
TSI	Total Solar Irradiance
VMGR	Vertical Mound Growth Rate
WNAW	Western North Atlantic Water

Chapter 1: Thesis overview

1.1 Thesis introduction

Documenting and understanding the background of natural climate variability underlying anthropogenic forcing requires high-precision accurate environmental archives calibrated with absolute chronologies in key locations. Cold-water corals form framework reef structures that can accumulate rapidly providing fossil carbonate remains that can be reliably dated. The shallow inshore *Lophelia pertusa* reefs system off western Scotland in the Sea of Hebrides, the Mingulay Reef Complex, is bathed by the North Atlantic Current (NAC), the surface limb of the Atlantic Meridional Overturning Circulation (AMOC), that is a key component of the climatic system. The present multi-disciplinary study highlights the potential of such a site for continuous and accurate short time scale and amplitude oceanic circulation reconstruction from classic sedimentological study and the skeletal chemistry of corals.

1.2 Rationale

1.2.1 Why cold-water coral?

Cold-water corals are globally distributed and occur over a wide range of water depths (e.g. Roberts et al., 2009). They often occur as reefal structures, large enough to be recognized by acoustic surveying techniques so as to focus spatial sampling techniques for direct analysis (Huvenne et al., 2007).

The skeleton of scleractinian coral, in aragonite, allows the use of U-series (absolute) and ^{14}C methods for dating (Adkins et al., 1998; Cheng et al., 2000a). Their growth rates can be high allowing fine scale temporal signals to be recorded. For such reasons corals are presently the most powerful tool for high temporal resolution and accurate past marine radiocarbon composition and therefore for oceanic circulation reconstruction (Burke and Robinson, 2012).

It is also anticipated that, as for their tropical counterparts, the geochemistry of cold-water coral skeletons (stable isotopes and trace elements) could be used for high resolution (decadal to seasonal) palaeo-environment reconstructions (i.e. temperature, salinity, productivity and others) (Mikkelsen et al., 1982; Smith et al., 2000). Presently, the biological mechanisms as well as the environmental parameters influencing on uptake of chemical isotopes and trace elements during coral calcification are not well understood or defined (Adkins et al., 2003; McConnaughey, 1989a; McConnaughey, 1989b). Therefore, there are currently many attempts to comprehend coral geochemistry and to develop new palaeo-climate tools based on coral skeletal chemistry.

Since the extensive distribution of cold-water corals became recognized from the 1980s many detailed analyses have been undertaken around the world.

1.2.2 Why the Mingualy Reef Complex?

The Mingulay Reef Complex is a shallow inshore reef off western Scotland formed by mound-like structures of the reef framework-forming scleractinian coral *Lophelia pertusa* associated with sedimentation processes. *Lophelia pertusa* was first reported in the Sea of the Hebrides in the mid-18th Century but it was only when the Mingulay Reef Complex was discovered in 2003 that an active research programme began there (Roberts et al., 2005).

Cold-water coral structures and continental shelves are both characterized by high accumulation/sedimentation rates (Frank et al., 2009; López Correa et al., 2012). It is assumed that shallow inner-shelf cold-water coral reefs may have especially high accumulation rates. Coring there offers great potential for high-resolution palaeo-environmental reconstructions integrating classic sedimentological study and the skeletal chemistry of corals described above.

The Mingulay Reef Complex is bathed by waters from the North Atlantic Current, which is a key component of the AMOC. Documenting its variability through time is therefore of prime interest to provide a better understanding of natural oceanic changes.

At the time this PhD project was initiated very few detailed studies on cold-water coral occurrence and reef systems build-up had been performed and none on the Mingulay Reef Complex in particular. Therefore, this work has expanded our knowledge on such intriguing geological feature have occurred as of significant interest.

In summary our interest in the Mingulay Reef Complex can be attributed to our curiosity for cold-water corals and the reef structures they form that provide diverse niches for highly diverse animal communities. However, its characteristics and location are also ideally suited for high quality palaeo-environmental reconstructions.

1.2.3 Why the Holocene?

It is necessary to concentrate our efforts on climate changes toward the most recent past to seek a more comprehensive view of the natural climate variability before human-induced climate change (Alley et al., 2003).

The current interglacial period, the Holocene (the last 11.5 kyr), has been more climatically dynamic than is commonly recognized (Mayewski et al., 2004). Until recently this period was considered as relatively stable climatically. This can be partly explained by the difficulty of finding palaeo-archives to document short-time scale and small amplitude climatic anomalies. As a result, little systematic knowledge about climate variability throughout this period is available. Therefore, it remains necessary to better document and understand the mechanisms leading to abrupt climate changes in the Holocene.

The Holocene is an important interglacial period since it sustained the growth and development of human society. Multiple examples of societal collapses are synchronous with abrupt shifts in climate changes. Therefore, a better understanding of climate changes during this period would provide a better appreciation as to what extent climatic changes have actually affected human civilization performance and stability.

1.3 Thesis aims

The main aim of this thesis can be subdivided into five major axes of research:

1) Provide a better understanding of cold-water coral reef build-up,

2) Document *Lophelia pertusa* temporal and spatial distribution to establish corals as a palaeo-indicator for environmental changes,

3) Conduct high temporal resolution hydrological reconstructions,

4) Link high temporally resolved oceanic shifts with *Lophelia pertusa* performance and,

5) Investigate cold-water coral skeleton trace elemental incorporation to develop their potential for palaeo-environmental reconstructions.

1.4 Thesis format

1.4.1 Introductory chapters

Chapter 1 outlines the rationale behind my PhD project and the specific aims of my thesis.

Chapter 2 provides an overview of the present understanding on cold-water corals and cold-water coral mounds/reefs, the present and former North Atlantic oceanic circulation and the climatic variability of the Holocene period is presented to sets the general context of my thesis.

Chapter 3 presents and describes the methods used to carry out the project. The main characteristics of our study site: The Mingulay Reef Complex, as well as the materials and tools used along this study are given.

1.4.2 Thesis body

The main body of this thesis is presented as a series chapters corresponding to papers submitted (chapter 4, chapter 5) or in preparation (chapter 6 and chapter 7).

Chapter 4 investigates the Holocene growth history of the Mingulay Reef Complex. This work compared with other studies from the NE Atlantic suggests that cold-water coral occurrence as well as changes in reef structure accumulation rate during the Holocene would be controlled by shift in palaeo-environmental regimes.

This work was presented at the 5th International Symposium on Deep-Sea Corals (ISDSC) in Amsterdam (Netherland) in April 2012 in an oral presentation entitled: Mélanie Douarin, Mary Elliot, J. Murray Roberts, Stephen R. Noble, Daniel

Sinclair, Lea-Anne Henry, David Long, Steven G. Moreton: *"The growth history of a shallow inshore Lophelia pertusa reef: the Mingulay Reef Complex"*, and was submitted to Earth and Planetary Science Research in June 2012 as: Mélanie Douarin, Mary Elliot, Stephen R. Noble, Daniel Sinclair, Lea-Anne Henry, David Long, Steven G. Moreton, J. Murray Roberts: "*High resolution chronology of coral reef growth of North-east Atlantic during the Holocene"*.

Chapter 5 describes the internal structure of the Mingulay Reef Complex. A new model of reef build-up involving environmental, faunal biodiversity and sedimentological regime changes through time is put forward.

This work was submitted in September 2012 to a special volume following the ISDSC in Deep Sea Research II as: Mélanie Douarin, Daniel Sinclair, Mary Elliot, Lea-Anne Henry, David Long, F. Mitchison, J. Murray Roberts "*Fossil biodiversity at the Mingulay Reef Complex: a model of coral reef build-up"*.

Chapter 6 presents centennially resolved marine radiocarbon ($\Delta^{14}C$ (‰)) variability between 1.7 and 4.2 ka BP and highlights significant North Atlantic surface circulation over the Holocene.

This work was presented at two international conferences; the Goldschmidt in Montreal (Canada) June 2012 and the Radiocarbon Conference in Paris (France) in July 2012 as: Douarin, M., M. Elliot, S.G. Morton, D. Sinclair, S.R. Noble, D. Long and J.M. Roberts: *"High resolution age reconstruction from cold-water corals in the North-eastern Atlantic during the Holocene (1.7 – 4.2 ka BP)"*.

Chapter 7 focuses on benthic foraminifer assemblages and benthic and planktonic isotopic reconstruction in view to explore potential relationship between hydrological and cold-water coral reef depositional environment changes.

This work was shown at the 5th International Symposium on Deep-Sea Corals (ISDSC) in Amsterdam (Netherland) in April 2012 as a poster presentation entitled: Douarin, M., M. Elliot, J.M. Roberts, S.R. Noble, D. Sinclair, L.-A Henry, D. Long and S.G. Morton: *"Accumulation rates and characteristics of shallow inshore Lophelia pertusa cores from the Mingulay Reef Complex"*.

1.4.3 Conclusion chapter

Chapter 8 highlights the main conclusions from the present multi-disciplinary study and suggests potential for further work.

1.4.4 Appendices

The appendices provide more detailed information on the main methods implemented to conduct this project.

Appendix 1 provides supplementary information for the sample preparation and U-series and radiocarbon analyses methodology.

Appendix 2 is the supporting material for chapter 6. Supplementary information on the methods and calculations as well as U-series and radiocarbon data tables are presented.

Appendix 3 investigates the reproducibility of trace/minor element ratio variability within the coral skeleton and to make accurate correspondence between coral's ultra-structures and trace/minor ratios composition.

Chapter 2: Background

2.1 Cold-water Coral

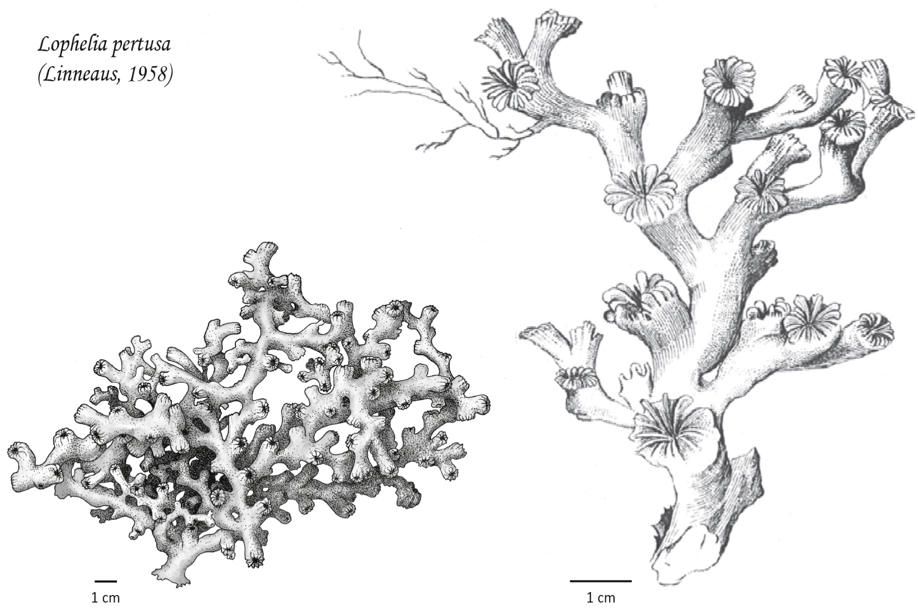

Figure 2 - 1: Drawings of *Lophelia pertusa* showing in left the framework formed by the colony (from Roberts et al., 2009) and in right details of individual polyp calices (Modified from Plate II from Gunnerus (1768)).

2.1.1 Definitions

Corals are commonly thought to be restricted to warm and shallow waters in tropical and subtropical regions. However, the exploration of deep water has revealed luxuriant coral reefs in dark, deep and relatively cold waters.

Most tropical corals receive their energy from the symbiotic association with unicellular dinoflagellate algae: the zooxanthella (Cairns, 1981). This photoautotrophic symbiont restricts the distribution of their host to the euphotic zone. In contrast to their tropical counterparts, most cold-water corals are azooxanthellate (lacking symbiotic zooxanthella) and have a heterotrophic regime. Thus they are not restricted only to surface waters.

Stony corals or Scleractinia have a calcareous skeleton made of aragonite, and can be both zooxanthellate and azooxanthellate.

Azooxanthellate scleractinians have been defined as "ahermatypic" (Wells, 1956), because they tend not to form reefs. Nevertheless, even though most of the 711 azooxanthellate scleractinians are solitary, 26% are colonial (Cairns, 2007). The colonial cold-water coral forms that tend to construct reefs are generally dendriform with anastomosing branches. The massive colonies common in tropical reefs are absent (Squires, 1964).

The most common and widespread cold-water framework-forming scleractinian is *Lophelia pertusa* (Figure 2 - 1) (Linnaeus, 1958; Roberts et al., 2009b) and this is the reef framework-forming species at the Mingulay Reef Complex. For this reason, the following sections will be focused on this specific coral species.

2.1.2 Geographical distribution

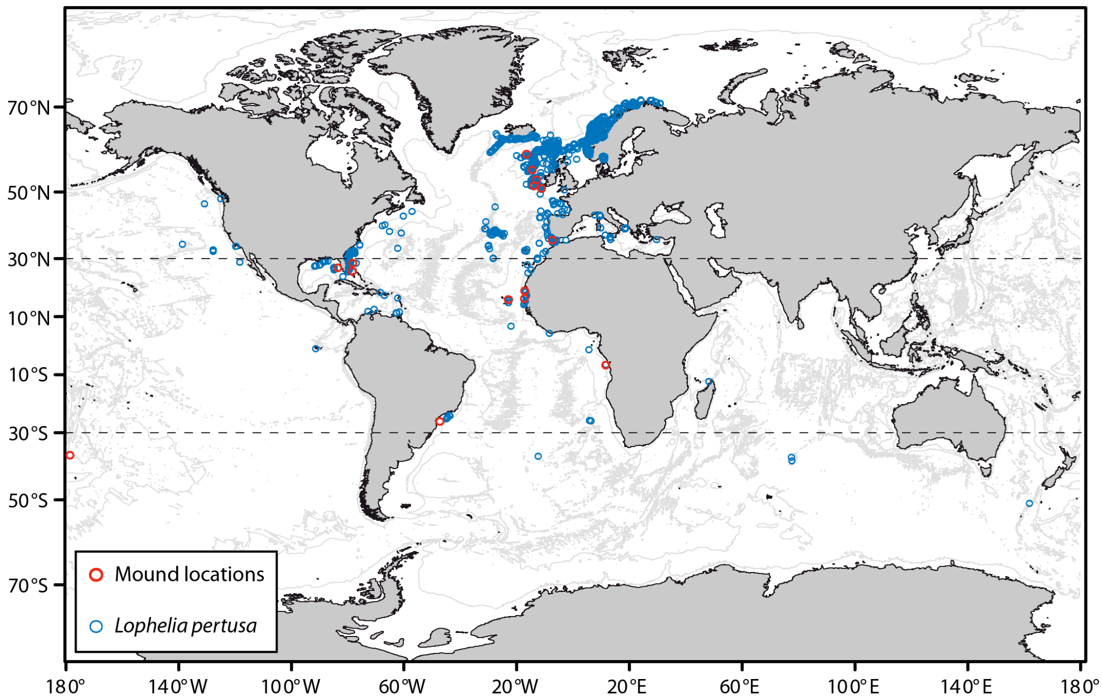

Figure 2 - 2: Cold-water coral distribution (from Roberts et al., 2009).

The full extent of cold-water coral distribution has yet to be defined, studies to date indicate that it could be equal or even exceed tropical coral coverage (Freiwald et al., 2004). Cold-water corals have a worldwide distribution and all species have specific ecological requirements (e.g. Roberts et al., 2009). *Lophelia* *pertusa* is widespread all along both sides of the Atlantic, including the Mediterranean Sea, Gulf of Mexico and the Caribbean Sea. A few records of *Lophelia pertusa* also exist in the Indian and Pacific oceans but are anecdotal compared to other locations, which have been studied more intensively (Figure 2 - 2) (Cairns, 1984; Freiwald et al., 2004; Roberts et al., 2006; Roberts et al., 2009b; Wheeler et al., 2007).

Lophelia pertusa is most commonly listed in the North-east Atlantic (Figure 2 - 3). Of the 2084 sites of *Lophelia pertusa* counted so far by the Institute of Palaeontology, Erlangen, Germany, 89% occur in the Atlantic and in the North-east Atlantic in particular (Rogers, 1999; Wheeler et al., 2007).

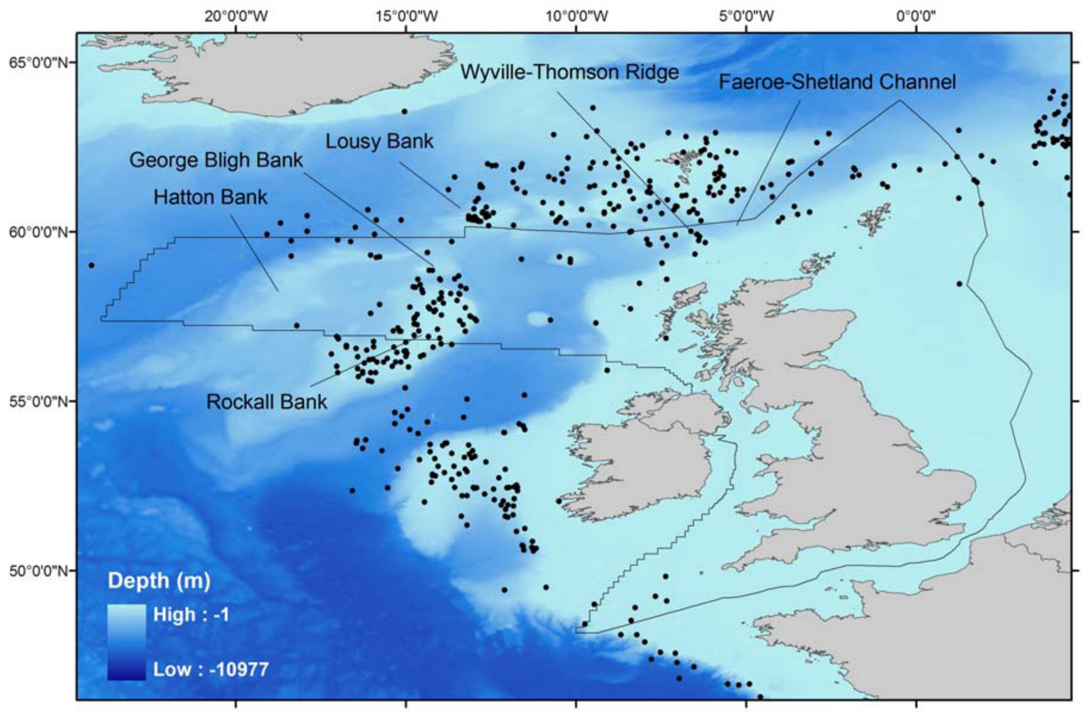

Figure 2 - 3: *Lophelia pertusa* distribution within the UK area (from Davies et al., 2009).

In the North-east Atlantic, *Lophelia pertusa* occurs preferentially along the European continental margin (De Mol et al., 2002; Kenyon et al., 2003; Wheeler et al., 2007) and is often (although not exclusively) associated with topographic highs, such as mounds or oceanic ridges but also local highs on continental shelves and slopes.

Most of the cold-water coral species occur in the mesopelagic (200 – 2000 m) zone (Roberts et al., 2009b). *Lophelia pertusa* occurs preferentially between 250 and 500 m water depth (Freiwald, 2002), but some live samples have been found under more extreme depths in a Norwegian fjord (Trendheimsfjord) at 39 m for the shallowest and at 3383 m for the deepest in the New England Seamount chain (Freiwald et al., 2004; Roberts et al., 2009b; Zibrowius, 1980). Studies suggest that the depth (or the hydrostatic pressure) does not exert a primary control on the distribution of corals (Freiwald et al., 2004; Roberts et al., 2009b). So any assessment of cold-water corals has to consider a wide range of factors that might influence their distribution.

2.1.3 Factors controlling cold-water corals distribution

a. Substratum

A large, contiguous and stable hard substratum is preferable for the settlement and metamorphosis of the planula (coral larva) and then to support a large colony subject to strong currents (Cairns, 2007; Wilson, 1979).

b. Hydrography

The environmental factors considered most likely to restrict *Lophelia pertusa* distribution are temperature (Freiwald, 2002; Roberts and Hirshfield, 2004), salinity (Freiwald, 2002; Freiwald et al., 2004), dissolved oxygen concentration (Dodds et al., 2007; Freiwald, 2002), and the aragonite saturation horizon (ASH) (Guinotte et al., 2006; Orr et al., 2005; Turley et al., 2007).

Temperature: Azooxanthellate corals occurring below the photic zone have been found growing in waters with temperatures ranging from -1.1°C to 29°C (Cairns and Stanley, 1981). *Lophelia pertusa* is generally found in waters ranging from 4 to 14°C (Freiwald, 2002; López Correa et al., 2010; Roberts et al., 2009b; Roberts and Hirshfield, 2004; Rogers, 1999).

Salinity: *Lophelia pertusa* typically grow in waters between 35 and 37 psu (Roberts et al., 2009b). However, once again there is evidence that corals can tolerate a wider range than this, with individuals in a Norwegian Fjord growing in water with salinity of 32 psu and in the Mediterranean in water with a salinity of 38.8 psu (Freiwald et al., 2004).

Stable salinities and temperatures seem to be necessary for high growth rates of *Lophelia pertusa*. Consequently, variable environments may cause local absence of the species (Freiwald et al., 2004).

Dissolved oxygen: *Lophelia pertusa* is most commonly found in waters with a dissolved oxygen concentration ranging from 4.3 to 7.2 ml l^{-1} (Dodds et al., 2007; Freiwald, 2002). This species seems able to regulate its oxygen consumption and to survive short periods of hypoxia (1 hour) and anoxia (96 hour) (Dodds et al., 2007).

Aragonite Saturation Horizon (ASH): The ASH is defined as the depth boundary between saturated and unsaturated water with respect to aragonite. In unsaturated waters, aragonitic organisms will not be able to calcify properly, resulting in weaker skeletons and/or a lower growth rate (Guinotte et al., 2006; Orr et al., 2005; Turley et al., 2007). This may partly explain why there is such a high concentration of cold-water corals in the North-east Atlantic where the ASH is far deeper (>2000 m) than other areas like the North Pacific for instance (50 m – 600 m) (Guinotte et al., 2006; Orr et al., 2005; Turley et al., 2007).

c. Food supply

Lophelia pertusa is a suspension-feeder preferentially eating live copepods rather than dead food particles (Mortensen, 2001).

It was once thought that, the distribution of cold-water corals was linked to light hydrocarbon seepage which supports a chemosynthetic food chain: The "hydraulic theory" has been however strongly debated and it is now currently admitted that "the environmental control theory" explains the connection between cold-water coral habitats and the quantity and quality of food supply (Henriet et al., 1998; Hovland, 1990; Hovland et al., 1994; Hovland et al., 1998b; Hovland and Risk, 2003). Cold-water corals occur therefore in areas where the local hydrodynamic processes either enhance the primary production in surface waters and its redistribution to deeper waters, or favour the re-suspension of organic particles from the seafloor (Davies et al., 2009; Frederiksen et al., 1992a; Genin et al., 1986; Mienis et al., 2009a; Mienis et al., 2007; White, 2007; White et al., 2005).

d. Current strength

Cold-water corals occur preferentially on topographic highs dominated by strong currents (Genin et al., 1986; Roberts et al., 2006; Rogers, 1999). Several factors may explain this. Firstly, the local hydrodynamic regime seems crucial for enhancing the recruitment of planula. Secondly, strong currents prevent sediment accumulation and stop the colony from being smothered by terrigenous or detrital particles. Lastly, enhanced currents appear to act as a mechanism increasing the food supply available for the suspension-feeder, *Lophelia pertusa* (Genin et al., 1986; Mienis et al., 2007; Mienis et al., 2009b; White, 2007; White et al., 2005).

2.2 Cold-water coral reef

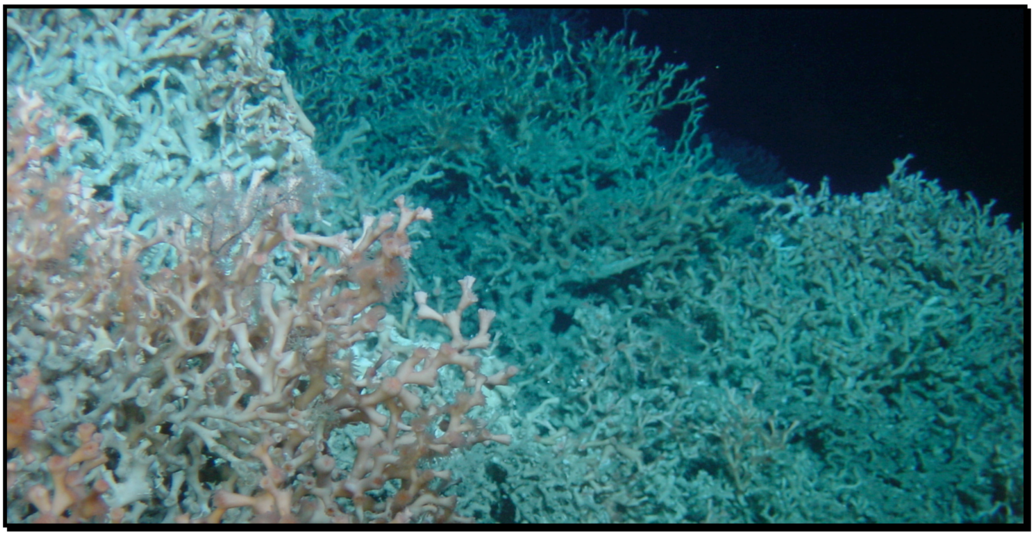

Figure 2 - 4: Photograph of a cold-water coral reef from the Celtic margin (CARACOLE cruise) ® Ifremer.

2.2.1 Definition

Coral carbonate mounds and cold-water coral reefs can be defined as local topographic highs, which locally are able to alter the hydrodynamic and the sedimentary regimes. These biogenic structures also form a structural habitat, similar to tropical coral reefs, favourable for other species (Freiwald, 2002; Roberts et al., 2006; Roberts et al., 2009b; Wheeler et al., 2007; Wilson, 1979). The single generation reefs are discriminated against larger coral carbonate mounds that are accumulations of multiple periods of reef growth (interglacial) and periods of intervening (glacial) sedimentation (Roberts et al., 2009b).

2.2.2 Reefs and mounds build-up

Several models of coral-mound ontogeny have been proposed to explain the initiation and development of such structures (De Mol et al., 2002; Dorschel, 2003; Eisele et al., 2008; Henriet et al., 2001; Roberts et al., 2006; Rüggeberg et al., 2007). These mostly agree on a complex interaction between sediment accumulation and cold-water coral colonization and growth under favourable environmental conditions.

Cold-water coral reef build-up starts with the settlement and metamorphosis of a planula (coral larvae) on a hard substratum. Under favourable environmental conditions (i.e. hydrology and food supply) a thicket resulting from an aggregation of several adjacent colonies (monotypic or polytypic) may form (Figure 2 - 4). The death of the underlying colonies and accumulation of debris (mostly coral skeleton debris) will eventually lead to the formation of a coral coppice. The succession of reef growth leads to the establishment of large topographic features such as cold-water coral reefs or coral carbonate mounds. At each step a new ecological niche and stratigraphic layer is formed (e.g. Squires, 1964).

The rate of growth of coral carbonate mounds is on average of about 0.2 mm a^{-1} (Frank et al., 2009; de Hass et al., 2009). This is about 100 times less than the growth rates of in situ *Lophelia pertusa* colonies and of live individuals maintained in aquaria, which are estimated at 26 mm a^{-1}, and 16 mm a^{-1}, respectively (Gass et Roberts, 2006; Orejas et al., 2008). Shallow cold-water coral reefs present even more significant accumulation rates reaching up to 6 mm a^{-1} (Freiwald et al., 1999; López Correa et al., 2012).

2.2.3 Reefs and mounds build-up and climate

L. pertusa is one of the dominant cold-water coral species in the North-east Atlantic. Therefore, the reef framework-forming cold-water coral environmental requirements have a significant impact on cold-water coral structure growth through time and climatic changes (Frank et al., 2011; Frank et al., 2009). The last 11 ka, as well as previous interglacials (marine isotope stages (MIS) 5, 7 and 9), have been favourable for coral growth and thus coral carbonate mound development in the North-east Atlantic between 50°N and 70°N (Douville et al., 2010; Frank et al., 2011; Frank et al., 2009). To date no *Lophelia pertusa* from glacial periods have been found at these latitudes (Dorschel, 2003; Dorschel et al., 2007b; Frank et al., 2004; Kenyon et al., 2003; Mienis et al., 2009b; Rüggeberg et al., 2007; Schröder-Ritzrau et al., 2003), hence glacial conditions are assumed to be detrimental to the growth of individual coral colonies and thus to coral carbonate mounds at these latitudes (Frank et al., 2011; Frank et al., 2009; Kenyon et al., 2003). In addition, any sediment accumulated during those times may be prone to erosion as soon as the currents speeds accelerate at the beginning of following interglacial period (Dorschel, 2003; Rüggeberg et al., 2007). Interestingly, at lower latitudes (between 20°N and 50°N) *Lophelia pertusa* reef growth is reported during cool events (such as the Younger Dryas) and glacial periods (MIS 2, 4, 6 and 8) in the Gulf of Cádiz, Mediterranean Sea and offshore Mauritania (Eisele et al., 2011; Frank et al., 2011; McCulloch et al., 2010; Wienberg et al., 2010; Wienberg et al., 2009).

2.3 Environmental settings in the North-east Atlantic region

2.3.1 The Meridional Overturning Circulation

The world ocean plays a major role in the Earth's climate system by its capacity to store and redistribute heat (Rahmstorf, 2002). As it covers 71 % of the globe, most of the Earth's solar radiation warms the surface waters which in turn transport heat from the low latitude (where the radiative balance at the top of the atmosphere is positive) to the high latitudes (where a net loss of radiative energy is observed) (Broecker, 1987; Trenberth and Solomon, 1994). Mechanisms driving the large inter-basin water masses exchanges or Meridional Overturning Circulation (MOC) are still debated (Kuhlbrodt et al., 2007) but would result in a combination of (1) thermohaline circulation (THC) driven by temperature and salinity gradients, (2) currents driven by winds and (3) tides (Rahmstorf, 2002) (Figure 2 - 5).

In the North Atlantic, which is the area of interest for this study, the surface water from the Gulf of Mexico absorbs heat but also evaporates, which leads to increased salinity. Those surface waters flowing northward and transported by the Gulf Stream lose heat to the atmosphere; which increases its density (high salinity, low temperature). In Greenland – Iceland – Norwegian (GIN) Sea and in the Labrador Sea the water mass reach a critical density and sinks forming the North Atlantic Deep Water (NADW) that re-circulates southwards towards the Southern Ocean (Marshall and Schott, 1999; Talley, 2008). As one of the three areas of deep water formation (the other two being the Ross Sea and the Weddell Sea in the Southern Hemisphere) the northern North Atlantic is a key area for global deep water formation (Rahmstorf, 2002) (Figure 2 - 5).

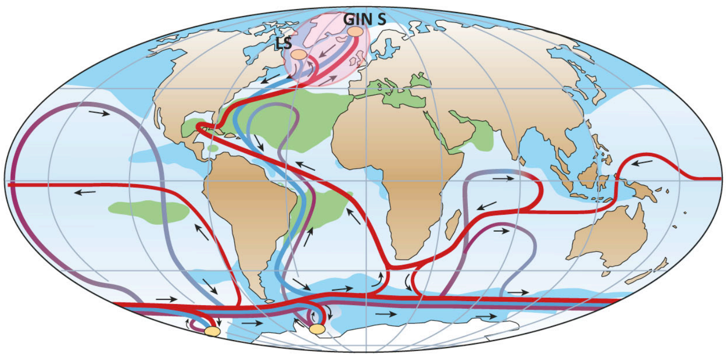

Figure 2 - 5: Simplified sketch of the global overturning circulation. Near-surface waters (red lines) flow towards three main deep-water formation regions, the North Atlantic (pink oval), the Ross Sea (RS) and the Weddell Sea (WS) (yellow ovals) and re-circulate at depth (deep currents shown in blue, bottom currents in purple; green shading indicates salinity above 36 psu, blue shading indicates salinity below 34 psu). In the North Atlantic there are two sites of deep-water formation, the Labrador Sea (LS), the GIN Sea (GIN S) (yellow ovals) (Rahmstrof, 2002).

2.3.2 Near surface North-east Atlantic currents

The surface oceanography of the north-eastern Atlantic is driven by the cyclonic North Atlantic Sub-Polar Gyre (SPG) and the anticyclonic Sub-Tropical Gyre (STG) (Häkkinen and Rhines, 2004; Hátún et al., 2005). Waters from the North Atlantic Current (NAC) follow the boundary between the two gyres (Hátún et al., 2005). The relative strength of the SPG and the STG is referred to as the gyre index. When the SPG is strong and develops an east-west shape then there is a greater influence of the SPG waters (lower salinity) relative to the STG waters (higher salinity) to the NAC to give a gyre index that is high. The trend is reversed giving a gyre index that is low when the SPG is weakened and presents a north-south shape, the relative influence of the STG waters to the NAC is enhanced (Hátún et al., 2005).

Such influence controls the intensity, position, and relative composition (salinity) of the NAC in the North-east Atlantic and therefore its inflow to the deep-water formation sites (Hátún et al., 2005) (Figure 2 - 6).

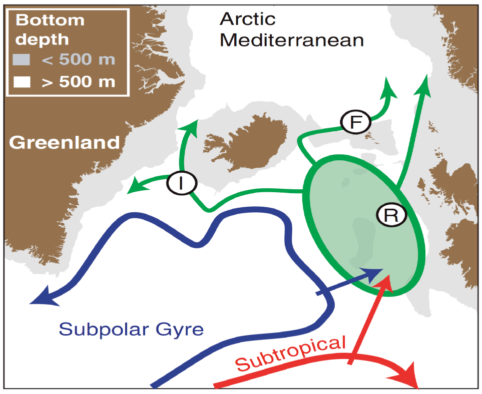

Figure 2 - 6: Sketch of the main features of the surface circulation in the NE Atlantic. The green shaded region shows where the subpolar and subtropical waters meet, mix and feed into the Arctic Mediterranean. Are reported on the map the Rockall Trough (R), the Faroe Current (F), and the Irminger Current (I) (Hátún et al., 2005).

2.4 The Holocene

Compared to glacial/interglacial cycles that characterize the Quaternary period (the last 2.6 Ma), the present interglacial, the Holocene (the last 11.5 ka) is considered to be relatively stable climatically. Nevertheless, Holocene climate variability has been punctuated by a series of low amplitude climate oscillations on timescales that impact upon ecosystem stability and human civilization (Bond et al., 1997; Mayewski et al., 2004; Wanner et al., 2011).

The Holocene period can be subdivided into three phases closely defined by climate forcing. This is shown in a selection of North Atlantic palaeo-climate records providing a comprehensive framework of the Holocene climate variability (Figure 2 - 7).

2.4.1 The Early Holocene 11 500 – 8 000 yr BP

The beginning of the Holocene is marked by maximal orbital forcing (high summer insolation in the Northern Hemisphere). The main feature of the period is the presence of extensive Northern Hemisphere ice sheets remaining from the previous glacial period melting rapidly causing rises in global sea level. Therefore, during this period changes in the ice sheet extent and ice sheet mass balance would have significantly impacted the global climate (Heikkilä and Seppä, 2003; Mayewski et al., 2004; Wanner et al., 2008).

2.4.2 The Mid Holocene from 8 000 to ~5500 yr BP

During the second phase of the Holocene, the Mid-Holocene or Holocene Thermal Maximum (HTM) there was still a high summer insolation in the northern hemisphere, but ice sheets were no longer large enough to have a significant impact on the climate (Kaufman et al., 2004; Renssen et al., 2009).

2.4.3 The Late Holocene from ~5500 yr BP to present

At about 5500 cal yr BP the post glacial rise in sea level was finished (Jansen et al., 2007) and the summer insolation in the northern hemisphere started declining (Berger et Loutre, 1991) with a corresponding rise in winter insolation (Figure 2 - 7). Nevertheless, this period is of great current research interest as it provides strong parallels with the major forcing that affect present-day climate. Therefore studies that help understand climate variability in the late Holocene may allow better discrimination between the effects of human activities and natural changes on the climate changes recorded over the last few centuries.

For the late Holocene five periods of significant rapid climate changes were documented worldwide at 6 000 – 5 000, 4 800 – 4 500, 3 300 – 2 500, 1 200 – 1 000 and 700 – 150 yr BP (Mayewski et al., 2004; Wanner et al., 2008; Wanner et al., 2011). The temperature and salinity variations of the western branch of the sub-surface North Atlantic inflow correlate with these rapid climate changes (Figure 2 – 7 (E); Thornalley et al., 2009). The North Atlantic inflow is warmer and saltier during enhanced freshwater flux to the sub-polar North Atlantic (Figure 2 - 7 (F); Bond et al., 2001; Bond et al., 1997). Strong westerlies over the North Atlantic are also reported at 6 000 – 5 000, 3 300 – 2 500, and 700 – 150 yr BP indicative that the North Atlantic inflow variability could be associated with atmospheric circulation changes (Figure 2 - 7 (D); Meeker and Mayewski, 2002). All the rapid climate changes reported here are associated with decreasing temperature in Greenland apart from the ones at 1 200 – 1 000 and 700 – 150 yr BP (Figure 2 – 7 (C); Mayewski et al., 2004). Decreasing solar output are also roughly correlates with the late Holocene climatic anomalies suggesting that solar variability could be a forcing factor, however this hypothesis remains strongly debated (Figure 2 – 7 (B); Berger, 1978).

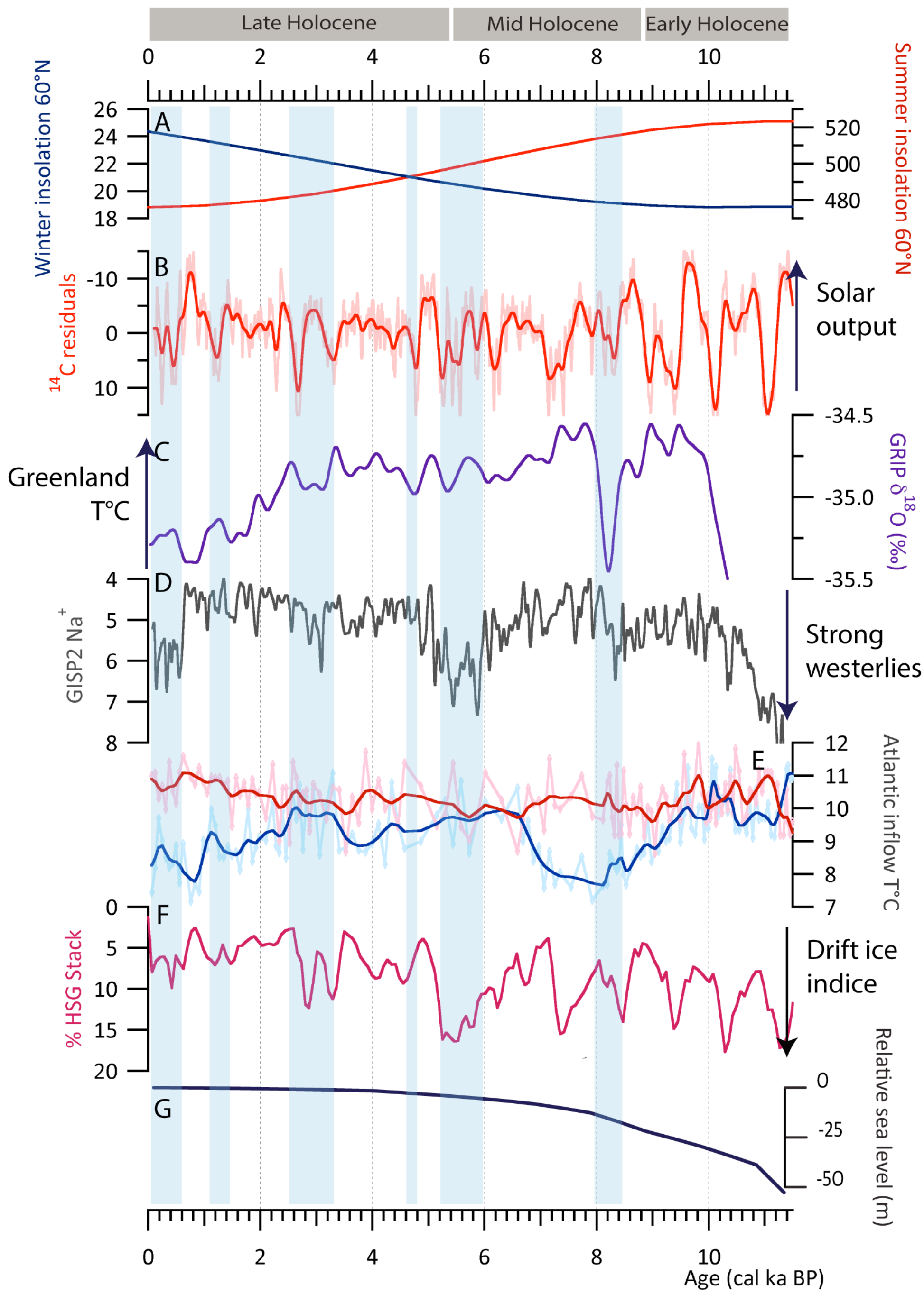

Figure 2 - 7: Climate forcing series and North Atlantic records. Blue bands represent timing of Holocene rapid climate changes (Mayewski et al., 2004; Wanner et al., 2011). (A) Winter (December) and Summer (June) insolation values (W m^{-2}) at 60ºN (Berger and Loutre, 1991), (B) $\Delta^{14}C$ residuals as proxy of solar output (Reimer et al., 2004), (C) GRIP $\delta^{18}O$ ‰ as proxy of Greenland temperature (Johnsen et al., 1997), (C) GISP2 Na+ (ppb) as proxy of atmospheric circulation (Meeker and Mayewski, 2002), (D) Near-surface (red) and sub-thermocline (blue) temperatures from South Iceland sediment core (RAPiD-12-1K; Thornalley et al., 2009), (C) Hematite-strained grains (%) from North Atlantic cores stack as proxy of freshwater flux to the sub-polar north Atlantic (Bond et al., 2001), (E) Relative Sea level changes (Jansen et al. , 2007).

Chapter 3: Materials and Methods

3.1 A study site: The Mingulay Reef Complex

3.1.1 Location

Mingulay Reef Complex is located in the Sea of Hebrides at the entrance to the Minch, between the west coast of Scotland and the Outer Hebrides island chain approximately 13 km east of the island of Mingulay, (56°50’N, 7°20’W) (Figure 3 - 1).

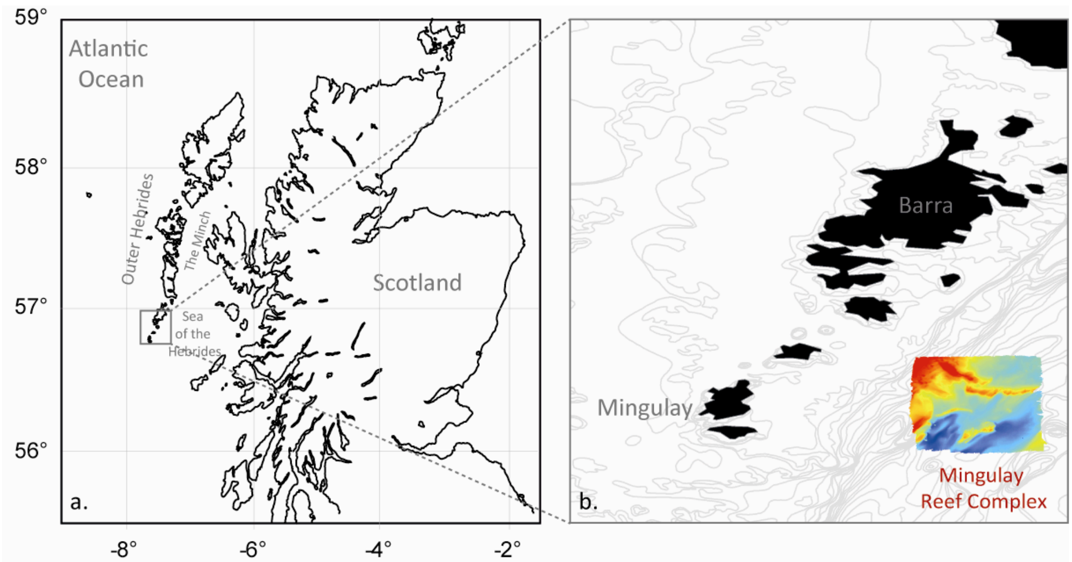

Figure 3 - 1: Regional setting of the Mingulay Reef Complex area relative to a global map of Scotland (a) and to the southern islands from the Outer Hebridean island chain (b).

3.1.2 Brief history of discovery and research

Research into the Mingulay Reef Complex began with the discovery of cold-water corals *Lophelia pertusa* in the early nineteenth century by fishermen (Wilson, 1979). The major advances in research and knowledge about the Mingulay Reef Complex, however, have occurred only in the last few decades due to the improvement of scientific techniques and technologies and the research efforts of the British Geological Survey (BGS) and the Scottish Association for Marine Science (SAMS) (See Davies et al., 2009b for review).

Research on the Mingulay Reef Complex gathered pace after extensive acoustic and video surveys during the Mapping INshore Coral Habitats (MINCH) project in 2003 (Long and Wilson, 2003; Roberts et al., 2005) followed by in-situ measurements of currents, temperature, turbidity, and fluorescence between 2006 and 2007 (Davies et al., 2009) and detailed study of local patterns in present-day species biodiversity (Henry et al., 2010).

3.1.3 Geological description

Most of the information about the Mingulay Reef Complex comes from reports and papers referring to the data obtained during the MINCH survey 2003 (Long and Wilson, 2003; Roberts et al., 2005; Roberts et al., 2004). During that project, five areas of the Mingulay Reef Complex were surveyed. Mingulay Reef 1 which is the location of the cores studied along this project will therefore be the primary focus of the following sections.

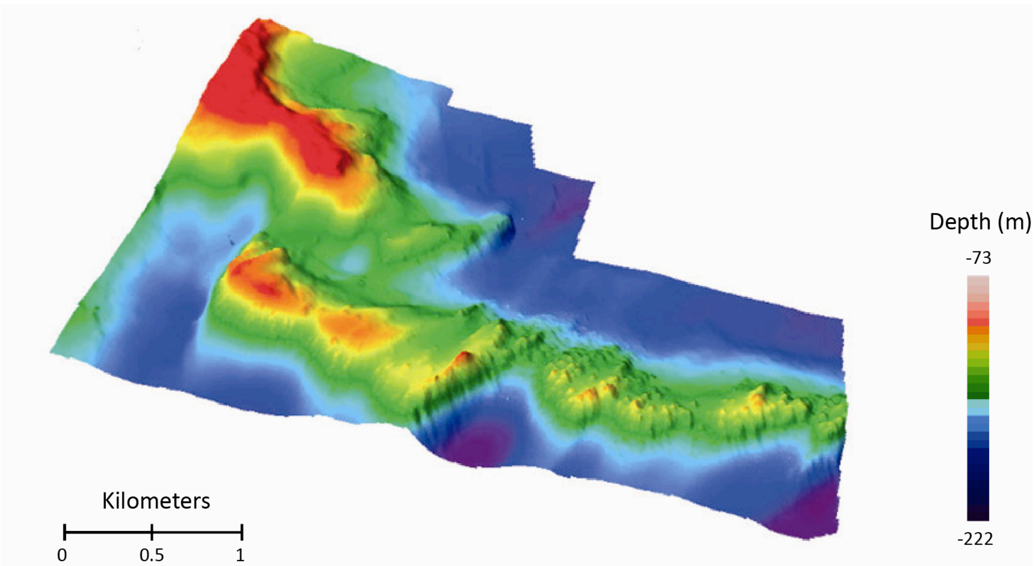

Figure 3 - 2: Three-dimensional visualisation of multibeam bathymetry from Mingulay 1.

Mingulay Reef 1 is the northernmost reef structures and also the largest area of the Mingulay Reef Complex, being approximately 4 km long and 500 m wide (Davies et al., 2009) (Figure 3 - 2). Mingulay Reef 1 rises 40 to 80 m above the average seafloor and is composed of two east-west orientated ridges. The water depth of Mingulay Reef 1 varies therefore from 72 to 215 m with the shallowest water being on the ridges (Roberts et al., 2005).

Prominent mound-like structures are predominately observed in the southern ridge. Those near-circular patches are up to 5 m high and have a general diameter of 15 m (Long and Wilson, 2003; Roberts et al., 2005; Roberts et al., 2004). The reefs are generally restricted to water depths of 110 m and below, but increasing in abundance up to this level (Long and Wilson, 2003). Video scanning of the seafloor and grab samples reveal that the mound-like structures are dominated by coral rubble as well as both living and dead reef framework formed by *Lophelia pertusa* (Long and Wilson, 2003; Roberts et al., 2005; Roberts et al., 2004). Live coral samples seem preferentially distributed on the top and flank of the mounds (Roberts et al., 2005). However, surface coral samples from Mingulay Reef 1 and Mingulay Reef 5 (North) have been radiocarbon dated to 3540±56 and 3 864±33 yrs BP (Roberts et al., 2005).

3.1.4 Modern oceanography

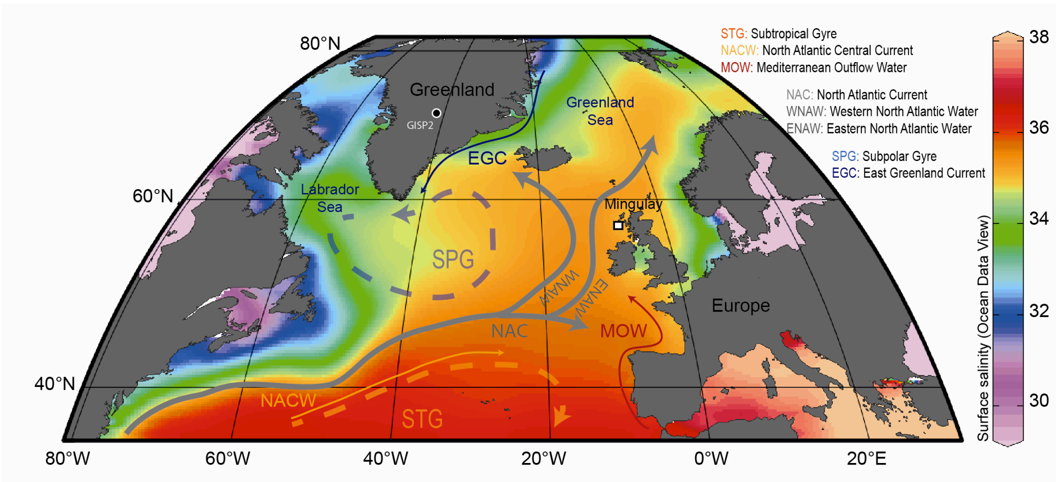

Figure 3 - 3: Simplified map of the major near surface currents of the North Atlantic superimposed on annual sea surface salinity.

Presently, waters from the North Atlantic Current occupy the outer parts of the continental shelf and the deeper (>100 m) coastal waters of west Scotland (Craig, 1959; Hill et al., 1997; Inall et al., 2009). At the surface the Scottish Coastal Current (SCC) brings northward colder and fresher waters from the Irish Sea and Clyde Sea (Ellett and Edwards, 1983).

The relative composition of the North Atlantic Current (NAC) at the Mingulay Reef Complex depends on the strength and shape of the Subpolar Gyre

(SPG) relative to the subtropical Gyre (STG) (Hátún et al., 2005; Inall et al., 2009). The North Atlantic Central Water (NACW), which lies underneath the surface mixed layer in between 100 and 700 m, is characterized by relatively warm, salty waters. This water mass circulates in the temperate Atlantic through the action of the STG. Thus, low SPG index (weak and a North-South SPG shape) would increase saltier, warmer and depleted in radiocarbon input from the STG waters to the NAC (Hátún et al., 2005). The East Greenland Current (EGC) is a major pathway of sea-ice and freshwater in the Atlantic Ocean. Thus high SPG index (stronger and an East-West shape) would induce a strengthened inflow of fresher, cooler SPG waters to the NAC to our study site. Waters of Mediterranean origin (MOW) may also have an influence on the NAC however; this point is still debated (Lozier and Stewart, 2008; New et al., 2001; Reid, 1979) (Figure 3 - 3).

At the southernmost point of the Outer Hebrides, the Barra Head mixing zone (Sadvidge and Lennon, 1987) is suspected to enhance the surface productivity in the surrounding area and may have favoured coral reef development in Mingulay Reef Complex (Roberts et al., 2005).

Multibeam backscatter images have revealed short trails (50 – 100 m) downslope of the southern flank of the southern ridge and longer trails (up to 500 m) on the northern flank of the same ridge (Roberts et al., 2005). Currents around the Mingulay Reef Complex are largely tidal and their strength and direction are altered by the topography of the reef (Davies et al., 2009). These trails lying perpendicular to the Mingulay Reef 1 seem therefore associated with the tidal current streams (SSW-NNE direction) (Long and Wilson, 2003; Roberts et al., 2005; Roberts et al., 2004).

Currents in the Mingulay Reef Complex are relatively strong. A recent study recorded mean amplitude of 29 cm s^{-1} (maximum recorded so far 81 cm s^{-1}) in the easternmost part of Mingulay Reef 1, and 22 cm s^{-1} (maximum recorded so far 67 cm s^{-1}) in the western part (Davies et al., 2009). The strong currents in this area create an advection onto the reef of deep bottom water rich in particulate matter. Moreover, the tidal flow induces a rapid downwelling of surface water to the reef. Both mechanisms enhance the food supplied to the corals at Mingulay 1 (Davies et al., 2009).

3.2 Material investigated

3.2.1 Core information

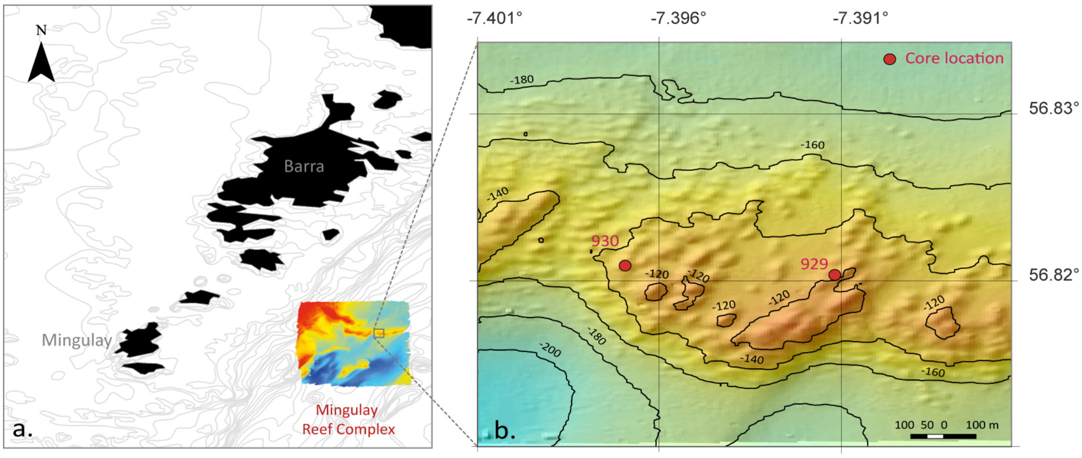

Figure 3 - 4: Location of cores sampling area relative to the Mingulay Reef Complex and the southern islands of the Outer Hebredian island chain (a) and zoom in on the position of the coral/sediment cores studied along this project (b).

In October 2007, the British Geological Survey (BGS) carried out a survey on board of the NERC vessel the *RRS James Cook* (Stewart and Gatliff, 2008). One of the aims of this project was to sample coral-mounds from Mingulay Reef 1 using the 6 m BGS vibrocorer. This corer is able to collect up to 6 m lengths of soft sediment embedded in a polycarbonate tube liner. The penetration into the seabed is controlled by vibration to preserve the collected core. The vibrocorer is retrieved by a controlled seabed winch. During the core sampling, real-time video footage was collected to ensure minimal damage to live corals. The cores were sliced into meter-length sections on board and then placed in a cold storage (4°C) at BGS until the beginning of this project (February 2009).

Analyses were carried out on the 2 longest cores: +56-08/929VE and +56-08/930VE (Figure 3 - 4 and Table 3 - 1), hereafter referred to as cores 929 and 930, because they potentially represent the longest time records.

Core name	Collection date	Location	Latitude o N/S	Longitude o E/W	Water depth (m)	Core recovery (m)
+56-08/929VE	04/10/07	Mingulay 1	56°49'19''	7°23'27''	127	3.61
+56-08/930VE	05/10/07	Mingulay 1	56°49'20''	7°23'47''	134	5.25

Table 3 - 1: BGS vibrocores information.

3.2.2 Surface coral sample information

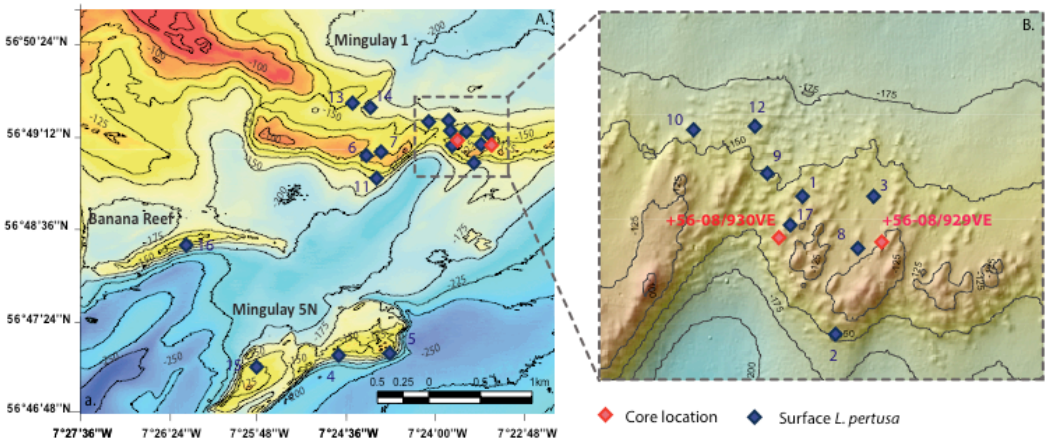

Figure 3 - 5: Location of the surface *Lophelia pertusa* samples sites. The information of the surface samples sites is reported in Table 3 - 2.

Lophelia sp. rubble from across the surface of the Mingulay Reef Complex (Mingulay 1, Mingulay 5 North, and Banana Reef area) were sampled between 2005 and 2011 using assisted video-grab on board of the *Esperanza* (2005), the *Discovery* (2009 and 2011) and the *Calanus* (2010) research vessels as part of on-going research examining the fauna associated with the reef complex. Other surface *L. pertusa* samples come from the top of cores recorded in 2007 by the British Geological Survey during a survey on board of the NERC vessel the *RRS James Cook*. Surface samples information is detailed in Figure 3 - 5 and Table 3 - 2.

Sample Name	Sample Collector	Collection Date	Location	Latitude o N/S	Longitude o E/W	Depth (m)
1. 2010-0223/002	Video-grab	23/02/10	Mingulay 1	56°49'24"	7°23'42"	125
2. 1151	Video-grab	15/05/05	Mingulay 1	56°49'08"	7°23'36"	121
3. 1154	Video-grab	15/05/05	Mingulay 1	56°49'24"	7°23'28"	146
4. 1156	Video-grab	15/05/05	Mingulay 5	56°47'14"	7°24'59"	140
5. 1157	Video-grab	15/05/05	Mingulay 5	56°47'15"	7°24'27"	122
6. 1168	Grab	18/05/05	Mingulay 1	56°49'11"	7°24'43"	125
7. 1169	Grab	18/05/05	Mingulay 1	56°49'14"	7°24'34"	128
8. 56-08/927 0-2cm	Vibro-core	24/09/07	Mingulay 1	56°49'18"	7°23'31"	123.5
9. HWU20110608/009A	Video-grab	08/06/11	Mingulay 1	56°49'27"	7°23'49"	162
10. HWU20110608/012A	Video-grab	08/06/11	Mingulay 1	56°49'33"	7°23'52"	162
11. HWU20110609/002A	Video-grab	09/06/11	Mingulay 1	56°48'59"	7°23'36"	162
12. HWU20110707/004A	Video-grab	07/07/11	Mingulay 1	56°49'32"	7°23'04"	135
13. HWU20110707/008A	Video-grab	07/07/11	Mingulay 1	56°49'42"	7°23'50"	134
14. HWU20110707/010A	Video-grab	07/07/11	Mingulay 1	56°49'40"	7°23'40"	154
15. 56-08/928	Vibro-corer	26/09/07	Mingulay 5	56°47'08"	7°25'48"	136
16. D340B/1488	Video-grab	01/07/09	Banana	56°48'19"	7°26'31"	118
17. D340B/1496a	Video-grab	02/07/09	Mingulay 1	56°49'21"	7°23'44"	125

Table 3 - 2: Surface *Lophelia pertusa* information.

3.3 Cores description and sampling

3.3.1 Cores opening

Sediment cores are typically split by running a taut wire through the mud. However, as this method would not be practical because the cores contained coral fragments embedded in sediment, they could not be cut using normal methods. Both cores were therefore frozen to avoid any shifting in the position and orientation of the coral fragments and to preserve any internal structure during the splitting procedure. While frozen, the cores were split at the BGS workshop using a diamond bladed circular rock-cutting saw. To avoid any potential contamination from the cutting fluid, the uppermost surfaces of the both halves were immediately removed. One of the core halves was preserved as an archive, while the other was designated as the working half.

3.3.2 Core photograph

Once opened and defrosted, the cores were photographed using a manual white-balance calibration to ensure accurate reproduction of colour. Each photograph was corrected for a slight spatial variation in exposure, and individual photographs were then stitched together into a photomontage (Figure 3 - 6).

3.3.3 Core description

The cores were described by a visual logging of the archive half: colour (using a Munsell colour chart: Munsell, 2000), textural group, and the distribution of corals and fossils.

Taken as a whole, the sediment of both cores consists mainly of olive grey mud. There are only small variations in the sediment composition and colour. Fragments of cold-water coral are present throughout the cores, albeit with varying abundance and preservation and with some areas presenting shelly-coral hash and/or pieces of shells have been observed. The shelly-coral hash layers defined in this study are layers presenting a significant amount of broken shells and/or heavily (bio)eroded coral fragments.

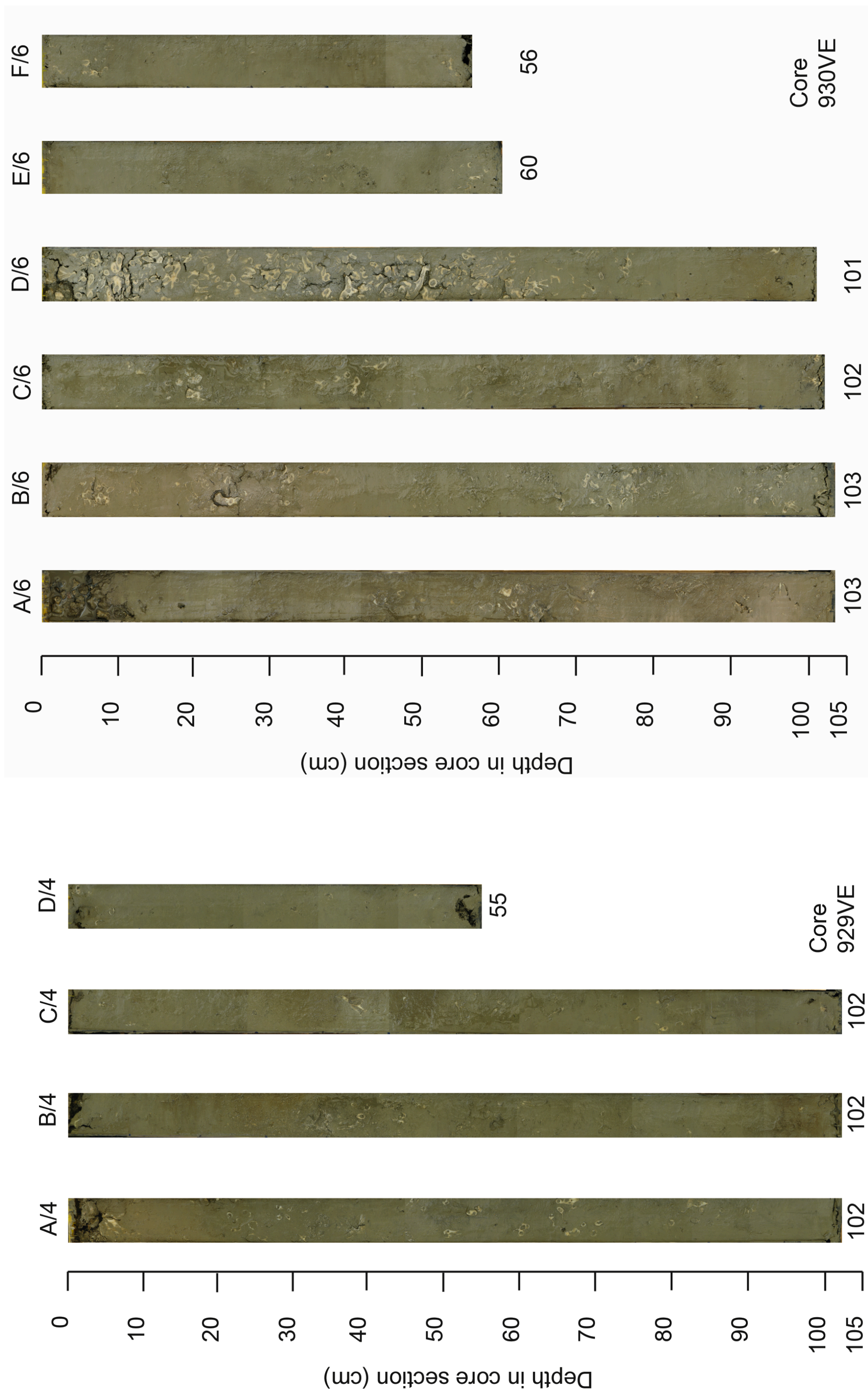

Figure 3 - 6: Photomontage of sections A/4 to D/4 of core 929 (left) sections A/6 to F/6 of core 930 (right). The length (in cm) of the each core section is indicated at the bottom.

3.3.4 Core dissection

The working half of the cores was sub-sampled for grain size analysis (see below) and dissected at 1 cm intervals, documenting the position and state of preservation of each coral fragment within the cores and archiving the sediment and coral fragments. After dissection, every fifth 1 cm sample (starting at 0 cm) was sieved through a 63 µm, 125 µm, 315 µm and 3 mm meshes. Coral and fossil fragments identification from the fraction above 315 µm and 3 mm was performed every tenth 1 cm sample (starting at 5 cm). Foraminifer isotopic measurements were performed on the fraction comprises between 125 µm and 315 µm every fifth 1 cm sample (starting at 0 cm) and benthic foraminifer's assemblages were done on 11 1 cm samples from the fraction between 315 and above and from 125 µm and 315 µm.

3.4 Core properties

3.4.1 Core CT scanning

The intact core sections were scanned using a Toshiba Aquilion 64 computed X-ray tomography (CT) at the Lorne and Islands District General Hospital in Argyll, Scotland. CT scanning uses X-ray detectors rotated through 360° to allow a reconstruction in 3 dimensions of the internal density structure of the cores. In this case, the coral (and fossils) fragments denser than the surrounding sediment are clearly revealed in white. CT slices of 1 mm thick were acquired along core 929 and 930. From the CT slices obtained and using the image J software longitudinal sections of each core sections were generated. Statistics were also generated from the CT scan slices the properties of the denser fragments (see Chapter 5 for more detail).

3.4.2 Multi sensor core logging

The two cores were passed through a GeoTek Multi-Sensor Core Logger (MSCL) at SAMS. Continuous measurements (every 1 cm) of wet bulk density (g cm^{-3}) and fractional porosity were obtained by gamma ray attenuation, as well as P-wave velocity (m s^{-1}), magnetic susceptibility (SI), and electrical resistivity (ohm m). The information retrieved from multi sensor core logging is corrupted by the presence of coral fragments. For this thesis only the density results were used to compare with our estimation performed from the CT scan data (Chapter 5).

3.4.3 Grain size analysis

A small (~ 1 g) sample of sediment was taken at 5 cm intervals from the working half of each core for particle size analysis. Particle size analysis was performed at SAMS using a Coulter LS230 laser sizer. This instrument measures the weight percentage of various grain size intervals between 0.04 and 2 000 µm in a sediment sample using laser diffraction. Measurements of grain size were performed on "bulk" samples, which were deflocculated using sodium hexametaphosphate solution and then on digested samples, which were treated with 20 % hydrogen peroxide (H_2O_2) and 10% nitric acid to remove organic carbon and carbonate.

The data generated has not been exploited during this project, other than to confirm the visual logging observations (see section 3.3.3).

3.5 Coral as a palaeo-proxy

3.5.1 Dating and marine radiocarbon reconstruction

While calcifying their skeletons, cold-water corals establish an equilibrium concentration of ^{238}U, ^{230}Th and ^{14}C isotopes with their surroundings. Assuming the coral aragonite maintains a closed-system behaviour when formed, the ^{238}U and ^{14}C lost by decay can therefore be used to determine the time of the skeleton was formed.

a. U-series dating

The relatively high uranium content of cold-water coral aragonite (between 3 100 and 5 500 ppb (Cheng et al., 2000a; Frank et al., 2005; Lomitschka and Mangini, 1999)) allows absolute U-series dating (Cheng et al., 2000a; Cheng et al., 2000b; Douville et al., 2010; Frank et al., 2005; Frank et al., 2004; Frank et al., 2009; Lomitschka and Mangini, 1999; Pons-Branchu et al., 2005).

The ^{238}U-series method is based on the radioactive decay series of ^{238}U in the sample itself. The main steps of the ^{238}U decay series lead to ^{234}U and ^{230}Th. The age of the aragonite mineralisation can be calculated by measuring the present-day activity ratios of $^{230}Th/^{238}U$ and $^{234}U/^{238}U$ (Ivanovitch and Harmon, 1992) (See Appendix 1 for more information about the principle of the U-series dating method).

b. Radiocarbon dating

The aragonite of cold-water corals is also ideally suited for radiocarbon dating, based on the ^{14}C decay to ^{14}N. The ^{14}C atoms created in the upper atmosphere by cosmic rays are rapidly oxidized to $^{14}CO_2$ and exchanged between the different active carbon reservoirs (Adkins, 2001). Since radiocarbon activity in the atmosphere is not constant through time, the radiocarbon decay has to be calibrated to calendar age using reference atmospheric records (Reimer et al., 2009). Atmospheric radiocarbon is transferred to the ocean primarily by air-sea gas exchange of $^{14}CO_2$. Surface waters equilibrated with the atmosphere are therefore enriched in radiocarbon but as they also exchange ^{14}C by mixing across the thermocline, marine radiocarbon composition is depleted compared with atmospheric ^{14}C. The relative age of the surface ocean is known as the reservoir effect (Stuiver et al., 1986). When dating marine carbonates time-dependant corrections can be made from the MARINE09 calibration curve, which incorporates global ocean reservoir correction of about 400 years (Reimer et al., 2009). However, for a given location the ^{14}C of the ocean surface deviates from this modeled marine curve (Stuiver et al., 1986). Thus, when dating marine carbonates it is essential to know the spatial and temporal difference (ΔR) between the modeled radiocarbon age of surface water and the known ^{14}C age of surface water at the time of formation of the marine carbonate sample.

Climatic and oceanic variations will result in temporal changes in the radiocarbon distribution within the reservoirs. Therefore, the radiocarbon signature of water masses can be use to trace ocean processes such as upper ocean ventilation and mixing, upwelling, deep-water formation (See Appendix 1 for more about the radiocarbon method principle).

c. Applications

- Dating techniques can be use to document cold-water coral's relative occurrence through time (see application in Chapter 4). Records of coral species geographical distribution through time can be used in turn as a useful palaeo-indicator for environmental changes.

- U-series dating on cold-water coral fragments from coral carbonate mounds coral/sediment cores allows quantification of the vertical mound growth rate (VMGR) and periods of active coral carbonate mound build-up (Frank et al., 2009) (see application in Chapter 4). Because the coral skeletal frameworks act as a sediment trap for both laterally and vertically advected sediment flux, the VMGR is consistently higher during favourable environmental conditions for coral growth. For instance, in mounds from the NE Atlantic the rate of growth during times of reduced or absent coral development is significantly smaller (< 0.05 mm a^{-1}) than when coral growth is active (> 0.3 mm a^{-1}) (Frank et al., 2009).

- When the radiocarbon age can be placed on an absolute age scale, such as U-series ages, estimation of the ^{14}C spatial and temporal deviation from the modelled curve could be used to reflect global ocean circulations variability associated with climate changes (see application Chapter 6).

3.5.2 Coral as a palaeo-environmental proxy

Studies to date have agreed that the elementary ratios in skeleton corals show a superposition of two signals: an environmental signal and a non-environmental signal (kinetic and/or vital effect). So far the lack of understanding of the mechanisms of calcification as well as what environmental parameters affect different elements have made the interpretation of trace elemental data difficult for palaeo-environmental reconstructions (Adkins et al., 2003; McConnaughey et al., 1989a; McConnaughey et al., 1989b).

3.6 Foraminifer assemblages and isotopic analysis

Foraminifers are zooplanktonic micro-organisms that can be benthic or planktonic. Most foraminiferal species have a shell made of calcite ($CaCO_3$), which incorporates the physicochemical characteristics of their surroundings. Also as calcite shells are relatively well preserved in the sediment after the death of the organisms, foraminifer's shells are therefore very useful for palaeo-environmental reconstruction.

3.6.1 Forminifer stable isotopic (C – O) composition

The calcitic shells of foraminifers are bio-mineralised through the incorporation of the calcium cation (Ca^{2+}), and the dissolved carbon inorganic species carbonate (CO_3^{2-}) and bicarbonate (HCO^{3-}). Foraminifer's calcite oxygen isotopic ($\delta^{18}O_{calcite}$) composition is a function of the seawater oxygen isotopic ($\delta^{18}O_{SW}$) composition and temperature (T°C) (Emiliani, 1955; Shackleton et al., 1977). Variations in $\delta^{13}C_{calcite}$ are primarily sensitive to carbon cycle and/or oceanic productivity (Zahn et al., 1986). Therefore, and despite some vital effects to take into consideration, carbon and oxygen isotopic measurements allow reconstructions of past-environments (i.e. salinity, temperature, productivity and carbon cycle).

3.6.2 Foraminifer assemblages

The ecology of benthic foraminifer communities are defined by hydrological parameters (e.g. salinity, temperature, dissolved oxygen), quantity and quality of organic flux to the seafloor, substrate availability (soft/hard surfaces – seafloor/elevated substrates) and current strength (Harloff and Mackensen, 1997; Jorissen et al., 1992; Jorissen et al., 1995; Jorissen et al., 2007; Murray, 2006). Therefore, foraminiferal assemblages can be used as bioindicators of certain environments.

Chapter 4: Growth of north-east Atlantic cold-water coral reefs and mounds during the Holocene: a high resolution U-series and ^{14}C chronology

4.1 Abstract

We investigated the Holocene growth history of the Mingulay Reef Complex, a seascape of inshore cold-water coral reefs off western Scotland, using U-series and radiocarbon dating methods. Both chronologies revealed episodic occurrences of the reef framework-forming scleractinian coral *Lophelia pertusa* during the late Holocene. Downcore U-series dating revealed unprecedented reef growth rates of up to 12 mm a^{-1} with a mean rate of 3 – 4 mm a^{-1}. Our study highlighted a persistent hiatus in coral occurrence from 1.4 ka to modern times despite present day conditions being conducive for coral growth. The growth history of the complex was punctuated at least twice by periods of reduced growth rates: 1.75 – 2.8 ka, 3.2 – 3.6 ka and to a lesser extent at 3.8 – 4 ka and at 4.2 ka. Timing of coral hiatuses and reduced reef growth rates at Mingulay were synchronous with those occurring across the wider northern European region, which suggests a close relationship between these ecosystems and large-scale shifts in palaeoenvironmental regimes associated with changes to the North Atlantic subpolar gyre.

4.2 Introduction

One of the most globally widespread cold-water corals is the reef framework-forming scleractinian *Lophelia pertusa*, which to date is known from all oceans except the Southern Ocean (Roberts et al., 2009). In the north-east Atlantic, *Lophelia* occurs preferentially along the European continental margin (de Mol et al., 2002; Kenyon et al., 2003; Wheeler et al., 2007) where it is often associated with areas of positive topographic relief such as banks, seamounts and ridges that create ideal environmental conditions (Davies et al., 2008). Local hydrodynamics are crucial for coral dispersal and recruitment, preventing corals from being smothered by sediments, and as a food supply mechanism for sessile suspension feeders such as corals (Genin et al., 1986; Frederiksen et al., 1992; White et al., 2005; Mienis et al., 2007; White, 2007; Davies et al., 2009; Mienis et al., 2009).

Some of the best studied *Lophelia* reefs are those found on coral carbonate mounds, which grow hundreds of metres high and several kilometres long (Wheeler et al., 2007). Several models of coral carbonate mound ontogeny have been proposed to explain the initiation and development of such structures, which generally converge on the importance of a complex interaction between sediment accumulation and cold-water coral colonisation and growth under favourable environmental regimes (Henriet et al., 2001; de Mol et al., 2002; Dorschel, 2003; Roberts et al., 2006; Rüggeberg et al., 2007; Eisele et al., 2008; de Haas et al., 2008). The last 11 ka, as well as previous warm interglacial periods such as marine isotope stages (MIS) 5, 7 and 9, have been favourable for coral growth and thus coral carbonate mound development in the north-east Atlantic between 50°N and 70°N (Frank et al., 2009; Douville et al., 2010; Frank et al., 2011). To date no *Lophelia* from glacial periods have been found at these latitudes (Dorschel, 2003; Kenyon et al., 2003; Schröder-Ritzrau et al., 2003; Frank et al., 2004; Dorschel et al., 2007; Rüggeberg et al., 2007; Mienis et al., 2009), hence glacial conditions are assumed to be detrimental to the growth of individual coral colonies and thus to coral carbonate mounds in this region (Kenyon et al., 2003; Frank et al., 2009; Frank et al., 2011). Interestingly, at lower latitudes (between 20°N and 50°N) in the eastern North Atlantic, *Lophelia* reef growth is reported during cool events and glacial periods such as the Younger Dryas and during MIS 2, 4, 6 and 8 in the Gulf of Cádiz, Mediterranean Sea and off Mauritania (Wienberg et al., 2009; McCulloch et al., 2010; Wienberg et al., 2010; Eisele et al., 2011; Frank et al., 2011). It has been suggested that the early Holocene northern migration of the polar front would have contributed to the restoration of optimal environmental conditions for *L. pertusa* occurrence (e.g. temperature, productivity, sedimentation processes) (Pirlet et al., 2011; Frank et al., 2011). Thus, it could be hypothesised that relative changes in AMOC associated with North Atlantic subpolar gyre (SPG) dynamics have also affected coral occurrence and growth over the last 11 ka.

U-series dating of cold-water coral fragments from coral carbonate mounds on the European continental margin allows quantification of the vertical mound growth rate (VMGR), a method that reveals periods of mound build-up coupled to palaeoceanographic changes (Frank et al., 2009). Because coral framework acts as a sediment trap for both laterally and vertically advected sediment flux, the VMGR is consistently higher during conditions favourable for coral growth. Such conditions are met when local hydrodynamics support repeated coral recruitment events that eventually coalesce to form large reef frameworks (Genin et al., 1986; Frederiksen et al., 1992; White et al., 2005; Mienis et al., 2007; White, 2007; Davies et al., 2009; Mienis et al., 2009; Frank et al., 2009; Frank et al., 2011; Chapter 5).

Since cold-water coral mounds and continental shelves are both frequently characterised by high growth and sedimentation rates, it is assumed that shallow inner-shelf cold-water coral reefs may have especially high growth rates. Sediment cores through these structures could therefore offer the potential for high-resolution palaeoenvironmental reconstructions. Cold-water coral reefs occur on the British continental shelf in the Sea of Hebrides (also known as The Minch), 13 kilometres east of the island of Mingulay (Figure 1; Roberts et al., 2005). Vibrocores containing mixed sediment/coral fragments were taken through the Mingulay Reef Complex in 2007 by the British Geological Survey, and are the subjects of our present study. The aims were to: (1) define the spatial and temporal evolution of the Mingulay Reef Complex, (2) estimate and compare north-east Atlantic *Lophelia* occurrence and reef/mound growth during the Holocene, and (3) establish whether large-scale shifts in palaeoenvironmental regimes have controlled coral occurrence and reef/mound growth during the Holocene.

4.3 Cold-water coral sampling

4.3.1 Vibrocores

Corals from two vibrocores on the Minguay Reef Complex were studied. The cores +56-08/929VE and +56-08/930VE (hereafter referred to as cores 929 and 930) were collected in October 2007 by the British Geological Survey during a survey on board the NERC vessel the *RRS James Cook* Cruise 015 (Stewart and Gatliff, 2008; Figure 4 - 1 and Table 4 - 1).

Table 4 - 1: Mingulay Reef cores information

	Core +56-08/929VE (hereafter referred to as **Core 929**)	**Core +56-08/930VE** (hereafter referred to as **Core 930**)
Latitude	56°49'19''N	56°49'20''N
Longitude	7°23'27''W	7°23'47''W
Depth	127 m	134 m
Recovery	3.61 m	5.25 m

Because the cores contained coral fragments embedded in sediment, they were frozen prior to splitting to avoid disrupting the position and orientation of the coral fragments and to preserve the core's internal sedimentary structure. While frozen, the cores were split using a diamond bladed circular rock-cutting saw. To avoid any potential contamination from the cutting fluid, the uppermost surfaces of both halves were immediately removed. Once opened and defrosted, the cores were dissected at 1 cm intervals, documenting the position and state of preservation of each coral fragment within the cores and archiving the sediment and coral fragments.

4.3.2 Surface sample locations

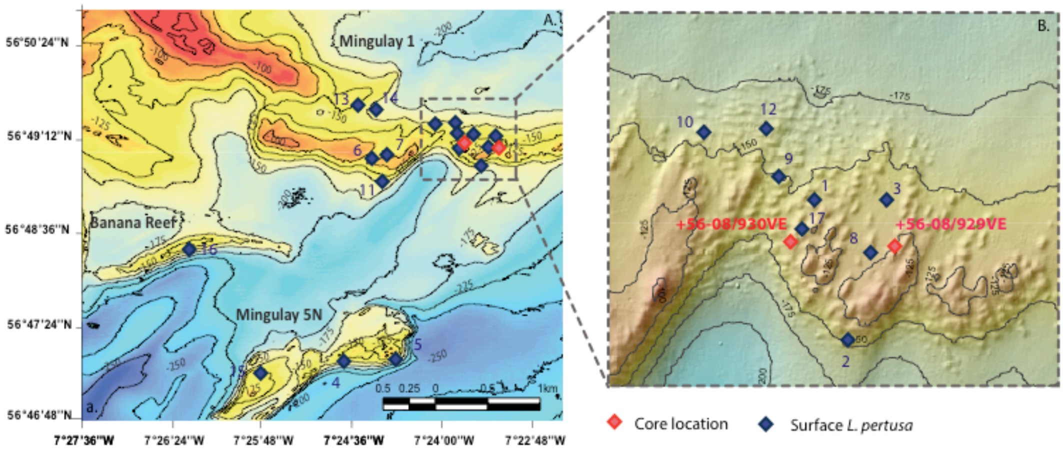

Figure 4 - 1: A. Location of the coral/sediment cores (red diamond) and surface *L. pertusa* samples sites (blue diamond) within the Mingulay Reef Complex, B. zoom in the position of the coral/sediment cores. The numbers indicated next to the blue diamonds correspond to the sample information reported in Table 4 - 3.

Surface videograb samples of coral rubble were taken from random locations at three reefs (Mingulay Reef 1, Mingulay Reef 5 North, and Banana Reef) during cruises on the research vessels MY *Esperanza* (2005), RRS *Discovery* Cruises 340b and 367 (2009 and 2011, respectively) and RV *Calanus* (2010). Three other surface samples were taken from the top of cores collected by the 2007 BGS cruise. Surface sample information is detailed in Figure 4 - 1 and Table 4 - 3.

4.3.3 Hydrological setting

Waters of Atlantic origin occupy the outer parts of the continental self and the deeper (>100 m) coastal waters of west Scotland (Craig, 1959; Hill et al., 1997; Inall et al., 2009). At the surface the northward flowing Scottish Coastal Current (SCC) brings cooler and fresher waters from the Irish and Clyde Seas (Ellett and Edwards, 1983). Today *Lophelia pertusa* reefs from the Mingulay Reef Complex are largely restricted to this Atlantic-origin water (Dodds et al., 2007) where strong SW-NE currents enhance the food supply to the coral reefs (Davies et al., 2009).

The Norwegian coral/sediment cores considered for this study were retrieved from Sjternsund (262 m) and Trænadjupet (315 m; López Correa et al., 2012). These two sites are bathed in North Atlantic Current (NAC) waters. The surface waters of the Norwegian shelf are characterised by the fresher Norwegian Coastal Current (NCC).

The NAC follows the boundary between the subpolar gyre (SPG) waters (fresher and cooler) and the subtropical gyre (STG; warmer and saltier) (Hátún et al., 2005). The NAC strength, direction and composition respond to SPG dynamics (Hátún et al., 2005): when the SPG circulation is stronger and presents a more pronounced east-west shape the SPG waters influence relative to the STG waters to the NAC is increased. Conversely, when the SPG circulation is weaker and forms a more pronounced north-south shape, a lower contribution of the SPG waters relative to the STG waters to the coral sites is observed (Figure 4 - 2).

Cold-water corals from sediment cores on Rockall Bank (core MD 01-2454G, 747 m water depth) and in the Porcupine Seabight (MD 01-2459G, 610 m water depth) were dated by Frank et al. (2009) and analysed by Colin et al. (2012) and Copard et al. (2012). The relative contributions of water masses at these coral sites are also directly influenced by SPG dynamics (Colin et al., 2010). The relatively homogenous Atlantic water flowing through Rockall Trough (Holliday, 2003) is formed by a mixture of SPG water, Subpolar Mode Water (SPMW) (Lacan and Jeandel, 2004) and water originating in the STG: the saline Eastern North Atlantic

Water (ENAW) and the saline and warm North Atlantic Central Water (NACW) (Piepgras and Wasserburg, 1987; Copard et al., 2010). The SPMW itself results from mixing of warm, saline NACW with relatively fresh, cold Sub-Arctic Intermediate Water (SAIW) (Piepgras and Wasserburg, 1987; Lacan and Jeandel, 2004).

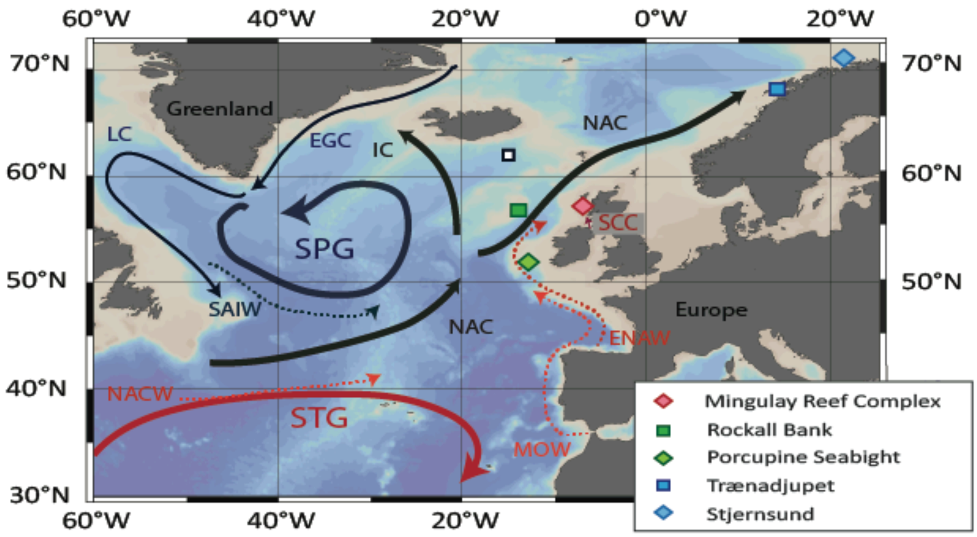

Figure 4 - 2: North-east Atlantic coral sites considered in this study relative to a simplified map of the North Atlantic surface currents and intermediate water masses. Are reported the East Greenland Current (EGC), the Labrador Current (LC), the North Atlantic Current (NAC) and its western branch the Irminger Current (IC), the North Atlantic Central Water (NACW) the Eastern North Atlantic Water (ENAW), the Sub-Arctic Intermediate Water (SAIW), the Mediterranean Outflow Water (MOW), the Scottish Coastal Current (SCC), the sub-polar gyre (SPG) and the sub-tropical gyre (STG). The location of the sediment core RAPiD-12-1K (Thornalley et al., 2009) is symbolised by a black square.

Finally, it is important to note that the northward flow of Mediterranean Outflow Water (MOW) and its influence at the different coral sites remains a matter of debate. Hydrological evidence suggests that MOW flows into the Porcupine Seabight (Holliday et al., 2000). However, at Rockall only episodic MOW influence occurs when the eastward extension of the SPG is reduced (Lozier and Stewart, 2008). It has been suggested that coral larvae from the Mediterranean Sea are transported along the north-east Atlantic margin through the action of MOW (De Mol et al., 2005). Thus, this water mass would be of significant importance for coral larvae recruitment in the north-east Atlantic.

4.4 Methods

Coral samples were dated using two methods. The downcore samples (n=34) were dated by U-series and the surface samples were radiocarbon dated (n=19).

4.4.1 Sample preparation

Before dating, only relatively pristine corals were selected and ultrasonically cleaned in distilled water to avoid contamination from sediments and surface deposits. Inner and outer surfaces of corals were mechanically removed using a DREMEL tool until samples appeared completely clean under a binocular microscope in order to remove contamination from iron and manganese oxides/hydroxides and surface sample re-crystallisation of aragonite into calcite. Following physical removal of the surfaces, samples were leached with hydrochloric acid (0.1 N) and rinsed three times with MilliQ water (e.g. Schröder-Ritzrau et al., 2003).

Once cleaned, a piece of each coral fragment was powdered using an agate mortar and pestle and screened by X-ray diffraction (XRD) at the University of Edinburgh for aragonite content and purity. Radiocarbon and U-series analyses were undertaken on fragments with >99 % aragonite content.

4.4.2 U-series dating

U and Th chemical separation and mass spectrometry were carried out at the NERC Isotope Geosciences Laboratory (NIGL), British Geological Survey, Keyworth. Samples were ultrasonicated in dilute HNO_3 and MilliQ water before dissolution in 15 M HNO_3. Dissolved samples were spiked with a mixed ^{229}Th-^{236}U tracer calibrated against gravimetric solutions prepared from CRM 112a U metal and Ames Laboratory high purity Th metal. All acids were prepared by double sub-boiling-distillation starting with RomilSpA grade stock. Pre-concentration by Fe co-precipitation prior to U-Th separation used a Fe in 1M HCl solution prepared from Puratronic Fe nitrate and the initial chemical separation of U and Th on 0.6 ml columns using AG-1 x 8 anion resin followed procedures established by Edwards et al. (1988). Separated Th aliquots were further purified using a second pass through AG-1 x 8 columns, while separated U was purified on UTEVA columns following

Andersen et al. (2008). Pilot U isotope data were obtained on a Thermo Triton thermal ionization mass spectrometer (TIMS) employing a Mascom SEM and RPQ. U was loaded as a nitrate on double zone-refined Re filament assemblies. Mass bias was monitored via replicate CRM 112a analyses, and SEM gain was corrected during sample analysis using $^{235}U/^{236}U$ measured sequentially on static SEM/Faraday and Faraday/Faraday detectors. Corresponding Th data were obtained on a Nu instruments NuHRmulticollector inductively coupled mass spectrometer (MC-ICP-MS). The bulk of the U and Th data for this study, however, were obtained on a latterly acquired Thermo Neptune Plus MC-ICP-MS. Samples were introduced with an Aridus II desolvating nebulizer in 0.2 M HCl - 0.05 M HF, while sample washout used sequential 0.25 M HCl – 0.1 M HF and 0.2 M HCl – 0.05 M HF following Andersen et al. (2008). U mass bias and SEM/Faraday gain correction of unknowns was based on standard bracketing; exponential correction for U mass bias was determined by analysis of CRM 112a spiked with a $^{233}U/^{236}U$ tracer (IRMM 3636), while SEM gain was monitored using the static SEM/Faraday measurement of $^{234}U/^{235}U$ on mass bias-corrected unspiked CRM 112a data. On peak zero, hydride and tailing corrections followed Heiss et al. (2013). Accuracy (within 0.1 %) and reproducibility (within 0.2 %) were monitored by replicate $^{234}U/^{238}U$ analyses of Harwell uraninite HU-1. Mass bias and SEM gain for Th measurements were corrected using an in-house ^{229}Th-^{230}Th-^{232}Th reference solution calibrated by ICP-MS against CRM 112a. Total ^{238}U and ^{232}Th blanks were <10 pg and <4 pg, respectively, during this study and were negligible relative to the sample U and Th. Data were reduced using an in-house Excel spreadsheet and ages calculated with Isoplot version 3 add-in (Ludwig, 2003a) following Ludwig (2003b) using the decay constants of Cheng et al. (2000). Correction for ^{230}Th from seawater followed Frank et al. (2005) ([$^{230}Th/^{232}Th$] = 10 ± 4). Quoted uncertainties (Table 2) for activity ratios, initial $^{234}U/^{238}U$, and ages are given at the 2 sigma level. These included a c. 0.2 % uncertainty calculated from the combined $^{236}U/^{229}Th$ tracer calibration uncertainty and measurement reproducibility of reference materials (HU-1, CRM 112a, in-house Th reference solution) as well as the propagated uncertainties from the seawater Th correction and measured isotope ratio uncertainty.

4.4.3 Radiocarbon dating

Nineteen surface *Lophelia* fragments were prepared to graphite at the NERC Radiocarbon Facility (East Kilbride). The samples were chemically etched to remove the outer 20 % (by weight) of each coral fragment by controlled hydrolysis using 0.02 M HCl. The samples were rinsed, dried and homogenised. A known weight of the pretreated sample was hydrolysed to CO_2 using 85 % orthophosphoric acid (H_3PO_4) at room temperature. An aliquot of CO_2 from each sample was taken to measure $\delta^{13}C$ (Table 4 - 3) on a dual inlet stable isotope mass spectrometer (VG OPTIMA) and was representative of $\delta^{13}C$ in the original, pre-treated sample material. The remaining CO_2 was converted to graphite by a two-stage reduction over heated Fe and Zn (Slota et al., 1987).

The ^{14}C in the samples was measured at the Scottish Universities Environmental Research Centre (SUERC) AMS Laboratory and corrected to $\delta^{13}C_{VPDB}$‰ -25 using $\delta^{13}C$ values provided in Table 3. Results are reported as conventional radiocarbon ka BP (relative to AD 1950) at the ±2σ level for overall analytical confidence and as calibrated age-ranges using the OxCal 4.1 calibration software (Bronk Ramsey, 2009) with the Marine 09 dataset (Reimer et al., 2009). A local marine reservoir correction (ΔR) of 0 was applied to sample ages < 1 ka, in line with the findings of Harkness (1983) and samples with older ages were corrected using ΔR= -79±17 years as per Ascough et al. (2004).

4.5 Results

4.5.1 U-series chronology

The downcore U-series dates acquired for this study are displayed in Table 4 - 2.

Sample Name	NIGL Batch/ Sample nb	Depth (cm)	^{238}U ppm	^{232}Th ppb	$^{230}Th/^{232}Th$ AR	$^{230}Th/^{238}U$ AR	$^{234}U/^{238}U$ AR	$\delta^{234}U_i$ (‰)	Age (ka)
1 929 A/4 3-9 cm	36/8	6.0 ± 3.0	3.356 ± 0.05	0.1409 ± 0.21	2562.6 ± 0.4	0.03533 ± 0.50	1.1455 ± 0.21	146.9 ±2.4	3.405 ± 0.019
2 929 A/4 12-17 cm	24/1	14.5 ± 2.5	3.748 ± 0.08	0.1361 ± 0.29	3108.8 ± 0.4	0.03708 ± 0.38	1.1485 ± 0.30	150.0 ±3.5	3.567 ± 0.018
3 929 A/4 38-41cm	38/1	39.5 ± 1.5	3.087 ± 0.05	0.1505 ± 0.30	2419.1 ± 2.7	0.03871 ± 2.74	1.1460 ± 0.21	147.6 ±2.4	3.734 ± 0.104
4 929 A/4 64-67 cm	38/2	65.5 ± 1.5	3.178 ± 0.05	0.1796 ± 0.18	2098.1 ± 0.2	0.03888 ± 0.39	1.1471 ± 0.21	148.7 ±2.4	3.747 ± 0.017
5 929 A/4 90-91cm	39/9	90.5 ± 0.5	3.049 ± 0.05	0.1250 ± 0.07	2925.7 ± 0.2	0.03939 ± 0.33	1.1462 ± 0.20	147.8 ±2.4	3.800 ± 0.015
6 929 A/4 100-101cm	38/3	100.5 ± 0.5	3.984 ± 0.06	0.1771 ± 0.07	2020.8 ± 0.2	0.02945 ± 0.40	1.1468 ± 0.21	147.9 ±2.4	2.828 ± 0.013
7 929 B/4 106-108 cm	36/9	107.0 ± 1.0	3.099 ± 0.05	0.1458 ± 0.21	2516.2 ± 0.4	0.03885 ± 0.50	1.1452 ± 0.20	146.7 ±2.4	3.751 ± 0.021
8 929 B/4 188-189 cm	35/3	188.5 ± 0.5	3.124 ± 0.05	0.2477 ± 0.11	1598.3 ± 0.1	0.04150 ± 0.45	1.1429 ± 0.21	144.5 ±2.4	4.019 ± 0.020
9 929 C/4 213-216 cm	38/6	214.5 ± 1.5	2.765 ± 0.06	0.2596 ± 0.07	1361.3 ± 0.2	0.04182 ± 0.52	1.1453 ± 0.21	147.0 ±2.4	4.043 ± 0.023
10 929 C/4 249-252 cm	38/7	250.5 ± 1.5	3.090 ± 0.05	0.2793 ± 0.07	1456.9 ± 0.2	0.04309 ± 0.50	1.1455 ± 0.21	147.2 ±2.4	4.166 ± 0.023
11 929 C14 284-290 cm	35/1	287.0 ± 3.0	2.725 ± 0.05	0.1465 ± 0.11	2487.6 ± 0.2	0.04391 ± 0.35	1.1455 ± 0.21	147.2 ±2.4	4.248 ± 0.018
12 929 D/4 310-312 cm	36/10	311.0 ± 1.0	3.077 ± 0.05	0.2044 ± 0.21	2010.2 ± 0.4	0.04378 ± 0.53	1.1446 ± 0.20	146.3 ±2.4	4.238 ± 0.025
13 929 D/4 349-353 cm	35/6	351.0 ± 2.0	2.981 ± 0.05	0.3327 ± 0.11	1213.6 ± 0.1	0.04427 ± 0.56	1.1445 ± 0.21	146.3 ±2.4	4.287 ± 0.026
14 930 A/6 4-6 cm	35/8	5.0 ± 1.0	3.474 ± 0.05	0.4740 ± 0.13	415.8 ± 0.2	0.01825 ± 1.53	1.1427 ± 0.20	143.4 ±2.3	1.750 ± 0.027
15 930 A/6 24-29 cm	35/7	26.5 ± 2.5	3.066 ± 0.06	0.1159 ± 0.11	1752.2 ± 0.2	0.02171 ± 0.42	1.1450 ± 0.21	145.8 ±2.4	2.081 ± 0.010
16 930 A/6 42-45 cm	39/1	43.5 ± 1.5	2.996 ± 0.07	0.2519 ± 0.07	814.2 ± 0.2	0.02229 ± 0.81	1.1465 ± 0.23	147.4 ±2.7	2.134 ± 0.018
17 930 B/6 107-110 cm	39/3	108.5 ± 1.5	3.230 ± 0.08	0.3177 ± 0.07	894.9 ± 0.2	0.02868 ± 0.74	1.1462 ± 0.22	147.4 ±2.5	2.754 ± 0.022
18 930 B/6 124-127 cm	35/9	135.5 ± 1.5	3.018 ± 0.05	0.3137 ± 0.13	875.1 ± 0.2	0.02963 ± 0.75	1.1418 ± 0.21	142.9 ±2.4	2.858 ± 0.023
19 930 B/6 134-137 cm	39/10	135.5 ± 1.5	3.020 ± 0.05	0.2414 ± 0.26	1144.5 ± 0.4	0.02989 ± 0.66	1.1464 ± 0.21	147.6 ±2.4	2.871 ± 0.020
20 930 B/6 142-146 cm	36/1	144.0 ± 2.0	2.805 ± 0.05	0.1327 ± 0.07	1866.4 ± 0.1	0.02894 ± 0.41	1.1455 ± 0.20	146.6 ±2.4	2.782 ± 0.013
21 930 B/6 142-146 cm	40/2	144.0 ± 2.0	2.824 ± 0.05	0.1503 ± 0.21	1674.8 ± 0.4	0.02920 ± 0.56	1.1456 ± 0.21	146.7 ±2.4	2.807 ± 0.017
22 930 B/6 199-202 cm	39/4	200.5 ± 1.5	2.770 ± 0.10	0.4841 ± 0.07	1364.2 ± 0.2	0.07800 ± 0.52	1.1431 ± 0.25	146.3 ±3.0	7.675 ± 0.046
23 930 C/6 214-217 cm	39/5	215.5 ± 1.5	3.568 ± 0.05	0.2422 ± 0.07	1410.4 ± 0.2	0.03133 ± 0.51	1.1460 ± 0.21	147.3 ±2.4	3.012 ± 0.017
24 930 C/6 251-254 cm	38/9	252.5 ± 1.5	3.025 ± 0.07	0.0999 ± 0.20	2949.4 ± 0.3	0.03199 ± 0.35	1.1448 ± 0.21	146.1 ±2.4	3.080 ± 0.013
25 930 D/6 312-314 cm	36/2	313.0 ± 1.0	2.747 ± 0.05	0.3625 ± 0.06	769.4 ± 0.1	0.03303 ± 0.84	1.1437 ± 0.20	145.0 ±2.4	3.185 ± 0.028
26 930 D/6 356-358 cm	39/7	357.0 ± 1.0	3.038 ± 0.05	0.2515 ± 0.07	1251.5 ± 0.2	0.03387 ± 0.55	1.1465 ± 0.21	147.8 ±2.4	3.259 ± 0.020
27 930 D/6 377-379 cm	36/3	378.0 ± 1.0	2.305 ± 0.05	0.3012 ± 0.07	851.8 ± 0.1	0.03625 ± 0.76	1.1450 ± 0.20	146.4 ±2.4	3.497 ± 0.028
28 930 D/6 377-379 cm	40/3	378.0 ± 1.0	3.803 ± 0.05	0.2619 ± 0.12	961.0 ± 0.4	0.02159 ± 0.76	1.1447 ± 0.21	145.5 ±2.4	2.070 ± 0.016
29 930 D/6 388-392 cm	24/8	390.0 ± 2.0	2.762 ± 0.05	0.2425 ± 0.09	1232.1 ± 0.2	0.03535 ± 0.56	1.1449 ± 0.21	146.4 ±2.5	3.409 ± 0.021
30 930 D/6 388-392 cm	40/4	390.0 ± 2.0	3.234 ± 0.05	0.3715 ± 0.09	875.8 ± 0.4	0.03278 ± 0.81	1.1447 ± 0.21	146.0 ±2.4	3.158 ± 0.027
31 930 D/6 408-409 cm	36/5	408.5 ± 0.5	2.429 ± 0.05	0.2659 ± 0.06	1203.9 ± 0.1	0.04307 ± 0.56	1.1465 ± 0.21	148.2 ±2.4	4.161 ± 0.025
32 930 E/6 438-440 cm	36/6	439.0 ± 1.0	2.781 ± 0.05	0.2672 ± 0.06	1175.8 ± 0.1	0.03691 ± 0.57	1.1415 ± 0.20	142.9 ±2.4	3.573 ± 0.022
33 930 E/6 459-461 cm	40/5	460.0 ± 1.0	2.615 ± 0.05	0.2042 ± 0.10	1556.7 ± 0.4	0.03981 ± 0.56	1.1447 ± 0.21	146.3 ±2.4	3.847 ± 0.024
34 930 F/6 505-510 cm	39/8	507.5 ± 2.5	2.871 ± 0.05	0.2703 ± 0.07	1227.6 ± 0.2	0.03779 ± 0.57	1.1468 ± 0.21	148.3 ±2.4	3.641 ± 0.022
35 Grab 15 5.5.10	35/2	seafloor	2.396 ± 0.05	0.1644 ± 0.11	20.2 ± 0.6	0.0002314 ± 59.65	1.1448 ± 0.21	144.8 ±2.4	0.022 ± 0.013
36 Grab 15 5.5.10	40/6	seafloor	2.527 ± 0.06	0.0678 ± 0.28	35.4 ± 1.5	0.0002243 ± 24.14	1.1485 ± 0.23	148.5 ±2.6	0.021 ± 0.005

Uncertainties are quoted at the ± 2s level, in % for activity ratios and absolute for other quantities

Table 4 - 2: U-series dates from downcore *Lophelia pertusa* samples. The depth represents the location of the coral fragments within the cores +/- half of its length.

Mingulay corals contained between 2.8 - 3.8 ppm of uranium. Sixteen and twenty-three U-series dates from *Lophelia pertusa* fragments were obtained for cores 929 and 930, respectively. These data permit the construction of age/depth profiles for the two cores (Figure 4 - 3).

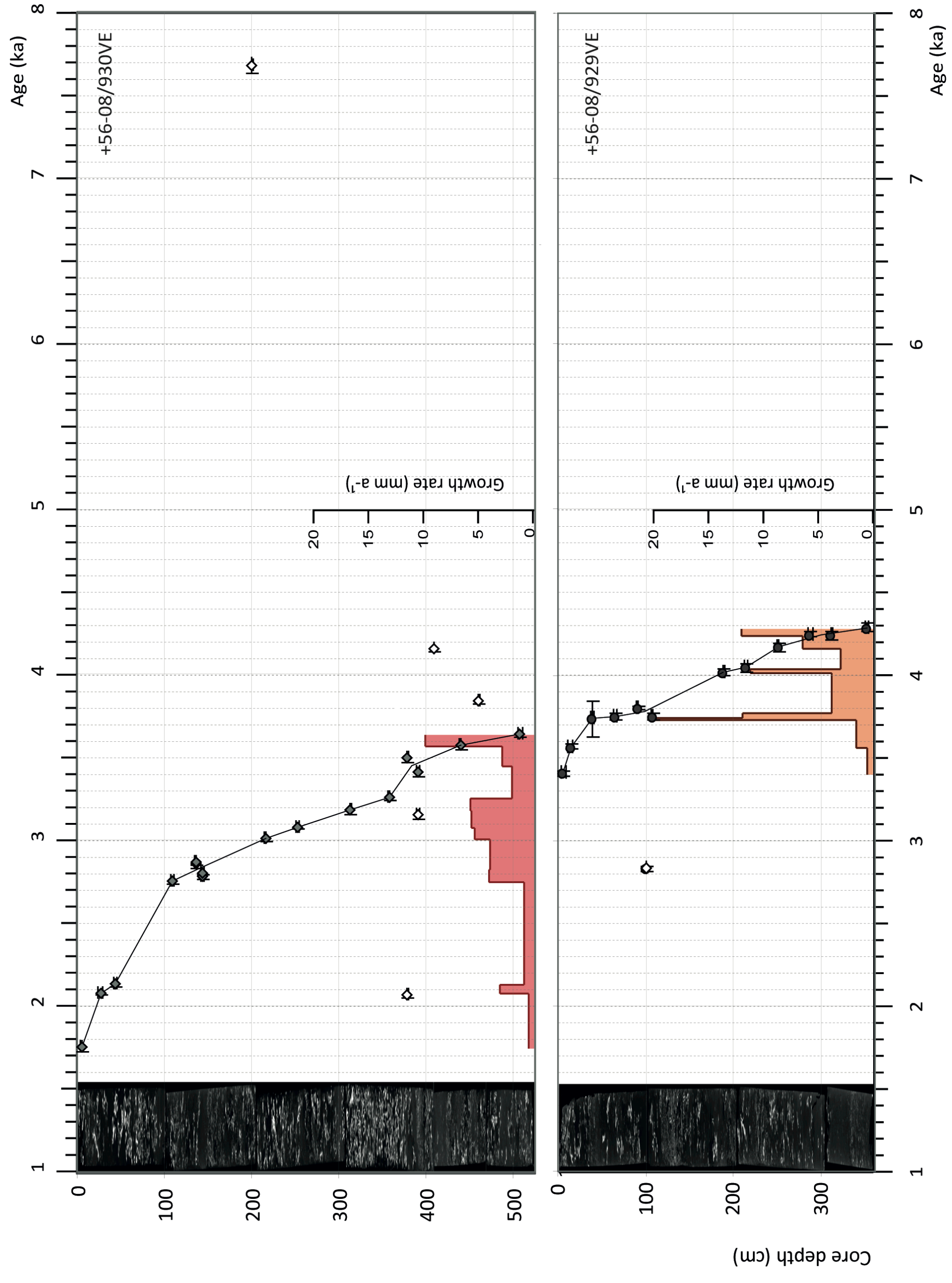

Figure 4 - 3: Age (ka) – Depth (cm) relationship of core 930 and 929. On the left of each profile is presented the CT scan image of the cores. All symbols in grey and white are U-series ages.

The $\delta^{234}U_{inital}$ values of the samples considered in this study ranged from 142.9 ± 2.4 ‰ to 150.0 ± 3.5 ‰ (2σ uncertainties). These values are indistinguishable from published $\delta^{234}U$ values of seawater (149.6 ± 3 ‰ 1SD, n=23; Delanghe et al., 2002 or 146.6 ± 2.5 ‰ 1se; Robinson et al., 2004) and are close to modern cold-water coral values from the Pacific, Atlantic, Indian and Southern Oceans sampled from various water depths (145.5 ± 2.3‰, 2σ, n=20; Cheng et al. 2000a). ^{232}Th values for all corals (Table 4 - 2) were relatively low at < 0.48 ± 0.07 ppb, supporting the notion that most of the corals analysed here are primarily aragonitic (Frank et al., 2004). Finally, one coral fragment collected alive was dated in duplicate, with measured ages of 22 ± 13 a and 21 ± 5 a. Assuming the growth rate of an individual coral is 15 – 17 mm a^{-1} (Orejas et al., 2008), and that the uppermost calices were removed during the cleaning procedure, the 1 to 2 cm of the coral fragments analyzed provide very accurate and reproducible ages giving us confidence in our fossil data.

After screening by $\delta^{234}U$ values, six dates were out of stratigraphic sequence (samples 6, 22, 28, 30, 31, 33; Table 4 - 2). Three hypotheses could explain this issue: (1) collapse and mixing of coral fragments from the same colony, (2) older material from adjacent reefs has been reworked and transported to the actively accumulating reef site, or (3) entrainment of young coral fragments into the deeper core section (de Haas et al., 2008, Frank et al., 2009). Samples 22, 31 and 33 were significantly older than would be interpolated from the U-series age/depth relationship (Figure 4 - 3). This indicates potential reworking and transport of older material from an adjacent reef. The base of the reef (the last 100 cm of core 930) included two age reversals toward older ages indicating that at the early stages of coral reef growth the height of the reef allowed more frequent transport of older material. These ages were not included in our growth rate estimations. Samples 6, 28 and 30 presented significantly younger ages given the U-series age/depth relationship, implying that the younger material may have become entrained during sampling. Note that two samples (27 and 29) from the same stratigraphic layer as samples 28 and 30 present ages in agreement with the stratigraphic sequence. Thus, we have only considered samples 28 and 30 for the rest of our study.

4.5.2 Mingulay Reef Complex growth rates

Sufficient reliable high-resolution U-series data were acquired to characterise cold-water coral reef growth. With the exception of a few age inversions, 80 % of the coral fragments present along the cores from the Mingulay Reef Complex were in stratigraphic order.

All fragments dated in this study were mid- to late Holocene. The stratigraphic model of core 929 exhibited ages from 3.41 to 4.29 ka and between 1.75 and 3.64 ka for core 930. The oldest *Lophelia pertusa* fragment age at 7.68 ka was measured from one out of stratigraphic order sample in core 930. Core 929 had a vertical growth rate averaging 4 mm a^{-1}, although this varied between 0.5 and 12 mm a^{-1} (Figure 4 - 3). Three major peaks in growth rate are centred at 3.7, 4, and 4.2 ka. The spike in growth rate reached 19.5 mm a^{-1} as estimated from one U-series age presenting an error of 0.1 a, therefore, it is possible that this value was slightly overestimated. Core 930 showed an average growth rate of 3 mm a^{-1}, ranging from 0.6 to 10 mm a^{-1} (Figure 4 - 3).

Two major reductions in growth rate (< 2 mm a^{-1}) were observed at 1.75 – 2.8 ka and 3.2 – 3.6 ka. Two minor reductions were noted in core 929 at 3.8 – 4 ka and at ~ 4.2 ka. The growth rate decline at ~ 3.5 ka was recorded in both cores, suggesting that coral growth was affected over a wider area across the reef complex.

4.5.3 Radiocarbon chronology

The age of the core tops (1.7 ka and 3.5 ka) were close to previously published radiocarbon dates from the surface of Mingulay Reef 1 and Mingulay Reef 5 (North), 3.54 ± 0.06 to 3.86 ± 0.03 ka BP, respectively (Roberts et al., 2005). These samples revealed that dead coral rubble found adjacent to living corals was much older than anticipated. Data from the 21 surface corals suggested that all samples were late Holocene (0 – 4.2 ka; Table 4 - 3 and Figure 4 - 4). The ages of dead coral spread more or less evenly across the period from 1.4 to 4 ka, with some evidence for clusters of ages 1.41 to 2.05 ka, 2.77 ka, 3.16 to 3.25 ka, 3.6 ka, 3.8 to 4 ka and 4.2 ka. This could indicate episodic mortality events and/or reductions in reef growth. Most importantly the absence of any coral between modern times and 1.4 ka strongly suggests that Mingulay reef growth was significantly disrupted sometime around 1.4 ka ago.

	Sample Number	Sample Name	Sample Collector	Collection Date	Location	Latitude o N/S	Longitude o E/W	Depth (m)	$\delta^{13}C^{PDB}$ ±0.1 (‰)	Conventional ^{14}C-age (ka BP)	Calibrated age-range ±2σ (cal ka BP)	
1	SUERC-33518	2010-0223/002	Video-grab	23/02/10	Mingulay 1	56°49'24"	7°23'42"	125	-8.8		Post bomb	
2	SUERC-33519	1151	Video-grab	15/05/05	Mingulay 1	56°49'08"	7°23'36"	121	-5.1	1.821 ± 0.035	1341	1540
3	SUERC-33522	1154	Video-grab	15/05/05	Mingulay 1	56°49'24"	7°23'28"	146	-6.8		Post bomb	
4	SUERC-33523	1156	Video-grab	15/05/05	Mingulay 5 N	56°47'14"	7°24'59"	140	-7.7		Post bomb	
5	SUERC-33524	1157	Video-grab	15/05/05	Mingulay 5 N	56°47'15"	7°24'27"	122	-6.7	0.404 ± 0.035	post1950	116
6	SUERC-33525	1168	Grab	18/05/05	Mingulay 1	56°49'11"	7°24'43"	125	-5.3	3.853 ± 0.035	3813	4057
7	SUERC-33526	1169	Grab	18/05/05	Mingulay 1	56°49'14"	7°24'34"	128	-4.3	3.247 ± 0.035	3058	3313
8	SUERC-33527	929 VE 3-9cm	Vibro-core	04/10/07	Mingulay 1	56°49'19"	7°23'27"	125	-5.2	3.728 ± 0.035	3633	3865
9	SUERC-33528	930 VE 4-6cm	Vibro-core	04/10/07	Mingulay 1	56°49'20"	7°23'47"	130	-5.4	2.283 ± 0.037	1877	2104
10	SUERC-33529	56-08/927 0-2cm	Vibro-core	24/09/07	Mingulay 1	56°49'18"	7°23'31"	123.5	-6.8	3.184 ± 0.037	2956	3227
11	SUERC-36967	HWU20110608/009A	Video-grab	08/06/11	Mingulay 1	56°49'27"	7°23'49"	162	-6.3	0.484 ± 0.037	229	0
12	SUERC-36968	HWU20110608/012A	Video-grab	08/06/11	Mingulay 1	56°49'33"	7°23'52"	162	-6.9	1.989 ± 0.035	1755	1528
13	SUERC-36969	HWU20110609/002A	Video-grab	09/06/11	Mingulay 1	56°48'59"	7°23'36"	162	-5.3	1.827 ± 0.035	1547	1345
14	SUERC-36972	HWU20110707/004A	Video-grab	07/07/11	Mingulay 1	56°49'32"	7°23'04"	135	-6.6		Post bomb	
15	SUERC-36973	HWU20110707/008A	Video-grab	07/07/11	Mingulay 1	56°49'42"	7°23'50"	134	-5.9	2.211 ± 0.035	2012	1798
16	SUERC-36974	HWU20110707/010A	Video-grab	07/07/11	Mingulay 1	56°49'40"	7°23'40"	154	-7.1		Post bomb	
17	SUERC-36975	56-08/928	Vibro-corer	26/09/07	Mingulay 5 N	56°47'08"	7°25'48"	136	-5.1	2.835 ± 0.035	2773	2548
18	SUERC-36976	D340B/1488	Video-grab	01/07/09	Banana	56°48'19"	7°26'31"	118	-4.8	4.026 ± 0.035	4293	4006
19	SUERC-36977	D340B/1496a	Video-grab	02/07/09	Mingulay 1	56°49'21"	7°23'44"	125	-4.7	1.742 ± 0.036	1475	1280
9	SUERC-36963	930 D/6 408-409cm	Vibro-core	04/10/07	Mingulay 1	56°49'20"	7°23'47"	130	-6.7	3.569 ± 0.035	3667	3441

Table 4 - 3: Radiocarbon age of *Lophelia pertusa* samples from Mingulay Reef Complex seabed. Post bomb samples are highlighted in blue and italic. Data presented in the table were calibrated using the program Oxcal 4.1 (Bronk Ramsey, 2009) and the dataset (MARINE 09) (Reimer et al., 2009), the ages were also corrected from local ΔR=79 ± 17 yr (Ascough et al., 2004).

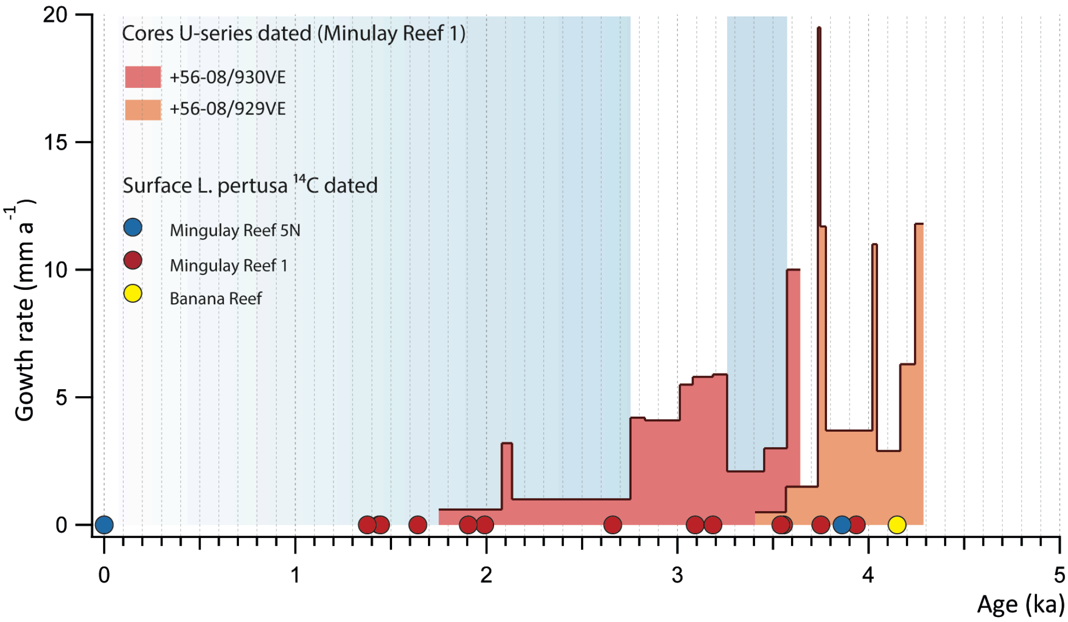

Figure 4 - 4: Growth rates estimated from cores 930 (pink) and 929 (orange). The round symbols represent the surface radiocarbon dates obtained from Mingulay 1 (red), Mingulay 5N (blue) and Banana reef (yellow). The blue bands represent the major decrease in growth rate recorded by the two cores.

4.6 Discussion

4.6.1 Holocene reef growth rates

Our data can be compared with other intensively dated coral-bearing sediment cores from the north-east Atlantic (Frank et al., 2009; López Correa et al., 2012; Figure 4 - 5). We chose to only consider *L. pertusa* dating in light of the probability that each cold-water coral species has specific environmental requirements.

The most intensively dated coral/sediment cores from mounds on the Celtic margin are cores MD 01-2454G from Rockall Bank and MD 01-2459G from the Porcupine Seabight (Frank et al., 2009). U-series dating revealed a VMGR from about 0.05 to 2.2 $mm.a^{-1}$ with values on average ~ 0.2 $mm.a^{-1}$ (Frank et al., 2009). By comparison, Holocene growth at Mingulay was on average 15 to 20 times greater (Figure 4 - 5). The lower resolution of the dating around one U/Th date every 450 years from the Celtic Margin cores (MD 01-2454G and MD 01-2459G) might have averaged out some of the peaks in growth rates, but probably not enough to explain the difference in VMGR with the Mingulay cores, which had on average one date every 100 a.

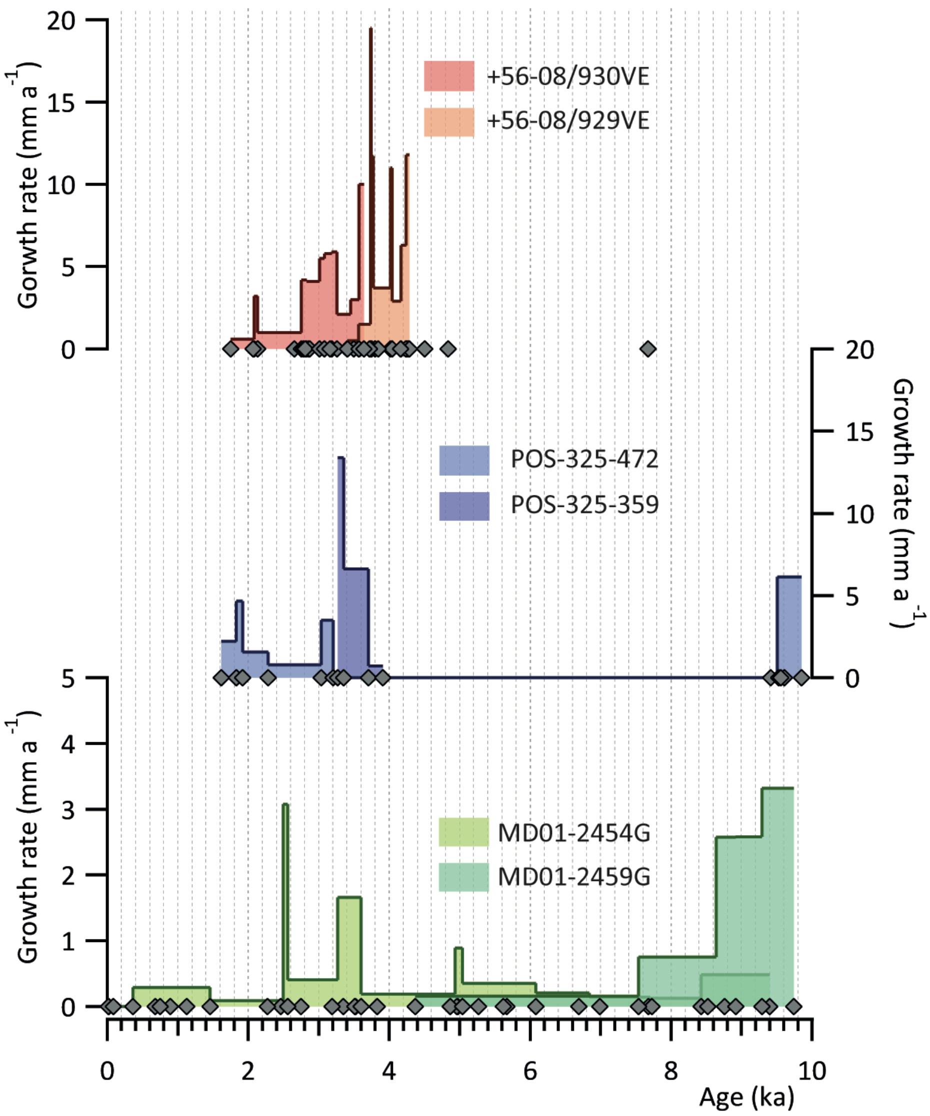

Figure 4 - 5: Summary of all the Holocene growth rates (mm a^{-1}) measured so far within the north-east Atlantic.

'Single generation' cold-water coral reefs (such as those within the Mingulay Reef Complex) are distinguished from larger 'coral carbonate mounds' in that they result from single intervals of growth rather than from multiple periods of reef growth (e.g. during interglacials) with periods of intervening sedimentation (e.g. during glacials; Roberts et al., 2006, 2009). Within the north-east Atlantic, most single generation Holocene-age cold-water coral reefs reported to date are from the Norwegian continental shelf and fjords (Hovland et al., 1998; Lindberg and Mienert, 2005; Lindberg et al., 2007; López Correa et al., 2012). The first estimates of growth rates from reefs on the Sula Ridge were about 2 – 3 mm yr^{-1} (Freiwald et al., 1999). Recently, studies from Stjernsund and Trænadjupet coral-sediment cores (POS-325-472 and POS-325-359, respectively) revealed growth rates of 2 – 6 mm a^{-1} (López Correa et al., 2012). The average growth rates measured from the Mingulay Reef Complex were more comparable with those from the Norwegian shelf, but were still far higher and more variable with growth up to 12 mm a^{-1} (Figure 4 - 5). However, this might be at least partially explained by the greater number of dates taken during the present study from the Mingulay reefs, revealing also high local reef growth rates, compared to the earlier studies. Overall our study at Mingulay confirms the trend for exceedingly rapid Holocene growth rates compared with bathyal coral carbonate mounds examined in the Rockall and Porcupine regions.

4.6.2 Holocene *Lophelia* occurrence in the north-east Atlantic

During the Holocene, centennial to millennial fluctuations in the influence of the SPG that affect the North Atlantic inflow and wider North Atlantic climatic conditions have been documented (Thornalley et al., 2009; Colin et al., 2010; Copard et al., 2012). These fluctuations had potentially adverse effects on Atlantic Ocean ecosystems (e.g. Stenseth et al., 2003). During the Holocene, changes in coral reef and mound growth rates have already been attributed to climate driven changes (Frank et al., 2009; López Correa et al., 2012). In this section we compile all the available *L. pertusa* ages from the north-east Atlantic alongside reef and mound growth rates to test whether the relative changes in the North Atlantic inflow to the coral sites could explain variations in *L. pertusa* occurrence throughout the entire region (Figure 4 - 6). We will especially focus our attention on the last 5 ka as the high resolution dating of the coral/sediment cores from the Mingulay Reef Complex may allow short-scale oceanic changes to be identified from changes in growth rates and coral occurrence.

a. Present – 2 ka: decline of Lophelia

From 2 ka to present, lower growth rates were observed across the entire Mingulay Reef Complex, along with a significant decrease in coral occurrence as evidenced by the total number of ages for the north-east Atlantic (Figure 4 - 6). At the Mingulay Reef Complex, we can exclude a bias in sediment core sampling strategy as 21 additional dates at the surface of the reef were obtained. There was a clear gap with no evidence of coral growth between 1.4 ka and the present, despite the fact that dense occurrences of live *L. pertusa* are documented today at the complex (Roberts et al., 2005, 2009). Interestingly, in Norway there is an interruption of reef growth at 1.6 ka recorded from coral/sediment cores and very little evidence of coral occurrence from 1.2 ka until recent times, and like Mingulay, corals occur there today (Mikkelsen et al., 1982; Hovland et al., 1998; Lindberg and Mienert, 2005; López Correa et al., 2012). Very few coral samples from the north-east coral carbonate mounds were dated from 0.8 to 2 ka (Frank et al., 2009; Schroder-Ritzrau et al., 2005). The compilation of coral mound growth rates from Rockall Bank and the Porcupine Seabight also show a reduction at 0.9 ka (Frank et al., 2009). However, this is not evident only from considering the age model of core MD 2454G, where a growth rate of 0.2 mm a^{-1} was estimated. This may highlight the need to perform a more intensive downcore dating strategy to reveal more short-term climatic events that could have impacts on coral occurrence and/or to compile growth rate estimates from several locations.

Several climatic anomalies over the last 2 ka have been documented that tend to group into three major episodes: 0.1 – 0.7 ka, 1 – 1.2 ka, and 1.4 – 1.8 ka (Mayewski et al., 2004; Thornalley et al, 2009; Wanner et al., 2011; Copard et al., 2012). A drop in neodymium isotopic composition (εNd) recorded from Rockall Bank cold-water corals highlighted a stronger influence of SPG water from 0.8 to 1 ka (Copard et al., 2012). Further north, the decreasing near-surface salinity and temperature at 1 ka suggested an enhanced influence of the SPG water to the NAC (Thornalley et al., 2009). Thus, despite the distinct temporal resolution of the records, they all imply an abrupt enhanced influence of the SPG water relative to the STG water to the coral sites. This oceanic shift could have significantly impacted cold-water coral growth and may thus explain the occurrences of *Lophelia* within the north-east Atlantic (Figure 4 - 6). Interestingly, Thornalley et al. (2009) reported that SPG strength declined 1.8 ka. Unfortunately, a gap in the SPG records from Rockall Bank does not allow us to easily confirm this interpretation (Figure 4 - 6). However, we cannot exclude that this would have contributed to destabilising cold-water coral ecosystems since our results show decreasing coral occurrence and growth within the north-east Atlantic from 1.8 ka (Figure 4 - 6). We hypothesise that the succession of abrupt oceanic shifts reported over the last 2 ka linked to the increasing influence of SPG circulation significantly destabilised this ecosystem.

b. 2 ka – 5 ka: Optimum conditions for Lophelia?

On Rockall Bank and in the Porcupine Seabight, three major high growth rate (>1 mm a^{-1}) events were recorded at about 2.5, 3.4 and 5 ka. Our records from inshore western Scottish waters also suggest persistent occurrence of *L. pertusa* and relatively high growth rates as early as 4.3 ka lasting until 2.7 ka. This period is however punctuated by a few events of lower occurrence/growth rates at 2.7 ka, 3.2 – 3.6 ka and to a lesser extent at 3.9 ka and 4.2 ka (Figure 4 - 6). The same trend has been observed in Norway, with two major peaks of growth recorded at 3 – 3.2 ka and 3.3 – 3.7 ka (López Correa et al., 2012). These coral records suggest that overall the 2 – 5 ka period was particularly favourable for *Lophelia* growth in the north-east Atlantic despite occasionally less intense coral growth across all locations at 2.6 – 2.8 ka and 3.2 – 3.6 ka.

During the late Holocene, the upper-intermediate waters from around Rockall were characterised by higher εNd values indicating less influence of the SPG water compared to the rest of the Holocene (Colin et al., 2010). Those conditions appear to have been relatively favourable for cold-water coral reef growth. However, the late Holocene has also been characterised by rapid climate changes (Bond et al., 2001; Mayewski et al., 2004). A small increase in the influence of the SPG was recorded in the North Atlantic at about 3.4 ka (Thornalley et al., 2009; Colin et al., 2010). This event seems to have affected coral growth within the Mingulay Reef Complex as reflected by a decrease in growth rates recorded in between 3.2 and 3.6 ka. In Norway, a cooling event was also reported at 3.3 ka in Stjernsund and associated with an overall cooling of the NAC that could also explain the decline in reef growth rate reported in this area (López Correa et al., 2012; Joseph et al., 2012). The rapid climate change occurring ~ 2.7 ka ago is probably one of the best documented periods of rapid climate change in the late Holocene (Mayewski et al., 2004). This relatively cold event has been associated with a shift in the SPG circulation

(Thornalley et al., 2009). Such changes have apparently significantly affected shallower north-east Atlantic cold-water coral reefs by reducing their growth and could also partly explain the lack of a εNd record due to a lower availability of coral samples from Rockall Bank and Porcupine Seabight (Colin et al., 2010; Figure 4 - 6). At Mingulay this event is clearly highlighted by an abrupt decrease of coral reef growth rate and no evidence of intense coral growth has been recorded in this area from then until the present day. For these shallower coral reef systems (Norway and Mingulay) ocean dynamics did not allow the system to fully recover while coral carbonate mounds from the Celtic margin showed a faster recovery.

c. Early and Mid Holocene Lophelia occurrence

No corals older than 4.3 ka were dated from Mingulay, with the exception of one out of sequence coral fragment dated at 7.7 ka, the oldest age from the complex so far. Despite potential sampling biases for this period, the data reveal that *L. pertusa* occurrence and growth within the north-east Atlantic are in agreement with the global hydrological changes over this period (Figure 4 - 6). Therefore, the compilation of coral data from this region should enable us to investigate the long-term changes in *L. pertusa* occurrence and growth from 5 to 11 ka.

Holocene *L. pertusa* occurrence within the north-east Atlantic appears to have started as early as 11.3 ka in Rockall Bank and 10.9 ka in Stjernsund (Norway) (Frank et al., 2009; López Correa et al., 2012). Subsequently, high growth rates were measured at 9.7 – 10 ka (>3 mm a^{-1}) in the Porcupine Seabight. Rockall Bank sediment cores show relatively high growth rates (0.6 mm yr^{-1}) between 8.5 and 9.5 ka (Frank et al., 2009). In Stjernsund, high growth rates (>6 mm a^{-1}) were similarly recorded from 9.4 to 9.8 ka.

The early Holocene (11 to 8 ka) was characterised by maximal orbital forcing (high summer insolation in the Northern Hemisphere). However, the large North Hemisphere ice sheets and major sea level changes still had a significant influence on climate, water mass organisation and circulation (e.g. Wanner et al., 2008). The growth rate records we discuss from the coral reef frameworks in the early Holocene suggest processes allowing the return of *Lophelia pertusa* ecosystems to high latitudes in the north-east Atlantic (50 – 70°N) and relatively favourable environmental conditions for coral settlement and growth (Frank et al., 2009; Frank et al., 2011; López Correa et al., 2012). This could be explained by the early establishment of near-modern North Atlantic circulation that produced suitable hydrological conditions (temperature, productivity, sedimentation processes) for coral occurrence (Frank et al., 2004; Thornalley et al., 2009, Colin et al., 2010; Frank et al., 2011; Pilet et al., 2011; López Correa et al., 2012; de Mol et al., 2005; Figure 6).

Data available from the Norwegian shelf coral/sediment cores show a long-term hiatus from 3.9 – 9.4 ka (López Correa et al., 2012). However, *Lophelia* samples aging from 6 – 8 ka were reported within the area (Mikkelsen et al., 1982; Hovland et al., 1998; Lindberg and Mienert, 2005). The available coral/sediment cores from the area did not allow us to report the relative occurrence of *Lophelia* during this period, but surface sample dating revealed its presence from 6 – 8 ka. Rockall Bank and Porcupine Seabight cores presented very low growth rates from 6 to 7.6 ka, followed by increasing VMGR until 5 ka (Frank et al., 2009).

Cold-water coral based εNd records show a strengthened mid-depth SPG influence to Rockall Bank from 5 – 8 ka (Colin et al., 2010). In response, the Irminger Current was significantly reduced but a constant influence of NAC to the Northern Norwegian water remained (Koç et al., 1993; Colin et al. 2010; Thornalley et al., 2009; Joseph et al., 2012). The stronger influence of SPG water to Rockall Bank may have impacted on the relative occurrence and growth rate of coral mounds from Rockall until 6 ka. Along the Norwegian shelf however, the constant influence of the NAC water would have maintained a suitable environment for coral growth until 6 ka. Although the number of cold-water coral ages covering this period remains limited, long-term changes in *L. pertusa* occurrence and growth seem coherent with local hydrological changes

d. The last century

Dense occurrences of living *Lophelia pertusa* corals and reef framework are presently observed at the Mingulay Reef Complex, which indicate that the environmental conditions are conductive for coral growth in this area (Roberts et al., 2009). Coral εNd data from Rockall Bank suggest that the last century was mostly dominated by a strong SPG (Copard et al., 2012; Figure 4 - 6), but that higher resolution records are needed to confirm these observations. However a weakened SPG has been documented at interannual to interdecadal time scales including the last two decades (Hakkinen and Rhines, 2004; Hátún et al., 2005, Sherwin et al. 2012), which supports our hypothesis that environmental conditions associated with the SPG are more conducive to coral growth in the north-east Atlantic. Large centennial time scale shifts in SPG dynamic seems to have influenced coral occurrence and reefs/mounds growth during the Holocene. The mechanisms associated with the SPG variability on interannual to interdecadal and its response to the global climate change need to be better constrained to evaluate the potential impacts of SPG dynamics on coral growth.

e. Summary

The compilation of the *Lophelia pertusa* dates from the north-east Atlantic coral reefs and mounds reveals periods of synchronous *L. pertusa* occurrences during the Holocene. Estimates of the growth rates provide additional information about the relative increase in coral growth due to stable and/or favourable environmental conditions.

The comparison of our data with centennial SPG circulation changes suggests that corals are very sensitive to changes in water mass properties probably associated with changes in productivity, hydrology, sedimentation processes and dispersal. We therefore propose that changes in the relative composition, intensity and direction of the Atlantic inflow during the Holocene on centennial time scale (resulting from changes in the strength and position of the SPG) have significantly influenced the growth, abundance and distribution of *L. pertusa* in the NE Atlantic.

In the deeper mounds off the Celtic margin, it appears that *Lophelia pertusa* was almost always present during the Holocene although significant variations in growth rates imply that they are vulnerable to changes in oceanic regimes. However our data suggest reefs from shallow inshore environments (such as in Norway and Mingulay) are even more sensitive to oceanic changes, and more time is needed for the ecosystem to recover after disruption. This could be partly explained by the local hydrology and geographic proximity to coral refuges.

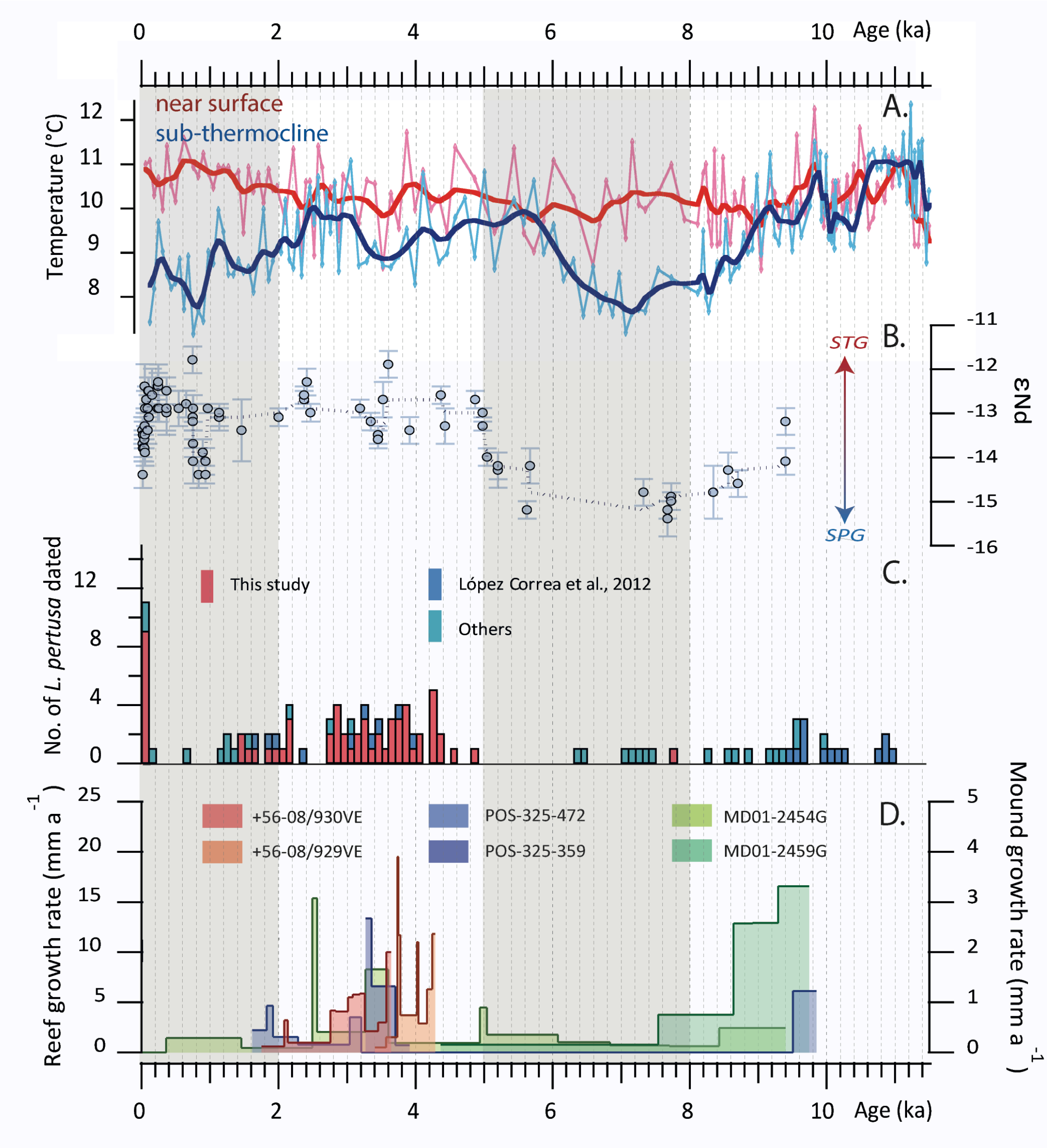

Figure 4 - 6: A. Near-surface (red) and sub-thermocline (blue) temperature reconstructions derived from South Iceland foraminifers analyses (core RAPiD-12-1K; Thornalley et al., 2009), B. Nd isotopic composition from cold-water corals from Rockall Bank (core MD01-2454G, 747 m water depth; Colin et al., 2010; Copard et al., 2012), C. Number of *Lophelia pertusa* fragments dated from shallow coral reef in Norway and Mingulay (this study, Mikkelsen et al., 1982; Hovland et al., 1998; Lindberg and Mienert, 2005; López Correa et al., 2012), D. compilation of cold-water coral structure growth rates from Rockall Bank and Porcupine Seabight (green) (Frank et al., 2009), Norway (blue) (López Correa et al., 2012) and Mingulay (red) (This study).

4.7 Conclusion

High-resolution downcore dating of two cold-water coral cores from the Mingulay Reef Complex has allowed us to examine variations in reef growth rates. The average dating resolution was about 100 yrs, allowing very accurate reconstruction of growth rate changes between 1.75 and 4.3 ka. Radiocarbon dates were also performed on surface samples from Mingulay reefs to map the age of the complex. By dating both downcore and surface samples we strove to avoid the effect of any patchy coral growth across the reef complex, and our results strongly implicate periods of favourable and unfavourable coral and reef growth.

The growth rates of shallow cold-water coral reefs were significantly higher than those observed for coral carbonate mounds. Growth rates for the Mingulay Reef Complex reached up to 12 mm a^{-1} which is the highest growth rate so far found in any cold-water coral reef. Two main phases of reduction/interruption of growth in the Mingulay Reef Complex were found at 1.75 – 2.8 ka, 3.2 – 3.6 ka, and to a lesser extent at 3.8 – 4 ka and 4.2 ka. We found no evidence of coral growth from 1.4 ka to modern times despite more than 50 dates collected within the complex suggesting that environmental conditions were not suitable for *Lophelia pertusa* growth, and this also seems to be the case for similar reefs in Norway.

From the compilation of dates from the north-east Atlantic cold-water coral reefs and mounds, the period from 2 – 5 ka was a remarkable period for *Lophelia pertusa* growth in this region, albeit punctuated by less favourable events. Holocene coral reef growth rates seem to have responded synchronously over a wide region likely as a result of large-scale shifts in palaeoceanographic regimes. We proposed here that changes in the relative strength and position of the SPG could have significantly impacted not only on the water mass properties but also food supply, sediment processes and dispersal within the coral sites, thus affecting both coral colony and reef growth. Our study further illustrates that the exceptionally high growth rates found in shallow cold-water coral reefs could provide novel records that allow very high-resolution palaeoenvironmental reconstructions of North Atlantic oceanography.

Chapter 5: Fossil biodiversity at the Mingulay Reef Complex: a model of coral reef build-up

5.1 Abstract

The downcore depositional history of cold-water coral reefs and mounds is characterized by variable amounts of coral fragments and associated biodiversity of reef fauna embedded in sediment. Our study aims to define the internal structure and evolutionary sequence of events leading to *Lophelia pertusa* reef build-up. Two coral/sediment cores from the shallow inshore *Lophelia pertusa* reef complex off western Scotland, the Mingulay Reef Complex, were scanned using computed x-ray tomography (CTscan) to: (1) reconstruct and quantify the relative contribution and preservation of coral fragments in the cores, (2) identify distinct reef facies, and (3) propose a model of reef build-up involving faunal biodiversity, sedimentological regime, and changes in erosional processes. Thirty-nine U-series dates were obtained on *Lophelia pertusa* clasts from the two coral/sediment cores to provide a temporal framework of the reef build-up. Three main parameters were considered: density of the coral/sediment cores, the number of fossil clasts, and the sum of the area of clasts detected by the CTscan. Parameters were validated by comparing these with density measurements from a multi-sensor core logger (MSCL) and physical dissection and analysis of fossils in the cores. Our analysis of CTscan images demonstrated clear intervals of distinct reef facies: coral-rich, sediment-rich and shelly-coral hash layers. The succession and the rapid cycle of reef development, disturbance and recovery suggested by our data allows us to provide for the first time a complete model of cold-water coral reef build-up including shifts in biodiversity, physical/chemical/biological processes and the sedimentary regime.

5.2 Introduction

Cold-water corals have a worldwide distribution. *Lophelia pertusa*, the most common and widespread reef framework-forming cold-water coral (see Roberts et al., 2009b for review), is an "ecological engineer" sensu Jones et al., (1994) and Wright and Jones (2006) and provides a complex three-dimensional habitat for many other species including rich biological communities of suspension-feeding invertebrates such as sponges and other corals (Henry and Roberts, 2007).

Growth models of cold-water coral reef and mound genesis through time have been proposed (De Mol et al., 2005; Dorschel et al., 2005; Henriet and Guidard, 2002; Kenyon et al., 2003; Roberts et al., 2006; Rüggeberg et al., 2007). Key steps in this succession begin with: 1) settlement and metamorphosis of coral larvae, 2) formation of a thicket resulting from an aggregation of several adjacent colonies (monotypic or polytypic) under favourable conditions for coral growth (i.e. hydrology and food supply), 3) formation of a coral coppice following the death of the underlying colonies and accumulation of debris (mostly coral skeleton debris), and finally, 4) the succession of reef growth leading to the establishment of large topographic features such as cold-water coral reefs or coral carbonate mounds. At each step a new ecological niche and stratigraphic layer are formed (e.g. Squires, 1964). The reconstruction of fossil communities associated with each step of reef build-up from geological records is challenging (De Haas et al., 2009; Mienis et al., 2009b) mainly because the succession of reef build-up phases is not clearly revealed and because erosional phases corrupt the signal. However, distinct reef macrohabitats are distributed along this succession gradient: from the reef or mound summit down to the flanks, these range from live cold-water coral framework, mixed live and dead framework, coral rubble, and silicilastic sediments (De Haas et al., 2009; Dorschel et al., 2007a; Mortensen et al., 1995; Roberts et al., 2005). Macrohabitats can therefore be used as analogues to reconstruct the different stages of reef build-up from coral/sediment cores.

Sedimentation within coral framework, reef and mound areas is also an important component of reef build-up (Dorschel et al., 2007a). The environmental settings of *Lophelia sp*. reefs are characterized by high current regimes (Davies et al., 2009; Frederiksen et al., 1992b; Genin et al., 1986; Mienis et al., 2007; Mienis et al., 2009b; White, 2007; White et al., 2005), and as a result erosion, sediment trapping and deposition are significantly affected by the relative occurrence of corals trapping the vertical and lateral flux of sediment (Dorschel et al., 2007a; Frank et al., 2009; Kenyon et al., 2003; Mienis et al., 2009b). The internal structure of a coral reef is therefore comprised of an accumulation of debris of coral and associated fauna, terrigenous sediment carried through the coral reef, and entrapped biogenic sediment resulting from the activity of associated coral infauna and epifauna (Wheeler et al., 2011).

Shallow inshore cold-water coral reefs are also characterized by very high accumulation rates (Chapter 4, López Correa et al., 2012). Therefore, the study of the internal structures of such reefs constitutes a unique opportunity for highlighting the different stages of reef build-up. The 'Mingulay Reef Complex' off the west coast of Scotland is formally defined as a reef, rather than a coral carbonate mound, as it results from a single generation of reef growth during the Holocene interglacial period. In contrast, coral carbonate mound structures result from successive growth during distinct interglacial periods (Roberts et al., 2006; Roberts et al., 2009b). In this study, metrics generated from computed x-ray tomography (CTscan) images, and downcore fauna were analysed to 1) reconstruct and quantify the relative contribution and preservation of *Lophelia pertusa* fragments within the reef, 2) identify cold-water coral reef facies characterizing the reef structures and 3) construct a conceptual model of reef development involving environmental, faunal biodiversity and sedimentological regime changes through time.

5.3 Materials

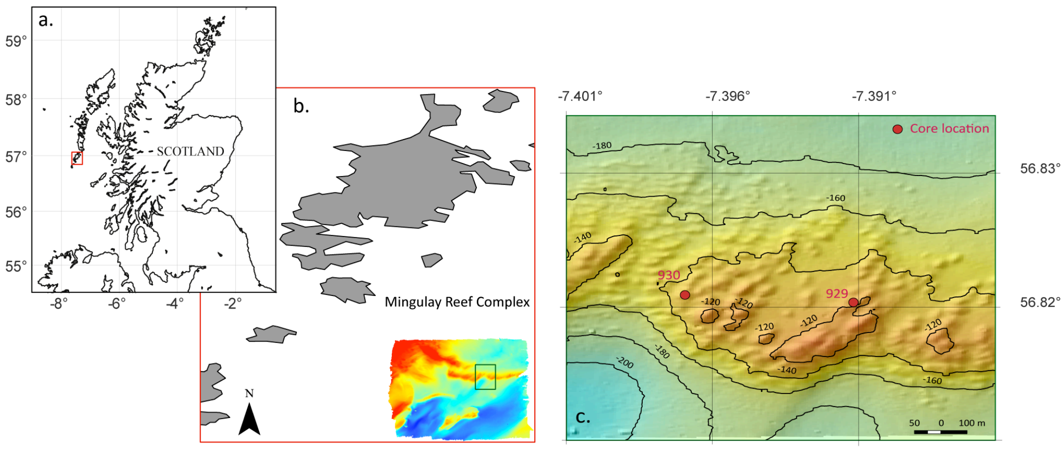

Figure 5 - 1: a. Location of the Mingulay Reef Complex relative the Scotland, b. bathymetric map of the Mingulay Reef Complex and c. location of the coral/sediment cores relative to a 3-dimensional multibeam map of Mingulay Reef 1.

Two coral/sediment cores +56-08/929VE and +56-08/930VE (hereafter referred to as cores 929 and 930) were retrieved from the Mingulay Reef Complex in October 2007 by the British Geological Survey (BGS) during a survey on board the NERC vessel the RRS James Cook (Stewart and Gatliff, 2008); see Figure 5 - 1 and Table 5 - 1. Real-time video footage was collected to ensure minimal damage to live corals. The cores were sliced into metre-length sections on board and then placed in cold storage (4°C) at BGS. The total recovery of core 929 (56°47’19’’N, 7°23’27’’W) and 930 (56°49’20’’N, 7°23’47’’W) was 3.61 m and 5.25 m, respectively. These cores were characterized by numerous *Lophelia pertusa* clasts (and their associated fauna) in sandy-mud. The cores were frozen prior to splitting to avoid any shifting in the position and orientation of the coral fragments and to preserve the internal sedimentary structure. While frozen, the cores were split using a diamond bladed circular rock-cutting saw at the BGS. To avoid any potential contamination from the cutting fluid, the uppermost surfaces of both halves were immediately removed. The age model of the cores is summarised in Chapter 4.

Core	Latitude	Longitude	Water depth	Length of recovered core
+56 -08/929VE	56°4 9’19’’N	7°23’27’’W	127 m	3.61 m
+56 -08/930VE	56°49’20’’N	7°23’47’’W	134 m	5.25 m

Table 5 - 1: Location depth and length of cores

5.4 Methods

5.4.1 CT scanning

Prior opening and sampling, intact core sections were scanned using a Toshiba Aquilion 64 computed X-ray tomography (CT) at the Lorne and Islands District General Hospital in Argyll, Scotland. CT scanning uses X-ray detectors rotated through 360° allowing a three dimensional reconstruction of the internal radiodensity of the cores allowing the size and position of clasts to be quantified. The biogenic clasts (e.g. corals, shells, spicules) denser than the surrounding sediment appeared white in the CT images. The sediment cores were CT scanned in one meter-long section. Each helical CT data object was then exported as 16-bit Hounsfield units (HU)-calibrated CT slices with an XY (image) resolution of 0.25 mm/pixel and a Z (slice) resolution of 1 mm/slice.

a. Image manipulation

The images generated by the CT scanner are calibrated in HU. Output from the CT scanner was routinely calibrated by measuring a block containing several different densities of material. The linear correlation between these two variables can therefore be used to convert HU into density (g cm^{-3}) following the linear equation given below (error bars represent 95% CIs):

(1) Density (g cm^{-3}) = 0.00106 (±0.00004) × HU + 1.03 (±0.02)

For ease of processing, each CT slice was converted to a contrast-enhanced 8-bit greyscale image using the software Image J (NIH). Conversion was linear, with pixels ≤ 692 HU mapping to 0 (black), and pixels ≥ 3200 HU mapping to 255 (white). The cutoff values were arbitrary, but were chosen to span the full range of density exhibited by coral clasts (which typically range from 1200 to 3200 HU) and some of the variation in the density of the mud (which typically ranged from 600 to 1100 HU). Combining the calibration equation from equation (1) with the greyscale mapping listed above, the calibration equation linking 8-bit greyscale intensity to density became:

(2) Density (8-bit-image, g cm^{-3}) = 0.0104 (±0.004) × greyscale + 1.76 (±0.03)

b. Average greyscale as a proxy for core density

A simple proxy for core density was calculated from the contrast-enhanced image slices by calculating the average greyscale for each image slice. This average is calculated from all pixels in the 390 x 436 pixel image, and is thus biased by non-sediment core pixels. This can be corrected by scaling the average by the ratio of pixels in the image (170 040) to pixels in the sediment core (90 792). The equation linking the average sediment density to the average grayscale was therefore:

(3) Avg density sed (g cm^{-3}) = 0.0104 (±0.004) × (avg greyscale × 1.873) + 1.76 (±0.03)

This metric will tend to overestimate the total density because some of the mud pixels (with a density < 1.7 g cm^{-3}) have been mapped onto an 8-bit greyscale value of zero (now equivalent to a density of 1.7 g cm^{-3}). Comparison of this density proxy with densities measured directly by multi-sensor core logger (MSCL) (Figure 5 - 1) confirms the overestimate, but the relationship is linear demonstrating that the proxy captured relative variation in density. From the comparison, the equation linking the CT density proxy to measured density was:

(4) Density – CTscan (g cm^{-3}) = 1.22 × Density – MSCL (g cm^{-3}) + 0.015

The pixel value re-mapping resulted in some suppression in the density of the mud fraction. As a result, the CTscan density proxy tended to be sensitive to variations in the amount of the higher density material (i.e. coral clasts) making it a useful measure of the coral and fossil content of the core. The average greyscale intensity of each contrast-enhanced CT slice should therefore be regarded as a convolution of 1) average mud density (including potential compaction toward the bottom of the cores), 2) area of coral clast, and 3) average density of the coral clasts.

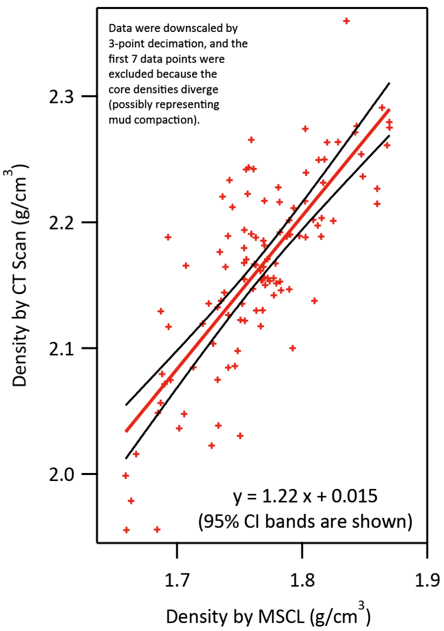

Figure 5 - 1: Correlation between density estimated by the MSCL and density estimated by the CTscan. There is a strong correlation indicating that the two methods capture density variations, but the slope is greater than 1.0 suggesting that the CTscan is slightly biased towards the higher density clasts.

c. Clast metrics

The 8-bit greyscale images were converted to black and white binary images using a threshold value of 60 (a density cutoff of 2.38 g cm^{-3}, which represents the lower end of the coral clast density). Particle-statistics routines built into Igor Pro 6.0 (Wavemetrics, Lake Oswego, OR) were used to quantify the number, area, and position of clasts in each image. In this study three main parameters were considered to describe the internal structure of the cores:

(1) the average density of the cores (as an indicator of the relative abundance of denser clasts vs. sediment),

(2) the number of dense clasts detected (assuming there were mostly coral and associated fauna fossils),

(3) the sum of the area of the clasts detected (to estimate the total proportion of the cores occupied by fossils). This statistics, combined with the previous two, can also be used to estimate the relative contribution of *Lophelia pertusa* vs. other fossil groups, (assuming that the coral clasts are generally bigger that the other fossils groups), and the relative state of preservation of the clasts (a large area occupied by a small number of clast implies the presence of well-preserved coral clasts, while a large area occupied by numerous small fragments likely represents heavily degraded fossils).

These parameters were selected because they were assumed to provide accurate information about: 1) the relative abundance of coral fragments, 2) the relative abundance of fossils representing the fauna associated with coral, 3) the relative state of preservation of the coral fragments and 4) the relative compaction of the sediments.

5.4.2 Multi-sensor core logger analysis

The two cores were passed through a GeoTek MSCL at the Scottish Association for Marine Science in Argyll, Scotland. Continuous measurements (every 1 cm) of wet bulk density (g cm^{-3}) were obtained by gamma ray attenuation (Rothwell and Rack, 2006). The average bulk density of a wet mud/clay mixture is usually between 1 to 2 g cm^{-3}, depending on the water (1 g cm^{-3}) content and the compaction of the sediment, which is significantly lower than the density of coral aragonite (2.7 g cm^{-3}). Thus an increase (decrease) in the proportion of the volume occupied by coral fragments within the core would measurably increase (decrease) the density measured by gamma attenuation.

5.4.3 Core dissection

The working half of each core was dissected at 1 cm intervals, documenting the position and state of preservation of each coral fragment (~ > 1 cm). The relative position of the coral fragments (~ > 1 cm) was then artificially re-sampled every 10 cm using Analyseries (Paillard et al., 1996) to make this information more comparable with the counted fraction (3 – 10 mm).

After dissection, every tenth 1 cm (starting at 5 cm) was sieved through a 3 mm mesh. The coral and fossil fragments that were recovered from sieving were identified and counted. A 3 mm mesh was chosen to: 1) facilitate fossil identification by separating out the size fraction that contained the most intact fossil fragments and avoiding the most eroding/broken clasts, 2) make the count data more comparable with the CT scan data (blurring of the CT image rendered fossil fragments that were less than about 2 – 3 mm undetectable).

As the counted fossil fragments were extracted from the only half of the cores the results were multiplied by two to be comparable with the CTscan data, which represented the whole core.

5.5 Results

5.5.1 Biodiversity associated with coral framework

Changes to the relative contribution of different fossil fragments to the core were estimated by counting different fossil pieces in the dissected core halves. Herein, coral pieces larger than about 1 cm are referred to as 'coral clasts' and coral pieces from the 3 – 10 mm size fraction are referred to as 'coral fragments' (Figure 5 - 2).

Within the 3 – 10 mm size fraction, coral fragments represented 0 – 77 % and 0 – 100 % of the fossils counted in cores 929 and 930, respectively. Bivalves varied in contribution, representing 0 – 97 % and 0 - 100 % for core 929 and 930 respectively. In general, there was no correlation between the contribution of coral fragments and bivalves. Bryozoans, brachiopods, gastropods and echinoderms exhibited sporadic distributions with low abundances, but seemed to occur in greater proportions when peaks in bivalve numbers were observed. In contrast, more fossils of polychaete worm tubes were detected when coral fragments increased in abundance.

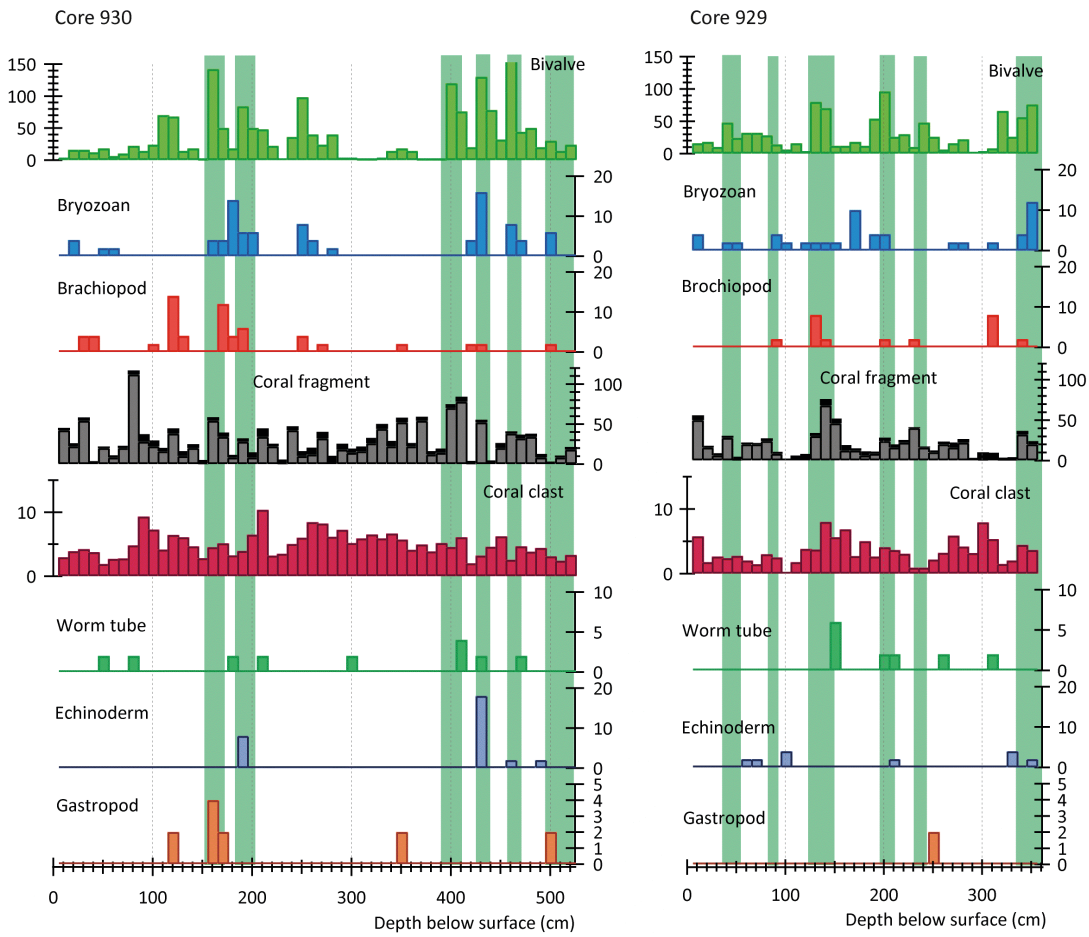

Figure 5 - 2: Fossil fauna identified in the *Lophelia pertusa* cores. The areas highlighted in green represent the shelly-coral hash layers identified from the CTscan data.

5.5.2 CT scan analyses

a. Density

The robustness of the CTscan densities estimated from the greyscale calibration was tested by comparing densities measured with the MSCL (Figure 5 - 3). Both records were comparable and were linearly correlated (Figure 5 - 1). The slope of the correlation, however, is > 1 meaning that the CT scan data show higher and more pronounced changes of the overall density (Figure 5 - 1).

When selecting which density record to work with, several factors had to be considered. On the one hand, the gamma densitometer on the MSCL provides density for only a 1 cm strip through the centre of a core half. Because the cores were very heterogeneous on cm distance scales (mainly due to the presence of large coral clasts) the MSCL density may not accurately represent the whole core. On the other hand, while the CT scanner captured the density of the whole core, the image processing biases the density measurement towards the higher density clasts (see Section 1.4.1 b), explaining the offset and steep slope observed in Figure 5 - 1 and Figure 5 - 3. We selected the CTscan density data to work with because it better highlighted the variation in the fossil clasts (but we note that the absolute density values were biased towards higher numbers).

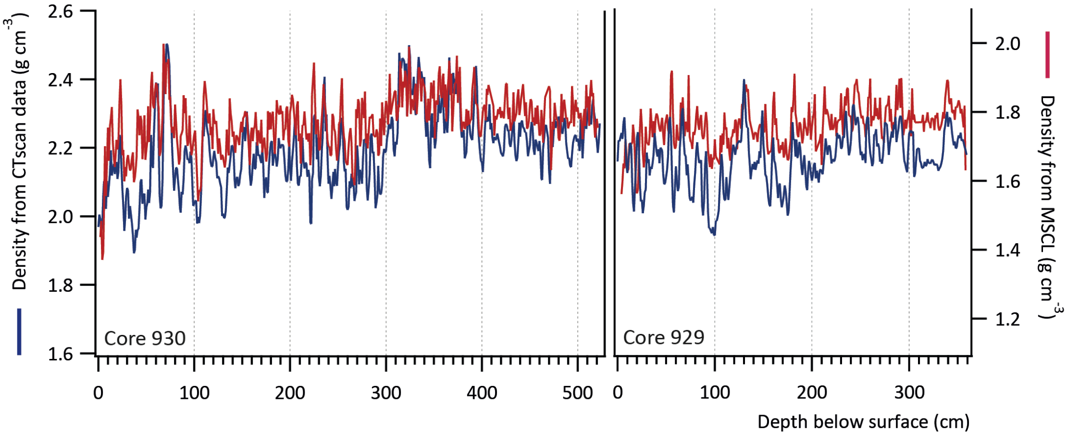

Figure 5 - 3: Density measured with a MSCL (red) and estimated from the CTscan greyscale data (black) for core 930 (left) and core 929 (right).

b. Fossil abundance and size

The CTscan data can be easily converted to an estimate of the fraction of the core occupied by fossil clasts by summing the total area of high-density clasts in each image and comparing this to the known area represented by the sediment core. Using this approach we see that clasts represented up to 47 surf.% and 48 surf.% of the material in cores 929 and 930, respectively.

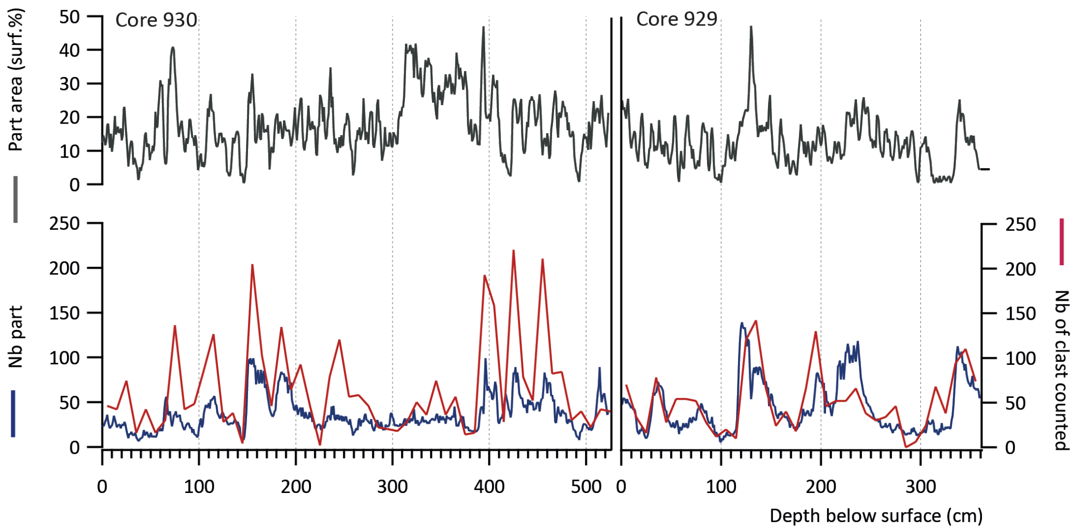

Figure 5 - 4: Selected statistics for the sediment cores from the CTscan data and dissection. (Top, grey line) – Total grey area, presented as percentage of each CT slice occupied by clasts. (Bottom, red and blue lines) – Comparison between the number of clasts detected by the CTscan data (blue) and the number of clasts > 3 mm diameter (including corals and other fossils) counted from the dissected cores.

The number of clasts detected in each CT scan image varied from 7 – 100 and 6 – 140, with the total area co-varying with the number of clasts except where the presence of a small number of large coral clasts dominated (Figure 5 - 4). Because clast-counting by CTscan occurs from a two-dimensional slice, the total numbers would not be expected to match the number of clasts counted within a three-dimensional volume (e.g. via dissection). However, in order to evaluate how well the CT scan clast-counting reflected the actual number of clasts, we graphed the CTscan numbers alongside the numbers of clasts counted by core dissection and sieving (see Section 1.4.3; Figure 5 - 4). In general there was good correlation between CTscan clast numbers and the number of clasts from dissection, although there were several instances where the CTscan particle numbers did not capture the full number of clasts found by dissection. This could occur either because the clasts were so densely packed that the CTscan was unable to resolve them as different particles, or because clasts were thin and the blurring of the CT image reduced their greyscale value below the threshold used for detection. This was especially evident in the shelly-coral hash layers and in the coral-rich layers. For the shelly-coral hash layers small thin fossils fragments were not well resolved by CTscan and for the coral-rich layers, densely-packed coral clasts could not be differentiated.

c. Layer distinction and inter-core comparison

There was a wide range of relative abundances, preservation states and sizes of coral/fossil fragments along the cores, and it is therefore useful to define a few distinct facies, which can be used to interpret the sedimentology. We analyzed the CTscan metrics and identified three main parameters that provided information about the abundance and preservation of fossil fragments: particle area, core density, and particle numbers (see Section 1.4.1 c). These parameters were graphed against depth down the core (Figure 5 - 4). From this, we defined three endmember sediment facies we refer to as 'Coral-Rich Layers', 'Sediment-Rich Layers' and 'Shelly-Coral Hash Layers' (Figure 5 - 5 and Table 5 - 2).

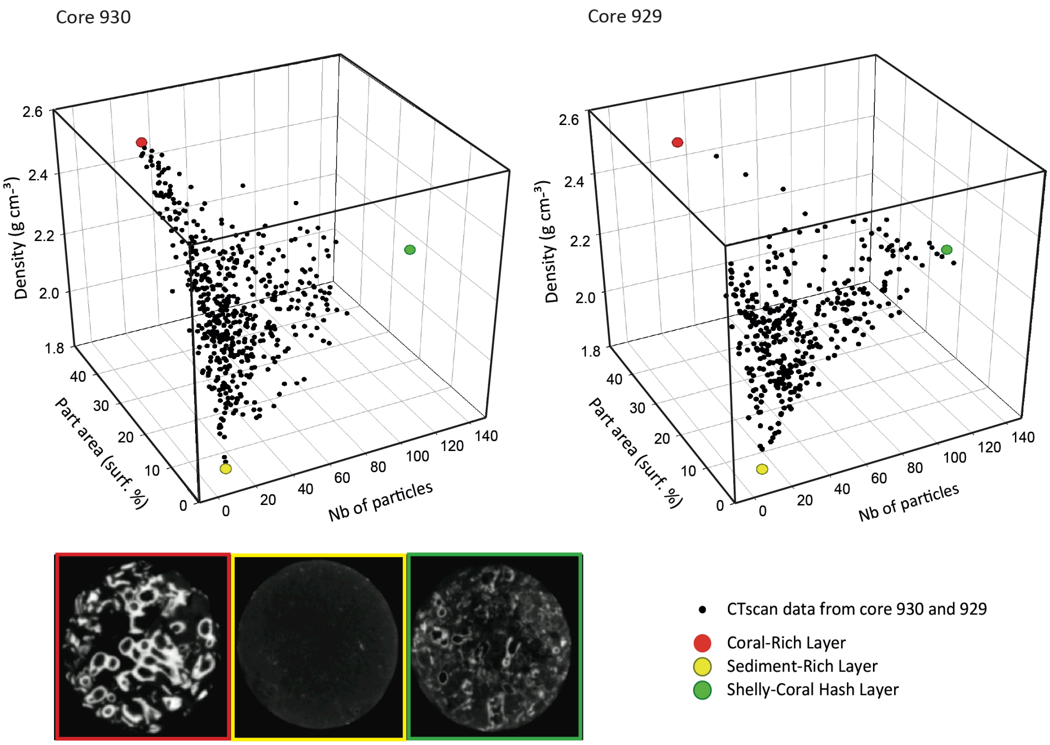

Figure 5 - 5: 3-Parameter correlation graph. The parameters graphed are: 1) the number of clasts detected, 2) the sum of the clasts' area (surf.%) and 3) the average density (g cm^{-3}) for each CT-slice. The red, yellow and green dots represent typical layers defined as coral-rich layer with well preserved fragments, layer without corals and shelly-coral hash layer with poorly preserved coral fragments.

Coral-Rich Layers had the largest amount of pristine coral fragments and were characterized by the highest overall CTscan density with values above 2.3 g cm^{-3} reflecting the greater contribution of denser clasts. The area occupied by the clasts in each CTscan image was therefore high (up to 20 surf.%) for an intermediate number of clasts (20 – 50). By contrast, *Sediment-Rich Layers* had very few clasts detected (< 20) and the sum of their area was below 10 surf.%. Consequently they had the lowest density with values below 2.1 g cm^{-3}. The *Shelly-Coral Hash Layers* were characterized by the largest number of fragments (above 50) but relatively low area with values (10 – 20 surf.%). These layers had intermediate density values (between 2.1 and 2.3 g cm^{-3}).

	Density (g cm^{-3})	Number of particles	Particles area (surf.%)
Coral-Rich Layer	> 2.3	20 – 50	> 20
Sediment-Rich Layer	< 2.1	0 – 20	0 – 10
Shelly-Coral Hash Layer	2.1 – 2.3	50 – 140	10 – 20

Table 5 - 2: Reef facies highlighted by the CTscan data

5.6 Discussion

5.6.1 Reef facies

The CTscan and core dissection data suggest that the internal structure of the Mingulay Reef Complex is characterized by 3 main facies resulting from distinct depositional environments.

a. Coral-rich layers

Coral-rich layers were characterized by a high contribution of large coral clasts but few fossils from other taxa. The relative contribution of corals and fossils can reach up to 45 surf.% of the total area. Other studies of coral carbonate mounds from the North-east Atlantic have also identified layers with a high contribution of coral clasts wherein the coral carbonate content reaches between 30 and 40 wt.% (Dorschel et al., 2007b; Titschack et al., 2009). Because of the high representation of coral clasts, we infer that these layers reflect favourable environmental conditions for an extensive growth of coral framework. An alternative explanation could be that the flux of sediment declines during these intervals resulting in a lower clast/mud ratio. A reduced sediment flux, however, might be expected to result in a visible change in sediment characteristics, but none of the sedimentological parameters (colour, grain size) show any discernible change across these intervals. Thus we favor the interpretation that these coral-rich layers represent favorable environmental conditions.

With the exception of polychaete worm tubes (some species of which are known to be associated with live coral reef (Mortensen, 2001; Roberts, 2005)), the coral layers did not contain many fossilized taxa. This suggests either a low biodiversity associated with live coral framework and/or that the fauna associated with live framework were not well represented and/or preserved. Lower diversity compared to that found on coral rubble facies is documented in the contemporary coral-associated fauna (Frederiksen et al., 1992b; Henry and Roberts, 2007; Roberts et al., 2009a; Roberts et al., 2006). However, coral framework may form a massive three-dimensional structure of a meter or so in diameter (Squires, 1964). Therefore, quantification of the fauna associated with such structures is difficult, and it is likely that the estimates remain biased by the sampling methodology and the lack of preservation of the soft-bodied fauna.

b. Shelly-coral hash layers

Shelly-coral hash layers were characterized by a high number of fossil fragments (sometimes more than 200 fragments in a 1 cm section of a core). These layers were mostly characterized by (bio)eroded coral fragments and a very high concentration of bivalves, but also contained other faunal groups (bryozoans, brachiopods, echinoderms and gastropods) which can be broken and reduced to small pieces. These layers appeared to capture the high benthic biodiversity characteristic of contemporary fauna inhabiting coral rubble facies (Frederiksen et al., 1992b; Henry and Roberts, 2007; Roberts et al., 2009a; Roberts et al., 2006), and may indicate a relatively dynamic environment where physical-erosion and likely biological-erosion occurred. It is worth noting that these layers were observed throughout the cores and not as a function of the depth downcore. Thus they are primary depositional features and do not result from changes to the relative preservation of the sediment material with time.

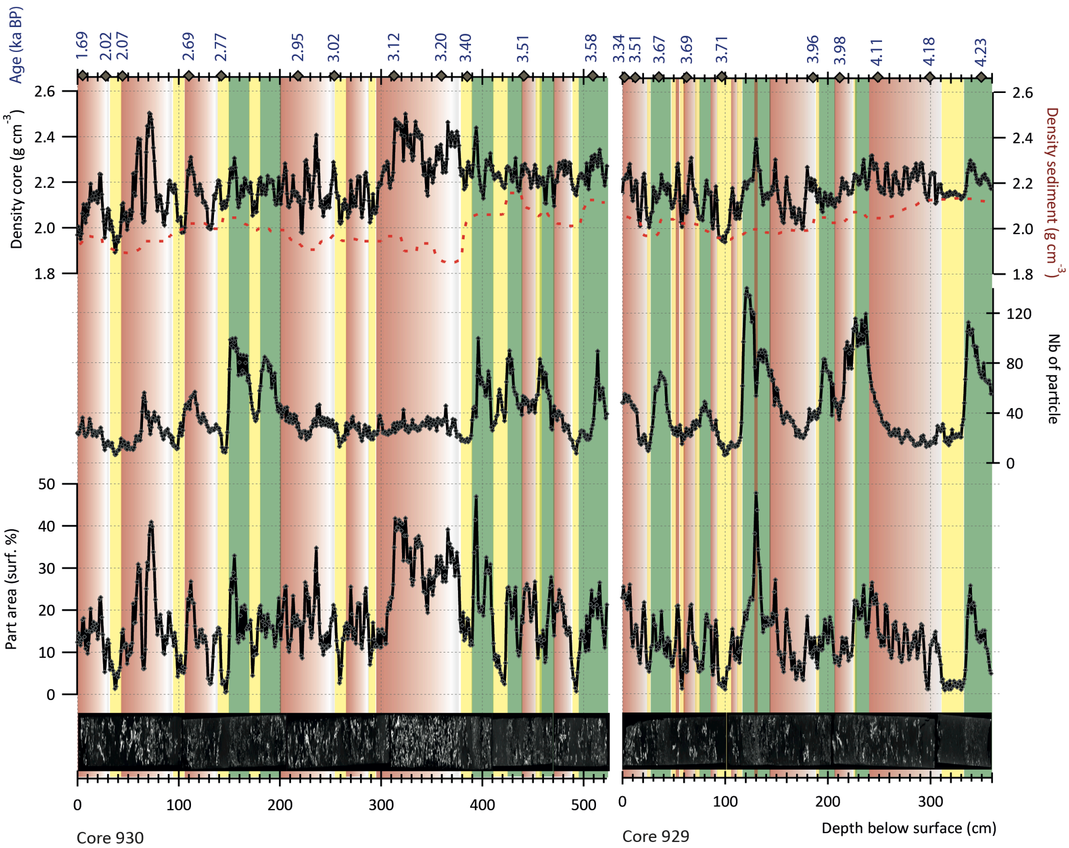

Figure 5 - 6: Abundance and state of preservation of cold-water coral present along core 930 and 929. Data highlighted in green reflect shelly-coral hash layers. Data highlighted in red reflect coral-rich layers. Data highlighted in yellow reflect sediment-rich layers.

c. Sediment-rich layers

Sediment-rich layers were characterized by the near absence of coral fragments and other fossils. Cold-water coral reefs and mounds are characterized by strong current regimes (Davies et al., 2009; Dorschel et al., 2007a; Genin et al., 1986; Roberts et al., 2006), which maintain a high concentration of fine particulates in suspension. Sediment-rich layers may result from a protracted period of reduced current that allows the fine sediment to settle and blanket the reef. However, it seems unlikely that drastic current decrease could occur as the topography of the area highly contributes to enhance the hydrodynamic processes (Genin et al., 1986; Mienis et al., 2007; White et al., 2005). Nevertheless, considering that periods of reduced current strength had occurred, the surface sediment freshly deposed would be prone to erosion as soon as the currents speeds accelerated (such as during the glacial/interglacial transition for coral carbonate mounds from the Celtic margin

(Dorschel, 2003; Rüggeberg et al., 2007). It is therefore unlikely that the compaction and consolidation of the relatively thin sediment-rich layers deposited over few decades in Mingulay would resist enhanced current strength. Therefore, Sediment-Rich Layers, often followed by progressive increase of coral fragments, are more likely to be deposited adjacent to physical barriers against strong currents, such as coral frameworks.

5.6.2 Model of reef growth

Our observations from the CTscan and the counting data indicate distinct cycles of coral growth, biodiversity and clast preservation within the reef. Below we propose a model of reef development through time and space. This model includes biodiversity succession associated with coral reef facies, but also mechanical, chemical and bioerosion processes (Figure 5 - 7).

- Step 1, reef initiation: the initiation of a cold-water coral reef may start as soon as the recruitment and settlement of planula larva on a substratum occurs (e.g. Squires et al., 1964). This may imply a favourable hydrodynamic regime allowing the transport of coral larvae to the reef site. The development of a coral framework subsequently changes local hydrodynamic conditions (Dorschel et al., 2007a): adjacent coral frameworks may provide a relatively efficient protection against current allowing the deposition of a species-poor, faunally depauperate sediment-rich layer.
- Step 2, framework expansion: if the environmental conditions remain favourable for coral growth (i.e. current strength, food supply, water mass properties…), the coral frameworks may grow as big as a few meters in diameter and colonize the entire area (e.g. Squires et al., 1964). Some coral branches might break down at this stage, but as the area remains relatively protected by the adjacent framework, sediments would quickly bury them. As observed in our records, the progressive increase of coral fragments trapped in sediments precedes and announces a coral-rich layer with a few associated taxa such as tube-building polychaete worms.
- Step 3, collapse of the framework: eventually the framework will die and collapse. Three main mechanisms could describe the collapse of such huge structures. First, the framework may collapse under its own weight and the

impact of bioerosion of sponges and fungi at its base. This implies that frameworks have a limited lifetime defined by their capacity to maintain a certain weight including the weight of an often dense aggregation of other large fauna superimposed on their capacity to resist (bio)erosive attack. Second, the vertical growth of the framework may not be able to cope with the high sedimentation regime characterizing the area. As a result coral framework becomes buried whereupon it breaks into pieces within the sediment. Third, death of the framework occurs due to environmental conditions becoming unfavourable, and the dead framework breaks up and is buried. The relative quantification of biodiversity associated with coral framework is not clear, but in sediment records very few fossils are associated with the framework. The framework would be quickly buried as the coral branches would trap the vertical and lateral flux of sediment (Dorschel et al., 2007a; Frank et al., 2009; Mienis et al., 2007).

- Step 4, coral rubble: a high benthic biodiversity develops on the coral rubble lying on the seafloor (as shown in our study by the high abundance of bivalves and other taxa). The coral rubble would trap sediment at first and be rapidly but superficially re-covered by sediment. However, without the presence of an extensive framework, the surface sediment and rubble would be more prone to the intense current regime characterizing reef environments. As a result, at this stage intensive re-working may occur, resulting in poorer preservation of the coral fragments. In addition, the high biodiversity would also likely increase bio(erosion) processes at the top of the reef structure. If the environmental conditions allow, a larval recruitment phase may occur, and a new cycle would start again.
- Step 5, geological structure: the cyclic repetition of these different phases of coral/reef growth would form local topographic highs that may in turn affect the local hydrodynamic and sedimentary regimes (Freiwald, 2002; Roberts et al., 2006; Roberts et al., 2009b; Wheeler et al., 2007; Wilson, 1979). The dating results performed on the two cores (Chapter 4) suggest that the cycle of reef growth, disturbance/death and recovery occurs very quickly, within about 100 years. The position of the core site relative to the peak of the mound may influence the expression of these cycles within the different facies. Thinner facies

layers and a lower faunal diversity might imply that the core came from the reef edge. This could be the case for core 929, which had fewer coral fragments and less faunal diversity than core 930.

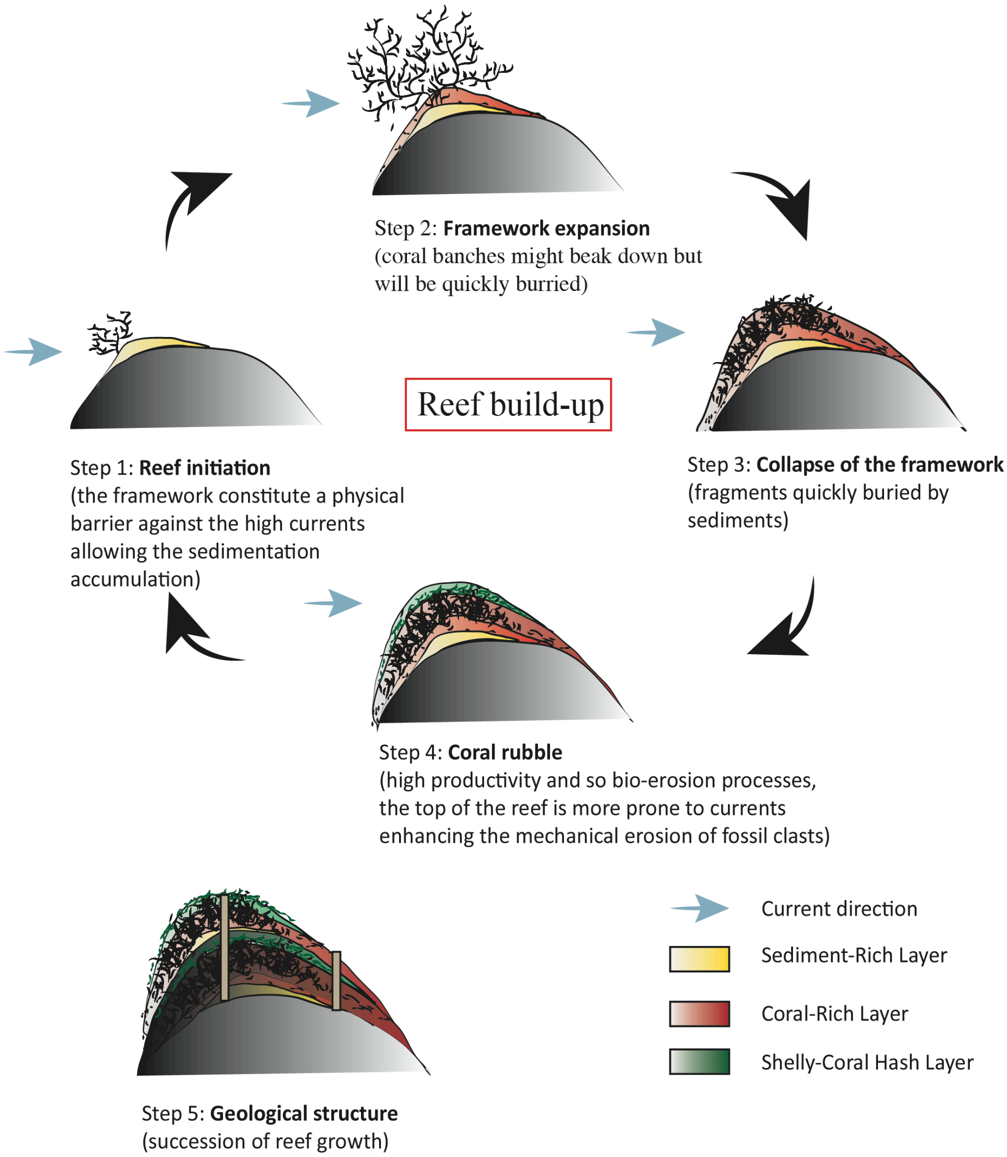

Figure 5 - 7: Schematic model of cold-water coral reef build-up.

5.7 Conclusions

CTscan images allowed the quantification of the relative abundance and state of preservation of the coral fragments and the fauna associated with cold-water coral reefs along coral-sediment cores. The images we retrieved from the shallow inshore

Mingulay Reef Complex, which present very high accumulation rates of 3 – 4 mm a^{-1} (Chapter 4), enabled us to reconstruct the depositional history of cold-water coral reefs in this region. Three main facies were identified and defined as: coral-rich layers, sediment-rich layers and shelly-coral hash layers. Coral-rich layers are assumed to represent extensive growth of coral framework under favourable environmental conditions followed by its collapse. Shelly-coral hash layers revealed a high benthic biodiversity and mechanical erosion due to the absence of coral framework acting as a physical barrier against strong currents characterizing the area. Finally the sediment-rich layers indicate a depositional environment relatively protected from the current, likely due to the presence of a coral framework and allowing the deposition of sediment.

These facies occurred in a systematic sequence within the cores suggesting cyclic depositional environments that drive a rapid cycle of reef growth, disturbance and recovery. From these observations we propose a model of cold-water coral reef build-up subdivided in five major steps (each characterized by changes in the relative biodiversity, sedimentological regime and changes in erosional processes): reef initiation, framework expansion, collapse of the framework and coral rubble.

Chapter 6: Decadal trends of the AMOC during Holocene 3.5 – 2.6 ka abrupt oceanic shifts

6.1 Abstract

Centennially resolved North Atlantic Current (NAC) marine $\Delta^{14}C$ reconstructions have been derived from coupled U-series and ^{14}C dating of fossil cold-water coral. These results enable to review the chronology and discuss mechanisms of a major Holocene climatic anomaly occurring from 2.6 to 3.5 ka BP. We propose a "$\Delta\Delta^{14}C$" index, to document changes in the relative atmospheric $\Delta^{14}C$ uptake by the deep-water formation strength, generated from existing ^{14}C residual and ^{10}Be datasets (Reimer et al., 2004; Steinhilber et al., 2009). Our coral records, compared with this index, suggest that following an initial perturbation occurring at 3.5 ka BP, shifts in the NAC composition and of the Atlantic Meridional Overturning Circulation (AMOC) occurred over the following 800 years. The sub-surface circulation regime has repeatedly affected cold-water coral growth, causing cold-water coral ecosystem decline till its temporary disappearance at 1.4 ka BP off coastal Scotland and possibly across the wider northern European margin. *Lophelia pertusa* has only very recently started re-occupying the area.

6.2 Introduction

The Holocene Epoch has been punctuated by repeated, abrupt climatic oscillations (Mayewski et al., 2004). Neither the forcing nor the mechanisms leading to such climatic disruptions are yet clearly understood. Most theories hypothesize that either freshwater pulses or changes in solar activity pushed the climate system over a threshold (Alley et al., 2003). The present increase of greenhouse gases induced by human activities could lead a similar abrupt change in global climate, in turn impacting upon ecosystems (Alley et al., 2003). It is thus critical to provide accurate reconstructions of natural climatic variability and evidence for ecosystem response to these changes.

A growing body of evidence has highlighted that shifts in the ocean circulation state would be a major component of abrupt climatic transitions (Clark et al., 2002). The Atlantic Meridional Overturning Circulation (AMOC) is a density driven circulation pattern in the Atlantic region, which transports heat generated in the tropical surface waters to the northern latitudes via the North Atlantic Current (NAC). In the Nordic Seas the dense water mass sinks and flows southward as the North Atlantic Deep Water (NADW) (Rahmstorf, 2002). The thermohaline circulation (THC) is the major vector of heat transport from the tropics to the high latitudes and is important for the sequestration and export of greenhouse gases to the deep-sea through the formation of NADW (Clark et al., 2002; Lozier and Stewart, 2008). Obtaining high-resolution records of ocean circulation variability is therefore essential to better understand natural climate variability.

Cold-water corals are distributed worldwide and can be found under a wide range of temperature and salinity (Freiwald et al., 2004; Roberts et al., 2009b). Their calcareous skeleton is ideally suited for both U-series and radiocarbon (^{14}C) dating enabling the reconstruction of past marine radiocarbon ($\Delta^{14}C$) and of the local deviation from the global average surface ocean activity (ΔR) (Adkins et al., 1998; Frank et al., 2004; Robinson et al., 2005). In the North-east Atlantic, the Holocene has been favourable for the near-continuous growth of cold-water coral reefs leading to the formation of large topographic features and allowing near-continuous and absolute dating of oceanic circulation changes (Chapter 4; Frank et al., 2009; López Correa et al., 2012). The shallow cold-water coral reef system of Mingulay, offshore Scotland, records above average accumulation rates of 3 – 4 mm a^{-1} (Chapter 4), which enables reconstructions of short time scale and small amplitude $\Delta^{14}C$ variability. The Mingulay Reef Complex measured accumulation rates varies significantly from 0.5 to 12 mm a^{-1} between 1.7 to 4.2 ka BP (Chapter 4). Although such ecosystems would be able to adapt to long term and progressive environmental changes it has been hypothesized that ecosystem performance would have been affected detrimentally by abrupt climatic and associated ocean shifts, causing reduction of occurrence and potentially disappearance (Alley et al., 2003; Stenseth et al., 2003).

In this study, North Atlantic sub-surface centennially resolved $\Delta^{14}C$ and ΔR variability was generated from paired U-series and ^{14}C dated cold-water corals from the Mingulay Reef Complex. The reconstructed changes were compared with the

"$\Delta\Delta^{14}C$" index generated from absolute ^{10}Be and ^{14}C residual data (Reimer et al., 2004; Steinhilber et al., 2009) to document AMOC instability during a major climatic anomaly between 2.7 and 3.5 ka BP. The oceanic shifts highlighted from the $\Delta^{14}C$ were compared to Mingulay reef accumulation rates (Chapter 4) and reveal cold-water coral sensitivity to abrupt oceanic circulation changes.

6.3 Material and methods

Coupled U-series and radiocarbon dates were performed on 20 cold-water scleractinian corals (*Lophelia pertusa*). The coral fragments were retrieved from two sediment cores at 127 m and 134 m depth below sea level from the Mingulay Reef Complex: 56°50'N; 7°20'W (Figure 6 - 1; Roberts et al., 2005). *Lophelia pertusa* fragments are present throughout the cores, albeit with varying abundance and preservation. The accumulation rate of 3 – 4 mm a^{-1} of the sediment cores enable reconstruction of $\Delta^{14}C$ and associated reservoir age variability with an average temporal resolution of ~150 years between 1.7 and 4.2 ka BP (TableA2 - 1 and Table A2 - 2 in Appendix 2).

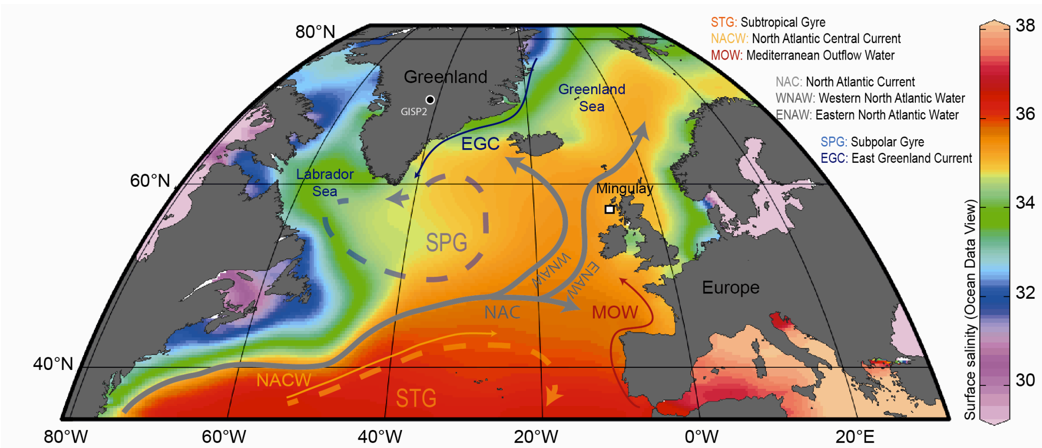

Figure 6 - 1: the Mingulay Reef Complex relative to a sea surface salinity map presenting the main North Atlantic surface currents.

The reservoir ages (R) of the NAC and derived branches have been shown to be centered at about 400 years (Mangerud, 1972). The records available for Ireland and the British Isles over the last 5 000 yrs have highlighted local derivation from the global average marine reservoir age of surface waters (ΔR) on the order of 400 yrs (with values ranging from –208 ± 75 ^{14}C to 207 ± 73 ^{14}C yrs) (Reimer, 2002 and

Ascough et al., 2004, 2006, 2007a and 2009). Regional climatic and oceanographic variations, inducing variation in the relative influence of subpolar waters to the NAC affecting in turn the North Atlantic Deep Water production and/or of local surface current to the sites may explained such a range of values (Ascough et al., 2007 and 2009). Indeed, the relative composition, intensity, and position of the NAC at the boundary between the anticyclonic Sub-Tropical Gyre (STG) and the cyclonic Sub-Polar Gyre (SPG) is affected by the strength and position of the latter (Häkkinen and Rhines, 2004; Hátún et al., 2005). Polar waters and the East Greenland Current (EGC) in particular are a major pathway of sea-ice and freshwater in the Atlantic Ocean. The relative radiocarbon content of this water mass is significantly depleted in radiocarbon compared to the NAC (Butzin et al., 2005; Franke et al., 2008). Thus, a high SPG index (stronger, and East-West shape) would induce a strengthened inflow of fresher, cooler and radiocarbon depleted SPG waters to the NAC. In contrast, the STG re-circulates in the temperate Atlantic's relatively warm, saline and well-ventilated waters. Thus, low SPG index (weakened state, and North-South in shape) would favor saltier, warmer and relatively ventilated inflow of STG waters to the NAC (Figure 6 - 1; Hátún et al., 2005). The weighted mean values of the ΔR for the British Isles estimated by Ascough et al. (2007) during the late Holocene is of -79 ± 17 ^{14}C yr, which is slightly lower than previous estimates of ΔR = –33 ± 93 ^{14}C yr (Reimer, 2002), and significantly different to the modern regional average ΔR for British waters of 17 ± 14 ^{14}C yr (radiocarbon.pa.qub.ac.uk). At present, in Mingulay, *Lophelia pertusa* reefs bath in Atlantic-origin water (Dodds et al., 2007). However, it is not excluded that in the past the Scottish Surface Current (SSC), enriched in radiocarbon relative to the NAC may also have influenced our study site (Ascough et al., 2007; 2009). Long-term records with a well-constrained and high temporal resolution from a single study site will allow to establish potential time-dependence in ΔR associated with changes in the local and global oceanography.

To compare our record with absolute dated and high temporal resolved AMOC changes, we generated a "$\Delta\Delta^{14}C_{atm}$" index from the ΔTSI total solar irradiance proxy derived from ice-cores ^{10}Be data and from the ^{14}C residual (Reimer et al., 2004; Steinhilber et al., 2009). Both records are commonly seen as solar input proxies. However, the ^{14}C residual is also highly dependent on the North Atlantic

Deep Water (NADW) strength affecting in turn the relative up-take of atmospheric radiocarbon ($\Delta^{14}C_{atm}$) (Clark et al., 2002). Thus, the solar output influence in the ^{14}C residual signal was discriminated from the total solar irradiance curve in order to obtain the "$\Delta\Delta^{14}C_{atm}$" index (see supplementary material).

6.4 Results

The North Atlantic inflow to the Mingulay Reef Complex exhibits high amplitude $\Delta^{14}C$ changes between 1.7 and 4.2 ka BP (Figure 6 - 2). From 2.07 ± 0.02 to 2.72 ± 0.01 ka BP and 3.51 ± 0.02 to 4.23 ± 0.03 ka BP, the $\Delta^{14}C$ values recorded at Mingulay follow the marine international average (Reimer et al., 2009). The corresponding ΔR values are centered at 16.6 ^{14}C yr, which is in agreement with the modern regional average for the British waters of 17 ± 14 ^{14}C yr and confirmed the major influence of the NAC in this region over these periods (Figure 6 - 2 A & B).

However the $\Delta^{14}C$ values recorded in Mingulay deviate significantly from the marine international standard (Reimer et al., 2009) between 2.75 ± 0.02 and 3.44 ± 0.03 ka BP (Figure 6 - 2 C). The continuous record obtained from the cold-water corals, emphasized high frequency ΔR variability with values from -180 ± 40 to 268 ± 40 years over the specific Holocene climatic anomaly. The well-defined succession of sub-surface radiocarbon changes suggests significant AMOC variability over an 800 yr period. One other prominent anomalies is observed at 1.69 ± 0.03 ka BP, with ΔR values of -180 ± 40, but is only defined by data point each (Figure 6 - 2 A & B).

The index of $\Delta^{14}C_{atm}$ up-take by the NADW shows strong variability of the THC over the studied period. Two major drops of the THC circulation are centered at 3.3 and 2.7 ka BP and a major increase of THC is observed centered on 3 ka BP (Figure 6 - 2 E).

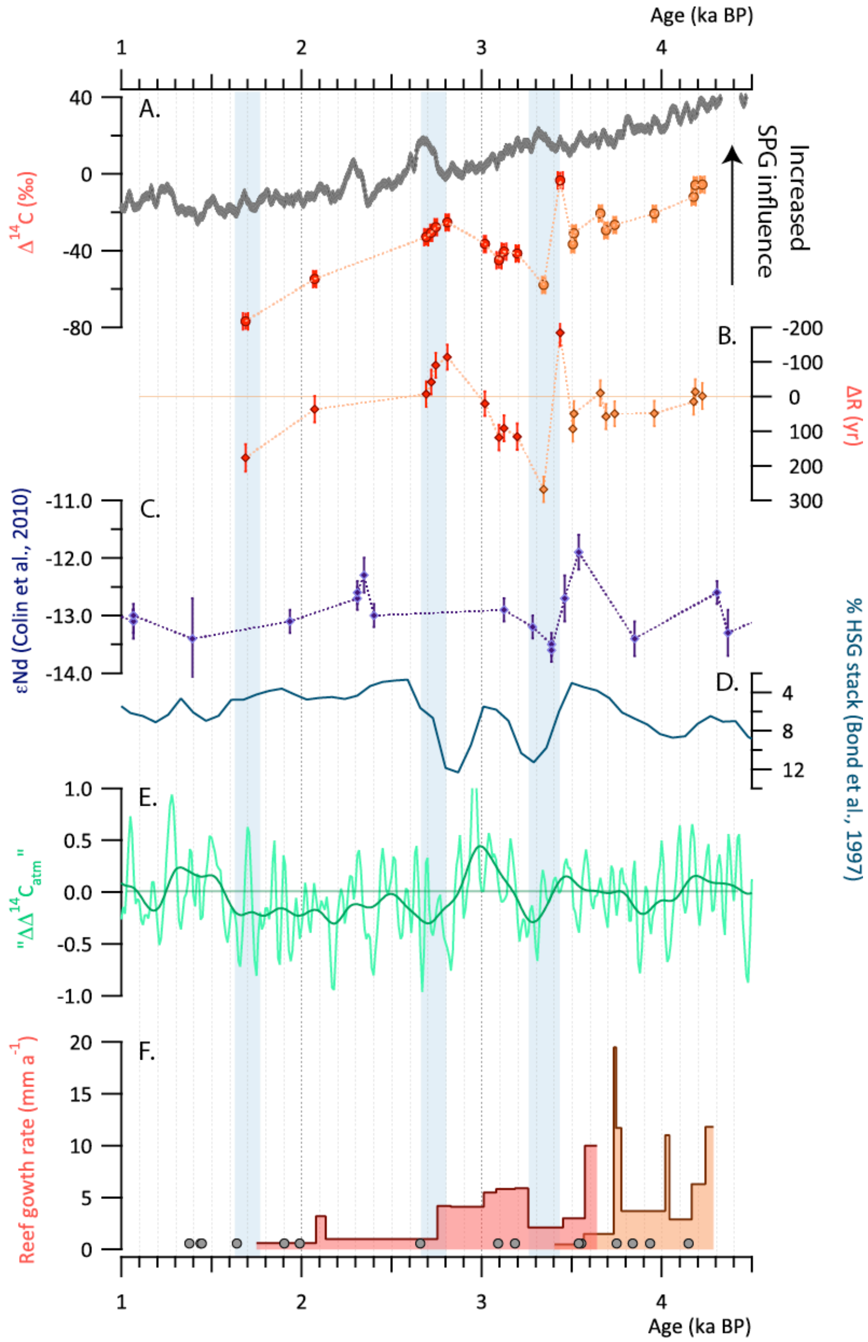

Figure 6 - 2: (A) Marine $\Delta^{14}C$ (‰) relative to the atmospheric radiocarbon (Intcal09) (Reimer et al., 2009) and (B) ΔR calculated from coupled U-series and radiocarbon ages performed on *Lophelia pertusa* corals from cores 929 (56°47'19''N, 7°23'27''W, 127 m down the surface, in orange) and 930 (56°49'20''N, 7°23'47''W, 134 m water depth, in red). (C) Nd isotopic composition from cold-water corals from Rockall Bank (core MD01-2454G, 747 m water depth; Colin et al., 2010). (D) Hematite-strained grains (%) from North Atlantic cores stack as proxy of freshwater flux to the sub-polar north Atlantic (Bond et al., 2001). (E) $\Delta\Delta^{14}C_{atm}$ as an index of $\Delta^{14}C_{atm}$ up-take by the NADW (this study), (F) Mingulay Reef Complex accumulation rates estimated from downcore (core 929 and 930, red and orange histograms, respectively) and reef surface corals radiocarbon ages (white cycles) (Chapter 4). Uncertainties are represented by 1σ error.

6.5 Discussion

Our results show a sharp depletion of the marine radiocarbon values and high ΔR in Mingulay NAC inflow 3.34 ± 0.02 ka BP ago (Figure 6 - 2 A & B). This shift in the $\Delta^{14}C$ in Mingulay is synchronous with depleted εNd values recorded from Rockall cold-water coral (Colin et al., 2010), indicative of a larger contribution of the polar waters depleted in radiocarbon to the NAC. The coeval increased hematite strained grains in the North Atlantic (Bond et al., 1997), suggests that a freshwater input to the North Atlantic was associated with modifications of the oceanic surface circulation and deep-water formation (Bond et al., 1997). The reconstruction of NADW strength derived from our "$\Delta\Delta^{14}C_{atm}$" index shows a significant reduction of the deep-water formation. Thus, as demonstrated for inter-annual to inter-decadal timescales and illustrated from millennial timescales, changes in the SPG influence would significantly affect the relative composition (salinity & temperature), strength and direction of the NAC (Hátún et al., 2005; Thornalley et al., 2009). This, in turn, would impact THC strength and regional climate. The subsequent lower accumulation rates of the Mingluay Reef Complex indicate that this first oceanic shift has significantly affected *Lophelia pertusa* growth (Figure 6 - 2 F).

This abrupt AMOC shift is followed by a progressive return to modern-like NAC characteristics with an overshooting down to $\Delta^{14}C$ values of -25 ± 4 (‰) and a ΔR of 110 ± 40 years from 3.34 ± 0.02 to 2.81 ± 0.02 ka BP. The enriched $\Delta^{14}C$ values recorded in Mingulay indicate an increasing influence of well-ventilated sub-surface water, which could be either attributed to an increase of SCC water or of STG water to our study site. The apparent intensification of the NADW from our "$\Delta\Delta^{14}C_{atm}$" index is in agreement with a stronger influence of the well-ventilated but also saltier and warmer STG waters to the NAC, both acting to intensify the AMOC circulation (Hátún et al., 2005). Our results thus suggest that the progressive intensification and influence of the STG water on the NAC seems to have promoted reef growth and ecosystem recovery from the abrupt cooling events.

In between 2.81 ± 0.02 and 2.72 ± 0.01 yrs BP our coral records suggests a transient re-establishment of modern-like conditions. Here, the strengthened SPG water influence on the NAC is correlated with a relative decrease of "$\Delta\Delta^{14}C_{atm}$"

index. This final phase of minor amplitude, occurring alongside a reduction on coral growth in Mingulay and also in Norway (Chapter 4), seems therefore to have been sufficiently abrupt to destabilized cold-water coral ecosystem once more.

None of the 60 dated *Lophelia pertusa* specimens within the entire reef complex were aged from 1.4 ka BP to modern. Thus, we hypothesize that the last apparent shift in the NAC, as recorded by an abrupt increase in $\Delta^{14}C$ at 1.69 ± 0.03 ka BP (Figure 6 - 2A), resulted in the total disappearance of the ecosystem, which was already weakened by the previous climatic anomaly. Fossil *Lophelia pertusa* chronologies from Norway again show parallel disruptions in reef development and a lack of corals from 1.2 ka BP to modern (Chapter 4), indicative that this regime shift may have been widespread off northern Europe.

Our results thus show that slower reef growth at the Mingulay Reef Complex centered at 1.75, 2.75 and 3.50 ka BP appears directly associated with abrupt AMOC shifts. Coral growth has resumed in Mingulay recently (post-bomb period). However, our study demonstrates that the increasing probability of sudden changes in the AMOC strength could significantly alter ecosystem persistence in ways similar to those recorded in the past.

6.6 Conclusions

Centennially resolved marine $\Delta^{14}C$ reconstructions derived from absolute dating of fossil cold-water coral have enabled a review of the chronology and mechanisms of a major Holocene climatic anomaly occurring from 2.7 to 3.5 ka BP. Following an initial perturbation occurring at 3.5 ka BP, substantial modifications of the NAC composition occurred for 800 yrs, likely associated with a strong AMOC variability. The sub-surface circulation regime shifts have repeatedly affected cold-water coral growth, causing ecosystem decline off coastal Scotland and possibly across the wider northern European margin.

Chapter 7: Foraminifer assemblages and foraminifer $\delta^{18}O$ – $\delta^{13}C$ isotopic reconstructions from Holocene (1.7 – 4.2 ka) shallow coral reef system sediment cores

7.1 Abstract

A detailed investigation of downcore benthic foraminifer communities associated with Mingulay Reef Complex facies, coupled with measurements of benthic and planktonic foraminifer oxygen ($\delta^{18}O$) and carbon ($\delta^{13}C$) isotopes was conducted. The aim was to explore potential relationships between hydrological variability and changes to cold-water reef depositional environments. More than 100 benthic foraminifera were identified characterizing a highly diversified community and an environment dominated by strong bottom currents, high food availability and varied substrates. Our results suggest that there were no significant changes in benthic foraminifera communities associated with the observed changes in reef depositional environments between 1.7 – 3.5 ka.

Significant variability in benthic foraminifera *C. lobatulus* $\delta^{13}C$ (from 1 to 1.8 ‰) and planktonic *G. bulloides* $\delta^{18}O$ (from 1 to 2.1 ‰) profiles were documented. Depleted *C. lobatulus* $\delta^{13}C$ values are associated with shelly-coral hash facies. We suggest that the enhanced organic carbon decomposition rates associated with the high macro-benthic community characterizing such facies would be the dominant process affecting benthic $\delta^{13}C$ records. However, shelly-coral hash layers result from the episodic collapses of coral framework that appear associated with shifts in oceanic circulation. Thus the depleted benthic $\delta^{13}C$ signal may indirectly highlight hydrological changes.

G. bulloides $\delta^{18}O$ profile seems to reflect changes in the relative strength of the sub-polar gyre within the reef area. The comparison of the foraminifer isotopic data with absolute dated reservoir ages from coral fragments from the same cores

suggest significant age offsets between down-core coral fragments and the sediment matrix.

7.2 Introduction

Successive cold-water coral reef growth leads to large and fast growing topographic features (De Mol et al., 2005; Dorschel et al., 2005; Henriet and Guidard, 2002; Kenyon et al., 2003; Roberts et al., 2006; Rüggeberg et al., 2007). In the North Atlantic, coral-carbonate mounds resulting from successive growth during distinct interglacial periods have accumulation rates averaging 0.2 mm a^{-1} (Frank et al., 2009). Cold-water coral reefs result from a single generation of reef growth during the Holocene interglacial period and have even higher sedimentation rates (López Correa et al., 2012). The Mingulay Reef Complex off the west coast of Scotland, for instance exhibits unprecedented accumulation rate averaging 3 – 4 mm a^{-1} that would enable high-resolution palaeo-environmental reconstructions, integrating classic sedimentological studies and the skeletal chemistry of corals (Chapter 4).

The Holocene is generally a favourable period for NE Atlantic *Lophelia pertusa* occurrence and cold-water coral structure expansion (Frank et al., 2011). However, recent results have demonstrated that the Holocene was punctuated by periods that were less favourable for coral growth throughout the NE Atlantic (Chapter 4, Frank et al., 2009, López Correa et al., 2012). Neodymium isotopic composition and marine radiocarbon signature of absolute dated corals from this region have highlighted short-time scale and small amplitude changes in the Atlantic Meridional Overturning Circulation (AMOC) (Colin et al., 2010; Copard et al., 2012; Frank et al., 2009; López Correa et al., 2012). In Mingulay Reef Complex, for example, reduced reef expansion at 3.5 ka BP, 2.8 ka BP and 1.6 ka BP have been associated with abrupt shifts in marine radiocarbon (Chapter 6). Thus, cold-water coral sites from the NE Atlantic are sensitive locations and key to documenting AMOC changes.

Cold-water coral reef internal structure is comprised of an accumulation of coral fragments and associated fauna, terrigenous sediment carried through the coral frameworks, and entrapped biogenic sediment resulting from the activity of associated coral infauna and epifauna (Wheeler et al., 2011). Distinct reef facies characterizing changing depositional environment and coral occurrence were defined as: coral-rich, sediment-rich and shelly-coral hash (Chapter 5). Coral-rich facies represent extensive growth of *Lophelia pertusa* framework under favourable environmental conditions followed by its collapse. Shelly-coral hash facies reflect a high benthic biodiversity and mechanical erosion due to the absence of coral framework acting as a physical barrier against the strong currents characterizing the area. Finally, the sediment-rich layers indicate a depositional environment relatively protected from the current, likely due to the present of coral framework and allowing the deposition of sediments. The successive sequence of these facies suggests cyclic depositional environments driving cold-water coral reef build-up and characterized by distinct biodiversity, sedimentological regimes and erosional processes (Chapter 5). However, the hydrological role in reef collapse and in the successive depositional environmental changes still need to be better understood.

Mingulay Reef Complex downcore benthic and planktonic foraminifera oxygen ($\delta^{18}O$) and carbon ($\delta^{13}C$) isotope variability was reconstructed and compared with centennially resolved marine radiocarbon ($\Delta^{14}C$ (‰)) (Chapter 6) and reef accumulation rate changes (Chapter 4). These were generated from the same cores spanning the Holocene period between 1.7 and 4.2 ka BP. In addition, the benthic foraminifera communities associated with the distinct cold-water coral reef facies were investigated. The aims were to identify whether distinct foraminifera species associated with different environmental conditions.

7.3 Material

7.3.1 Coral/sediment cores

Two vibro-cores from the Mingulay Reef Complex were investigated for this study. The cores +56-08/929VE and +56-08/930VE (hereafter referred to as cores 929 and 930) were collected in October 2007 by the British Geological Survey during a survey on board the NERC vessel the RRS James Cook (Stewart and Gatliff, 2008). The total recovery of core 929 (56°47’19’’N, 7°23’27’’W) and 930 (56°49’20’’N, 7°23’47’’W) was 3.61 m and 5.25 m, respectively (Figure 7- 1).

The cores were sliced into metre-length sections on board and then placed in cold storage (4°C) at BGS. Because the cores contained coral fragments embedded in sediment they were frozen prior to splitting to avoid any shifting in the position and orientation of the coral fragments and to preserve internal sedimentary structure of the cores. While frozen, the cores were split using a diamond bladed circular rock-cutting saw. To avoid any potential contamination from the cutting fluid, the uppermost surfaces of both halves were immediately removed. Once opened and defrosted, the cores were dissected at 1 cm intervals, documenting the position and state of preservation of each coral fragment within the cores and archiving the sediment and coral fragments. After dissection, every fifth 1 cm slice was freeze-dried and washed through 315, 125 and 63 µm mesh sieves. The 3 size fractions were then dried in an oven at 45°C.

7.3.2 Hydrological setting

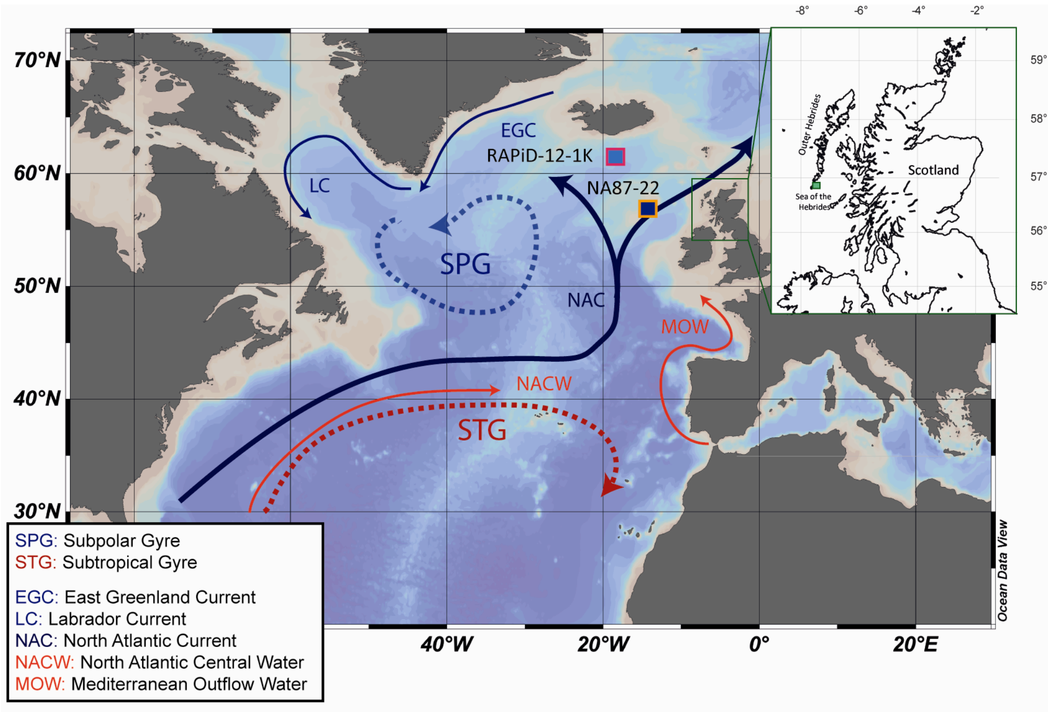

Figure 7- 1: Location of Mingulay Reef Complex study site (56°47'N, 7°23'W; Green square), core NA87-22 (55°30'N, 14°42'W) and core RAPiD-12-1K (62°05'N, 17°49'W) relative to simplified map of the North Atlantic surface currents.

At present, waters from the North Atlantic Current occupy the outer parts of the continental self and the deeper (>100 m) coastal waters of west Scotland (Craig, 1959; Hill et al., 1997; Inall et al., 2009). At the surface the Scottish Coastal Current (SCC) brings northward colder and fresher waters from the Irish Sea and Clyde Sea (Ellett and Edwards, 1983). The Mingulay Reef Complex baths in North Atlantic Current (NAC) waters (Craig, 1959; Hill et al., 1997; Inall et al., 2009). The hydrological characteristics (temperature, salinity) of the NAC depend on the strength and shape of the subpolar gyre (SPG) relative to the subtropical Gyre (STG) (Hátún et al., 2005; Inall et al., 2009) (Figure 7- 1). Relatively warmer, saltier and well mixed waters re-circulate in the temperate Atlantic through the action of the STG. By contrast, the polar waters transported throughout the SPG are fresher, cooler and depleted in radiocarbon. Thus, in low SPG index (weak and North-South SPG shape) a stronger influence of the STG waters to the NAC would occur (Hátún et al., 2005) and in high SPG index (stronger and East-West shape) a strengthened inflow SPG waters would contribute to the NAC. Waters of Mediterranean origin (MOW) may also have an influence on the NAC, however this point is still debated (Lozier and Stewart, 2008; New et al., 2001; Reid, 1979) (Figure 7- 1).

7.3.3 Age models

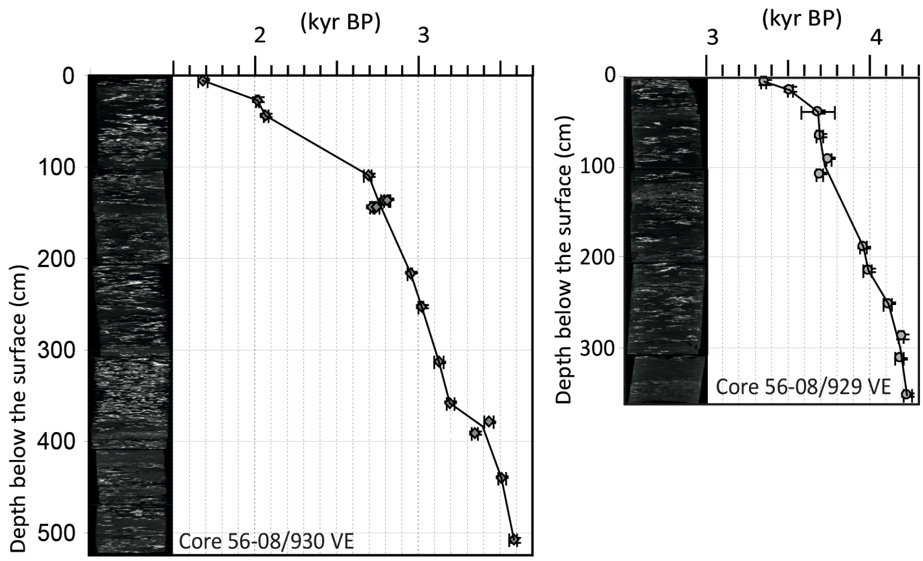

Figure 7- 2: Age model of core 930 (left) and 929 (right) obtained from cold-water coral (*Lophelia pertusa*) U-series dating (grey circle). On the left of each age model is presented the CT scan image of the core showing distinct stratigraphic layers.

The age models of the cores were obtained by 28 U-series dating performed on *Lophelia pertusa* fragments abundantly distributed all along the cores (Chapter 4).

The period recovered by the two cores is from 1690 ± 30 yr BP to 4230 ± 30 yr BP (Figure 7- 2) (Chapter 4).

7.4 Methods

7.4.1 Foraminifer assemblages

Sediments from distinct layers of core 930 were studied for benthic foraminifer assemblages. Eleven layers of sediment defined as sediment-rich layers, coral-rich layers, or shelly-coral hash layers (Chapter 5) were considered. All benthic foraminifer from the fraction above 315 µm, and between 125 and 315 µm were picked, sorted by species and counted. In the fraction above 315 µm, the sum of benthic foraminifers varied from 20 to 195 individuals. Thus, as the total number of foraminifer was not statistically sufficient, we did not consider this fraction further. For the fraction from 125 and 315 µm however, the foraminifer communities characterizing distinct cold-water coral facies were highlighted using Bray Curtis similarity clustering and non-metric MultiDimensional (nMDS) were ordinate with a stress value of 0.09 using the PRIMER software.

7.4.2 Foraminifera isotope profiles

Prior to analyses, well preserved benthic *Cibicides lobatulus* and planktonic *Globigerina bulloides* foraminifera were picked and ultra-sonically cleaned in ethanol and rinsed 3 times in distilled water. Stable isotopes analyses ($\delta^{18}O$ and $\delta^{13}C$) were carried out at Edinburgh University. Oxygen and carbon stable isotope analyses were performed on 0.02 - 0.1 mg appreciatively 12 (or more) *Cibicides lobatulus* and *Globigerina bulloides* from the fraction between 125 and 315 µm. The samples were reacted with 100 % orthophosphoric acid at 75°C in a KIEL CARBONATE III preparation device and the resulting CO_2 was then analyzed on a THERMO ELECTRON DELTA+ ADVANTAGE stable isotope ratio mass spectrometer.

The standard deviation (n=91) of a powdered coral laboratory standard (COR1D, $\delta^{13}C$= -0.648, $\delta^{18}O$= -4.923) run on the same days as the study samples [between 09/09/10 and 23/09/11], was ± 0.05 ‰ for $\delta^{13}C$ and ± 0.06 ‰ for $\delta^{18}O$. Isotopes ratios are quoted relative to the Vienna-PeeDee Belemnite V-PDB standard.

7.5 Results

7.5.1 Foraminifera assemblages

a. Planktonic vs. benthic

The proportion of planktonic tests for the fraction between 125 µm and 315 µm was calculated from (P/(P+B)*100) where P is the number of planktonic and B the number of benthic foraminifera. For this fraction, the eleven samples selected presented a planktonic percentage of about 8 to 17 % (Table 7- 1). This is consistent with a previous study which shows that the planktonic proportion within the Hebridean shelf, west of Scotland averaged 10 % (Austin and Kroon, 1996; Murray, 1985). No planktonic foraminifera were found in the fraction above 315 µm.

a. Benthic species identification

More than 100 species were counted in the 11 layers considered from Mingulay Reef Complex sediment cores. The 36 dominant species identified are presented in Table 7-1.

The Bray Curtis similarity clustering and non-metric MultiDimensional (nMDS) analyses performed on each layer show a high degree of similarity between the foraminifer assemblages from the 11 selected levels. Results shows that the 11 sections present more than 80 % of similarity, but samples “60-61 cm”, which presnt only 70 % of similarity with the other sections. This observation is confirmed by the two-dimensional dispersion nMDS plot of foraminifer communities (Figure 7- 3). Thus, all layers are grouped relatively close to each other except for layer 60-61. Interestingly, even if the distinct layers considered are very similar, 3 main clusters defined from the CTscan images as shelly-coral hash layers, coral-rich layers and sediment-rich layers can be drawn. However, this does not seem to be the main parameter impacting on foraminiferal communities and does not allow us to distinguish foraminiferal communities associated with each facies type.

	Core 930										
depth	15-16	60-61	135-136	145-146	155-156	260-261	330-331	375-376	400-401	420-421	510-511
% planktonic	14	17	8	17	10	12	16	12	10	16	12
Cibicides lobatulus	26	32	19	17	33	30	20	22	29	24	27
Bulimina marginata	20	9	20	18	13	17	23	15	15	17	17
Melonis barleeanus	11	4	16	10	12	10	12	18	9	9	10
Hyalinea balthica	7	4	4	4	4	8	5	5	5	5	3
Rosalina praegeri	7	5	4	6	4	5	3	5	3	7	3
Cassidulina laevigata	5	4	4	5	5	4	5	4	3	5	3
Rosalina anormala	3	11	5	7	5	5	6	8	8	7	5
Oolina melo	2	2	1	1	0	1	1	1	0	1	0
Eponides repandus	2	2	0	0	1	0	0	0	1	1	3
Cancris oblongus	2	0	0	0	1	0	0	0	0	0	0
Oolina hexagona	1	1	0	1	0	1	0	0	0	0	1
Spiroplectammina wrightii	1	0	3	0	2	3	1	3	3	4	5
Oolina williamsoni	1	2	1	1	0	1	1	1	1	1	0
Quinqueloculina seminulum	1	0	0	1	0	2	1	0	1	0	0
Oolina costata	1	1	0	0	0	1	0	0	0	0	0
Miliolinella subrotunda	1	5	1	3	1	0	0	1	2	2	2
Ammonia sp.	1	0	2	0	2	1	1	0	1	0	1
Trifarina angulosa	1	0	2	1	0	0	1	1	0	1	1
Cibicides refulgens	1	0	1	0	2	1	0	0	1	0	1
Textularia sagittula	1	0	2	4	4	2	5	0	3	4	6
Fissurina marginata	1	0	0	0	0	1	1	1	0	1	0
Nummulopyrgo globulus	1	3	1	3	1	0	1	2	2	1	1
Fissurina orbignyana	1	0	0	0	0	1	1	1	1	0	1
Oolina squamosa	0	1	0	0	0	0	0	0	0	0	0
Planorbulina mediterranensis	0	1	0	0	0	0	0	0	0	0	2
Nonionella turgida	0	4	0	4	0	1	0	1	2	1	1
Cassidulina crassa	0	0	1	0	0	0	0	0	1	1	0
Gaudryina rudis	0	0	0	1	0	0	1	0	0	0	1
Bolivina difformis	0	0	0	1	0	0	0	0	0	0	0
Cibicidoides variabilis	0	0	5	2	0	0	1	0	1	3	1
Nonion depessulum	0	0	0	1	0	0	0	0	0	0	0
Stainforthia fusiformis	0	0	0	1	0	0	0	0	0	0	0
Quinqueloculina stalkeri	0	0	0	1	0	0	0	1	0	2	1
Triloculina truncata	0	2	0	1	0	0	1	0	1	0	0
Spiroculina vivapara	0	0	0	1	0	0	0	0	0	0	0
Siphotextularia flintii	0	1	0	0	0	0	0	0	0	0	0
others	3	6	3	4	5	3	3	6	3	3	4
Count	571	283	639	1175	421	901	616	886	491	961	534

Table 7- 1: Summary of foraminifera counts, coral-rich layers are highlighted in red, sediment-rich layers are highlighted in yellow and shelly-coral rich layers are highlighted in green.

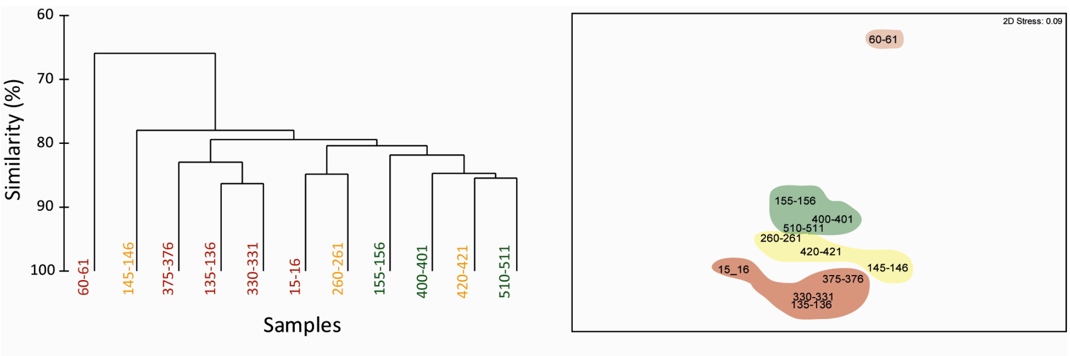

Figure 7- 3: Statistics analyses performed from the frequency of the benthic foraminifers in the 11 layers considered. A. "CLUSTER" analysis performed in PRIMER, showing how similar are the 11 layers of foraminifer assemblages. B. nMDS plot (non-metric scaling plot) showing the two-dimensional dispersion of foraminifer communities. Coral-rich layers are highlighted in red, sediment-rich layers are highlighted in yellow and shelly-coral rich layers are highlighted in green.

b. Isotopic data

The *G bulloides* $\delta^{18}O$ values reflect both the surface seawater temperature (SST) and the $\delta^{18}O$ of the seawater ($\delta^{18}O_{sw}$) in which they built their test. The $\delta^{18}O_{sw}$ varies as a function of the global ice volume and the sea surface salinity (SSS) (Shackleton et al., 1977). In the North Atlantic, *G. bulloides* is predominantly found in spring (April to June) and typically occupy the seasonal mixing layer (0 – 50 m below the surface) (Ganssen and Kroon, 2000). The *G. bulloides* $\delta^{18}O$ records from Mingulay Reef Complex sediment cores show values varying from 1 to 2.1 ‰. In more detail we observe from the bottom to the top of core 929 a progressive depletion of mean $\delta^{18}O$ values from around 1.6 to around 1.8 ‰, indicative of either increasing surface temperature and/or decrease in surface salinity. Relatively enriched values are however, observed at 90 – 120 cm and 230 – 361 cm, with values reaching 1.8 and 2.1 ‰, respectively. Core 930 present oxygen isotope values centered at 1.6 ‰ punctuated by relatively depleted values reaching 1 ‰ from 40 to 130 cm and 350 to 420 cm. In between these two core sections (130 to 350 cm), relatively enriched $\delta^{18}O$ values centered at 1.8 ‰ are observed (Figure 7- 4).

The *G. bulloides* $\delta^{13}C$ values are centered at -1 ‰ and range from -2.5 to -0.5 ‰. The controls on *G. bulloides* $\delta^{13}C$ remain poorly constrained. However, two periods of significant $\delta^{13}C$-depletion are observed in core 930 at 50 to 90 cm and 350 to 420 cm seem to be associated with depleted *G bulloides* $\delta^{18}O$ values and could reflect increasing productivity related to the spring bloom (Ganssen and Kroon, 2000) (Figure 7- 4).

The $\delta^{13}C$ of the epibenthic *C. lobatulus* is in the isotopic equilibrium with the sea water Dissolved Inorganic Carbon ($\delta^{13}C_{DIC}$) (Duplessy et al., 1984). Thus, this species is routinely used as a tracer of bottom water masses (Curry and Oppo, 2005; Duplessy et al., 1984). However, $\delta^{13}C_{DIC}$ is strongly influenced by biological processes through the carbon isotope fractionation occurring during photosynthesis and the formation of organic matter (vital effect) (Zahn et al., 1986). In Mingulay, the signal shows significant variability with values oscillating from 1 to 1.8 ‰. Interestingly, the most depleted values observed at 160, 190, 400 cm for core 930 and 130, 230 and 360 cm for core 929 are observed within shelly-coral hash layers (Figure 7- 4).

Finally, the *C. lobatulus* $\delta^{18}O$ records show values centered around 1.6 ‰, with a range from 0.7 and 1.8 ‰ (Figure 7- 4).

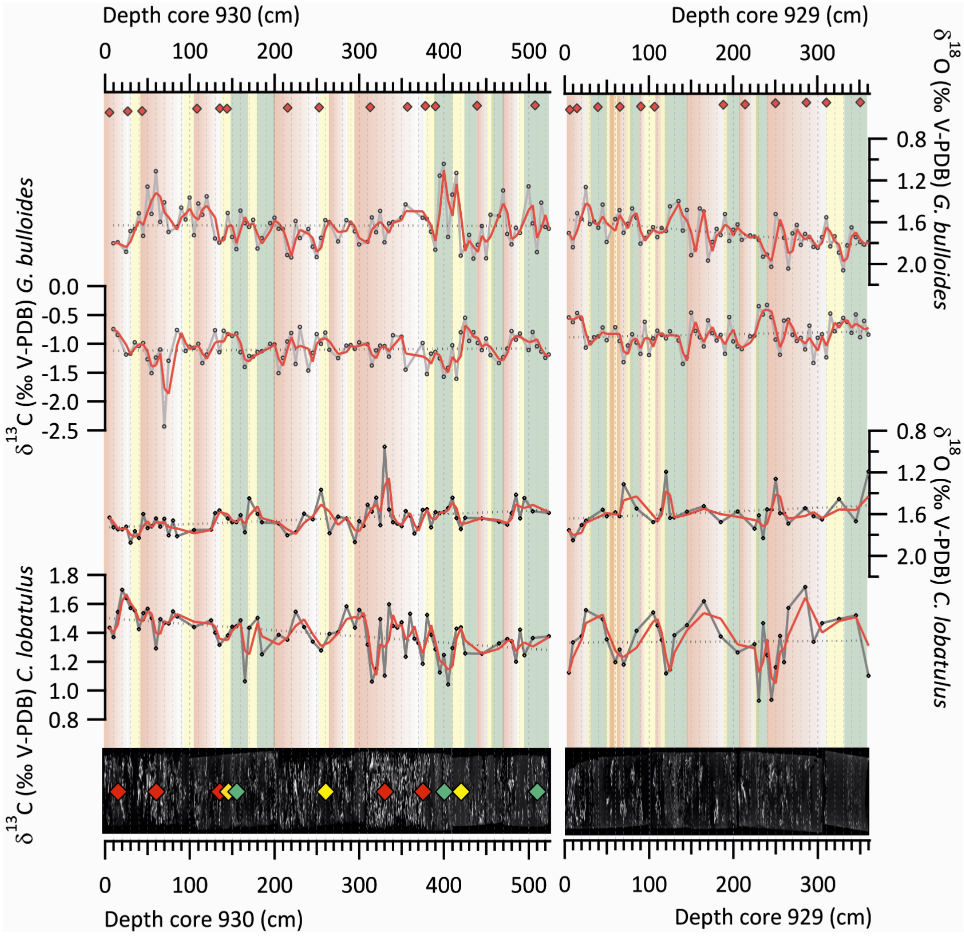

Figure 7- 4: Downcore isotopic profiles obtained from benthic foraminifera (*C. lobatulus*) and planktonic foraminifer (*G. bulloides*). Red diamonds on top symbolised the position of the cold-water coral fragments U-series dated. The CT scan images of each core are reported at the bottom of the graph. The Data green, red and yellow bands represent the shelly-coral hash layers, coral-rich layers and the sediment-rich layers, respectively. The sediment layers analysed for foraminifer assemblages are reported as red diamonds for coral-rich facies, yellow diamonds for sediment-rich layers and green diamonds for shelly-coral hash facies.

7.6 Discussion

7.6.1 Coral reef environmental background

The ecology of benthic foraminifer communities is defined by hydrological parameters (e.g. salinity, temperature, dissolved oxygen), quantity and quality of organic flux to the seafloor, nature of the substrate (soft/hard surfaces, seafloor/elevated substrates) and current strength (Harloff and Mackensen, 1997; Jorissen et al., 1992; Jorissen et al., 1995; Jorissen et al., 2007; Murray, 2006).

a. Benthic foraminifera assemblages: Hydrological interpretation

The water depth of the Mingulay Reef Complex varies from 72 to 215 m. At present, waters from the North Atlantic Current occupy the outer parts of the continental shelf and the deeper (>100 m) coastal waters of Western Scotland, providing a suitable environment for coral growth (Craig, 1959; Dodds, 2007; Hill et al., 1997; Inall et al., 2009; Roberts et al., 2005). The most abundant benthic foraminifera species identified in Mingulay are *Cibicides lobatulus*, *Bulimina marginata*, *Melonis barleeanus*, *Milionlinella subrotunda*, *Textularia sagittula*, *Oolina squamosa*, *Cassidulina crassa*, *Stainforthia fusiformis*, *Hyalina balthica*, or again *Spiroculina vivapara*. All are known from the inner shelf of the British Isles and/or from the temperate Atlantic waters (Murray, 1991a; Murray, 2000; Murray, 2004b). In the layers analyzed there were no significant changes in benthic foraminifera assemblages. This suggests that no significant hydrological changes have occurred and/or that the properties of the deeper shelf waters have not impacted on benthic foraminifer assemblages.

b. Benthic foraminifera assemblages: Environmental interpretation

Current strength and substrate are of significant importance for benthic foraminifera communities in cold-water coral reef area. Current strength favours the re-suspension of organic particles and sediment particles from the seafloor constituting an important food supply for suspension-feeders. The nature of the substrate contributes to increasing the proportion of epifaunal foraminifera able to live attached on elevated and firm substrates, thus avoiding burial by high sediment fluxes (Margreth et al., 2009; Rüggeberg et al., 2007; Schönfeld, 2002a; Schönfeld, 2002b; Schönfeld et al., 2011). The strong current regime observed in the modern settings around the Mingulay Reef Complex are largely tidal in origin (Davies et al., 2009; Inall et al., 2009). Furthermore, the current strength and direction are enhanced and re-oriented by the topography of the reef (Davies et al., 2009; Long and Wilson, 2003; Roberts et al., 2005; Roberts et al., 2004). The occurrence of live cold-water coral frameworks, coral rubbles and associated fauna therefore provide suitable substrata for species characteristic of high energy environment such as *Cibicides lobatulus,* which is also the dominant species within the Complex and other attached epifaunal foraminifers including *Rosalina anormala*, *Cibicides refulgens*, *Spirillina vivipara* or again *Textularia sagittula* (Murray, 1991b; Murray, 2004a; Murray, 2006; Rüggeberg et al., 2007; Schönfeld, 2002a; Schönfeld, 2002b). The species *Trifarina angulosa,* characteristic of environment dominated by strong current and coarse sediment substratum are also well represented (Harloff and Mackensen, 1997; Murray, 1991b; Murray, 2006).

However, the relative patchiness of the available hard substrata relative to softer/finer silisiclastic sediment zone is also revealed by the relatively high occurrence of the species *Bulimina marginata*, *Hyalinea balthica*, *Melonis barleeanus* and *Stainforthia fusiformis* which are commonly found in surface soft sediments (Murray, 2003). The inherent patchiness of these environments may partly explain why there is no significant variability in benthic species assemblages downcore and why there are so few distinctions between the different facies considered (coral-rich layers, sediment-rich layers and shelly-coral hash layers). Thus, the species such as *Hyalina balthica, Bulimina spp.*, *Melonis barleeanus* and *Cassidulina spp.* identified as off-mound species (Margreth et al., 2009), and species such as *Cibicides lobatulus* and *Bolivina sp.* identified as occurring preferentially on live coral facies (Margreth et al., 2009; Schönfeld, 2002a; Schönfeld, 2002b), cannot be distinguished from one substrata to another as they may co-exist in the layers we considered.

Within the Mingulay Reef Complex, the high availability of organic matter characterizing cold-water coral mounds area seems confirmed by our foraminifer assemblage (Kiriakoulakis et al., 2007). Indeed, the species *Bulimina marginata* is commonly found in area of high food availability (Jorissen et al., 1992; Murray, 2003; Murray, 2006). Other species such as *Miliolinella subrotunda* or *Cassidulina laeviga* are also found in areas of moderate to high organic flux (Altenbach et al., 1993; Altenbach et al., 1999).

Although we observed significant changes in accumulation rates and coral preservation (chapter 3 and chapter 4), our study of benthic foraminifera assemblages shows no significant changes during the period of study. We attribute this to the inherent patchiness of these reef settings where a variety of substrates are found within a small area. Our results suggest that the benthic assemblages do not reveal hydrological changes.

7.6.2 Sea surface hydrological signal

Presently, Mingulay Reef Complex sea surface temperatures (SST) and salinities (SSS) between 0 and 50 m, from April to June, which is the most likely depth and season of *G. bulloides* occurrence around this area, are of 8.5 to 12°C and 34.95 to 35.15 psu, respectively (Ganssen and Kroon, 2000; Levitus and Boyer, 1994). If we assume a constant salinity of 35.1 psu over the studied period, the temperature variability in Mingulay recorded from downcore *G. bulloides* $\delta^{18}O$ values would vary from 9 to 14.5 °C (Austin et al., 2006; Bemis et al., 1998). This is a very large range of temperature variability for the Holocene period. Thus, we assume that the shifts in *G. bulloides* $\delta^{18}O$ most likely reflect a combination of changes in SST and SSS.

In an effort to explain the *G. bulloides* $\delta^{18}O$ range of values in Mingulay, our records were compared with published North Atlantic *G. bulloides* $\delta^{18}O$ measurements performed from other localities influenced by the NAC (Figure 7- **5**). Cores NA87-22 (55°30'N, 14°42'W) (Duplessy et al., 1992) shows *G. bulloides* $\delta^{18}O$ values oscillating from 0.9 to 1.5 ‰ and core RAPiD-12-1K (62°05'N, 17°49'W) (Thornalley et al., 2009) exhibits values varying between 1.3 and 1.7 ‰ over the entire Holocene. By comparison, the Mingulay Reef Complex *G. bulloides* $\delta^{18}O$ values are more enriched from 1 to 2.1 ‰ (Figure 7- 1 and Figure 7- **5**) reflecting either the presence of colder SST and/or higher SSS.

The *G. bulloides* $\delta^{18}O$ range of values highlight distinct salinity/temperature gradient within the three locations considered. The enriched *G. bulloides* $\delta^{18}O$ values observed in core RAPiD-12-1K relative to NA87-22 can be explained by its more northerly location, where colder SSTs are expected. Presently, the surface (0 to 50

m) temperature and salinity from April to June where core RAPiD-12-1K was retrieved are on average 2°C and 0.2 psu lower than where core NA87-22 was collected (Levitus and Boyer, 1994) (Figure 7- 6). This suggests a stronger influence of fresher and cooler waters from the polar front to RAPiD-12-1K core site. The enriched *G. bulloides* $\delta^{18}O$ values recorded from core RAPiD-12-1K compared to core NA87-22 can be simply explained by a temperature gradient in between the two areas.

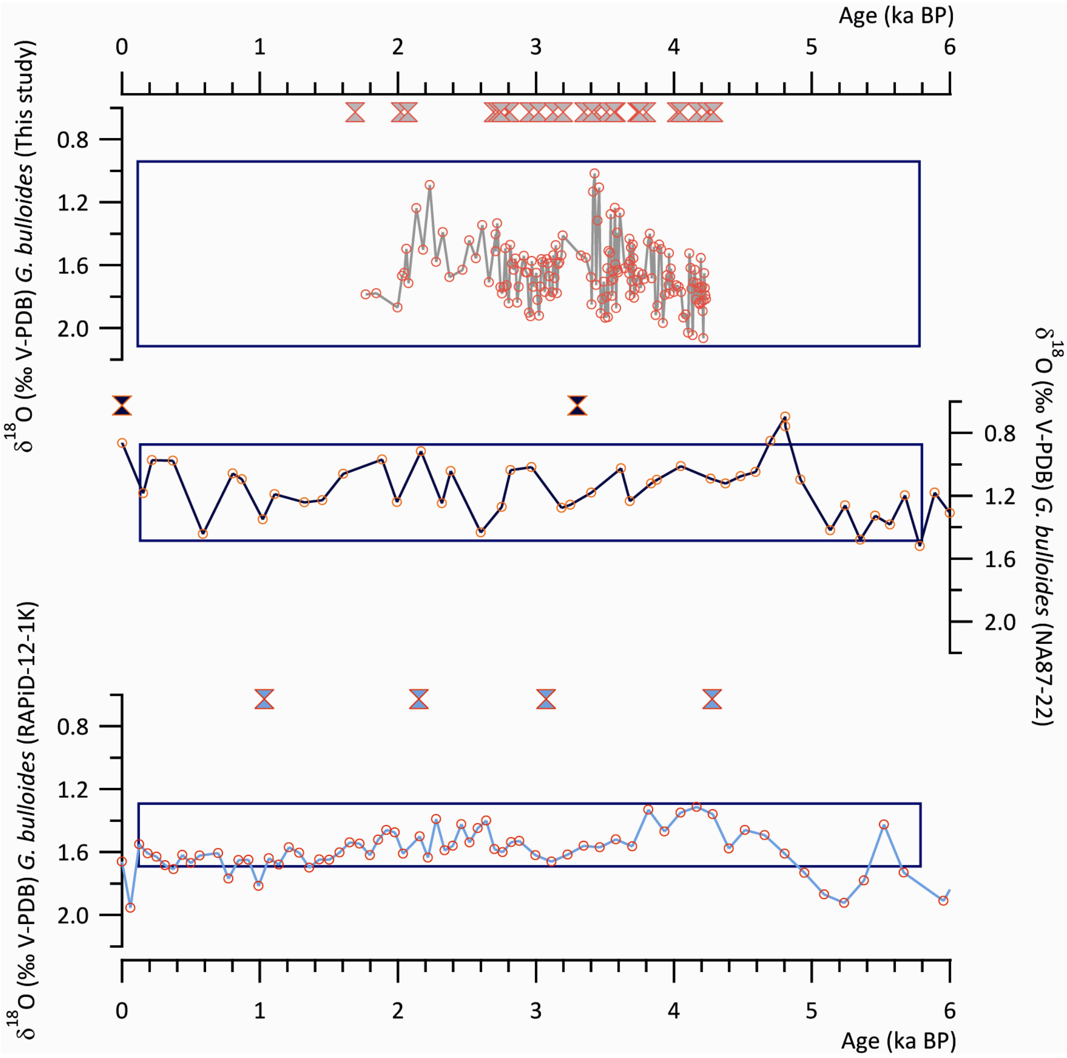

Figure 7- 5: Comparison of *G. bulloides* $\delta^{18}O$ records from Mingulay Reef Complex sediment cores (this study), core NA87-22 (Duplessy et al., 1992) and core RAPiD-12-1K (Thornalley et al., 2009). The hourglass symbols on top of each graphic represent the age constrain of each record, establish from foraminifer radiocarbon ages for core NA87-22 and core RAPiD-12-1K and cold-water coral U-series ages for Mingulay Reef Complex cores. The blue square represent the $\delta^{18}O$ range for the period comprise between 1.7 and 4.2 kyr BP.

Mingulay Reef Complex sediment cores and core NA87-22 are located at similar latitudes. Therefore, one would expect the same averaged *G. bulloides* $\delta^{18}O$ values for the two locations. However, in Mingulay Reef Complex the *G. bulloides* $\delta^{18}O$ values are on average 0.4 ‰ heavier than in core NA87-22 between 1.7 and 4.2 ka BP. From April to June, the SST and SSS (between 0 and 60 m below the surface) of the shallow cold-water coral reef system are presently about 2°C and 0.3 psu lower than where core NA87-22 was collected (Levitus and Boyer, 1994) (Figure 7-6). The Mingulay Reef Complex is therefore dominated by fresher and cooler surface waters. Along the western coast of Scotland, the surface Scottish Coastal Current (SCC) transports cold and fresh waters northwards from the Irish Sea and Clyde Sea (Ellett and Edwards, 1983). Thus, we can hypothesise that this current has had a significant influence on the *G. bulloides* $\delta^{18}O$ values. However, according to Austin et al. (2006) regional salinity vs. $\delta^{18}O_{sw}$ equation, the salinity difference between the two sites would only affect the $\delta^{18}O_{sw}$ by 0.05 ‰.

Thus, we could assume that the temperature difference between the two study sites is the major cause of such enriched *G. bulloides* $\delta^{18}O$ values in Mingulay. Strong SPG influence would also contribute to reducing the northward penetration of STG waters that flow along the continental shelf and the Mingulay Reef Complex area. Therefore the influence of the SCC would be relatively stronger (Ascough et al., 2009; Colin et al., 2010; Inall et al., 2009). Thus, it could be hypothesized that high SPG influence associated with a higher influence of colder SCC inflow to the Mingulay area would produce even more enriched *G. bulloides* $\delta^{18}O$ values. Conversely, during reduced SPG influence, the STG water would dominate and the SCC influence would be significantly reduced thereby depleting *G. bulloides* in $\delta^{18}O$, with expected values more comparable to those measured in site NA87-22. The enhanced $\delta^{18}O$ signal induced by the changing influence of the SCC in response to the SPG strength, make the Mingulay Reef Complex a very unique area to document Holocene low amplitude and short time scale hydrological changes from foraminifer isotopes. One possibility to distinguish these different interpretations would be to perform Mg/Ca measurement on *G. bulloides* from our cores to confirm our hypothesis.

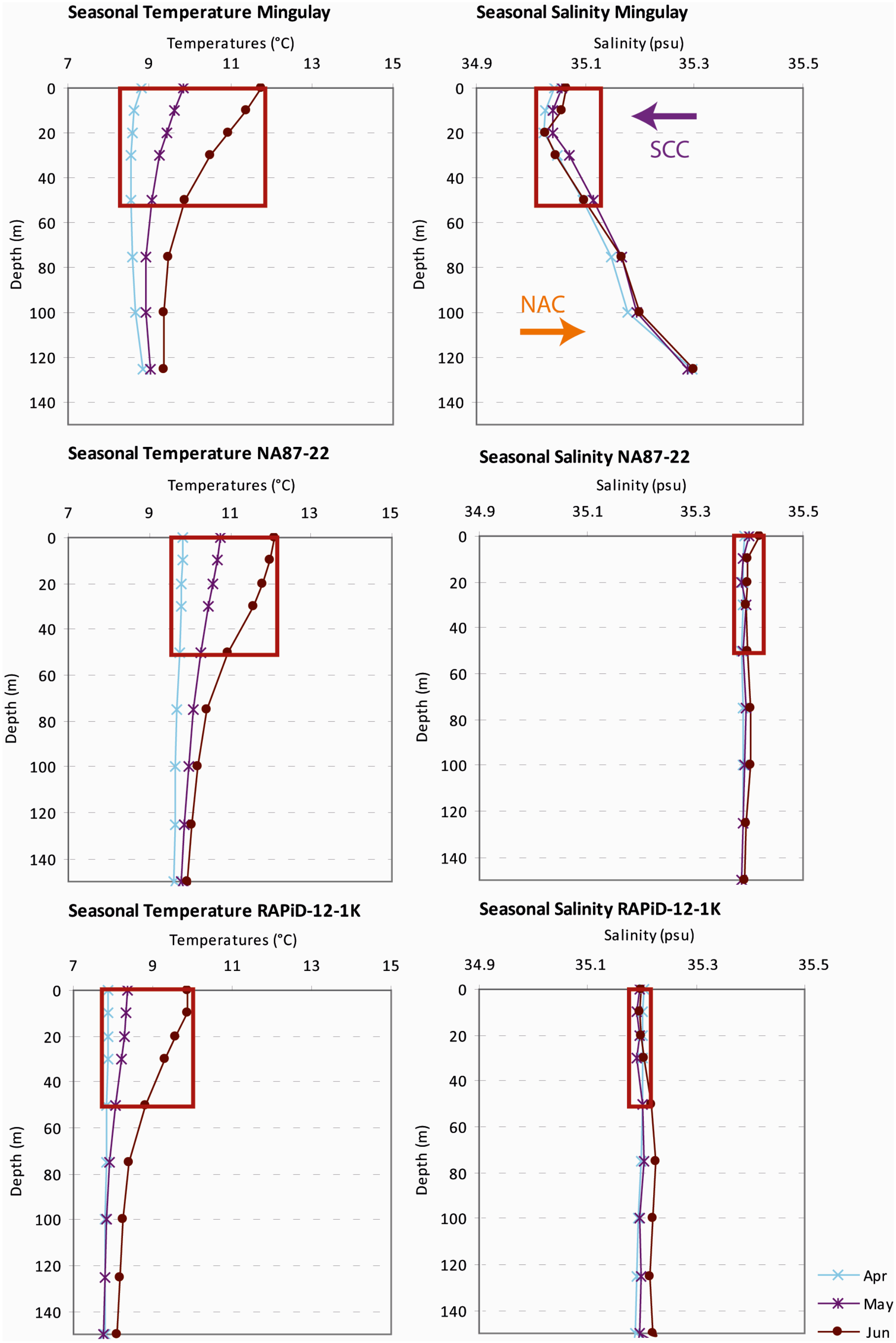

Figure 7- 6: Present, water column temperature and salinity profiles for Arpil (blue), May (purple) and June (brawn) for the 3 locations considered: Mingulay Reef Complex, core NA87-22 and RAPiD-12-1K area. The red square symbolise the ranges of depth, salinity and temperature of *G. bulloides*. The relative influence of the NAC and the SCC within the Mingulay Reef Complex area are symbolised by an orange and purple arrow, respectively.

7.6.3 Coral reef facies and C. lobatulus d13C

C. lobatulus $\delta^{13}C$ profile exhibits significant variability with values oscillating from 1 to 1.8 ‰ (Figure 7- 7). *Cibicidoides* $\delta^{13}C$ is routinely used as a tracer of deep bottom-water masses, typically at water depths of around 2000 meters or more (Curry and Oppo, 2005; Duplessy et al., 1984). However, it is known that other factors such as the incorporation of carbon derived from organic matter or variations in pore water $\delta^{13}C$ may also have a significant impact on benthic foraminifer $\delta^{13}C$ (McCorkle et al., 1997). In our records, depleted *C. lobatulus* $\delta^{13}C$ values appear within shelly coral-hash layers (Figure 7- 4). Such facies were defined in chapter 5 as reflecting high macro-benthic biodiversity (mostly bivalves). High productivity environments, where the organic carbon decomposition rates are enhanced would be reflected in benthic foraminifer shell chemistry, and would induce depleted $\delta^{13}C$ (McCorkle et al., 1997; Zahn et al., 1986). Thus, *C. lobatulus* $\delta^{13}C$ depleted values as recorded in the Mingulay Reef Complex sediment cores would most likely document depleted organic matter induced by an enhanced macro-benthic activity.

The collapse of the cold-water coral framework and the subsequent depositional environment led to the formation of shelly-coral hash layers (Chapter 5). Therefore, as abrupt oceanic shifts have repeatedly affected cold-water coral growth in Mingulay from 1.7 – 4.2 ka BP (Chapter 6), shelly-coral hash layer could be associated with oceanic shifts. The major shelly-coral hash layers documented at 2.75 – 2.85, 3.45, 3.55 ka BP seem relatively well correlated with marine reservoir age changes. However, there are additional thinner shelly-coral hash layers that are also associated with depleted *C. lobatulus* $\delta^{13}C$ which do not appear correlated with any hydrological changes (Figure 7- 7). Therefore, shelly-coral hash layers associated with depleted *C. lobatulus* $\delta^{13}C$ may indirectly be associated with hydrological changes, but not exclusively.

7.6.4 The temporal accuracy of coral reef foraminifer signal

A few studies have compared radiocarbon dates from foraminifera and U/Th dates from corals from the same level of the core. Coral carbonate mounds from the

Celtic margin show that Holocene foraminifera are between 650 and 2 000 years older than the cold-water coral fragments from the same depth (Eisele et al., 2008; Lutringer-Paquet, 2005; Mienis et al., 2009b). Shallow inshore sediment cores from Norwegian coral reef system however exhibit foraminifer ages that can be 260 years younger than the coral fragments from the same sediment layer (López Correa et al., 2012). Mingulay Reef Complex accumulation rates are relatively similar to those recorded in Norway (Chapter 4). Therefore, comparable age offsets between foraminifera and cold-water coal fragments, would make the comparison between the hydrological reconstructions derived from foraminifera and cold-water corals challenging.

Shelly-coral hash layers however, mark a cessation in coral growth, potentially provoked by drastic hydrological changes. Therefore, it could be tempting to use such levels as temporal anchors to discuss the temporal accuracy of the sediment matrix relative to the downcore coral fragments considering that 1) the accumulation of coral rubbles on the seafloor is quickly buried by sediment, which would potential induce a lower age offset between the coral fragments and the sediment matrix, 2) these layers reflect predominantly major oceanic shifts and therefore significant shifts in the foraminifer profiles and 3) the extremely high sedimentation rates and efficient sediment trapping by the coral fragments partly compensate the re-working and mixing characterizing such facies.

Changes in reservoir ages as well as *G. bulloides* $\delta^{18}O$ values reflect changes in the relative influence of the SPG waters and STG waters to the NAC (chapter 6 and section 3.7.2). High reservoir ages and enriched *G. bulloides* $\delta^{18}O$ values reflect a strengthened SPG. By contrast, low reservoir ages and depleted $\delta^{18}O$ values reflect a weakened SPG and a stronger influence of the STG water to our study site. Thus, *G. bulloides* $\delta^{18}O$ profiles could reflect relative changes of the SPG influence to the NAC and be compared with our absolutely dated records of reservoir age changes (Chapter 6).

At 3.45 ka BP within a shelly-coral hash layer the depleted *G. bulloides* $\delta^{18}O$ values suggest an enhanced influence of the STG to the NAC, which are well temporally correlated with a drop of the reservoir ages. However, for the rest of the isotopic signal any correlation with the reservoir age changes would be speculation. It is therefore necessary to conduct foraminifera radiocarbon dating to be able to document short-time scale and amplitude hydrological changes from cold-water coral reef sediment cores.

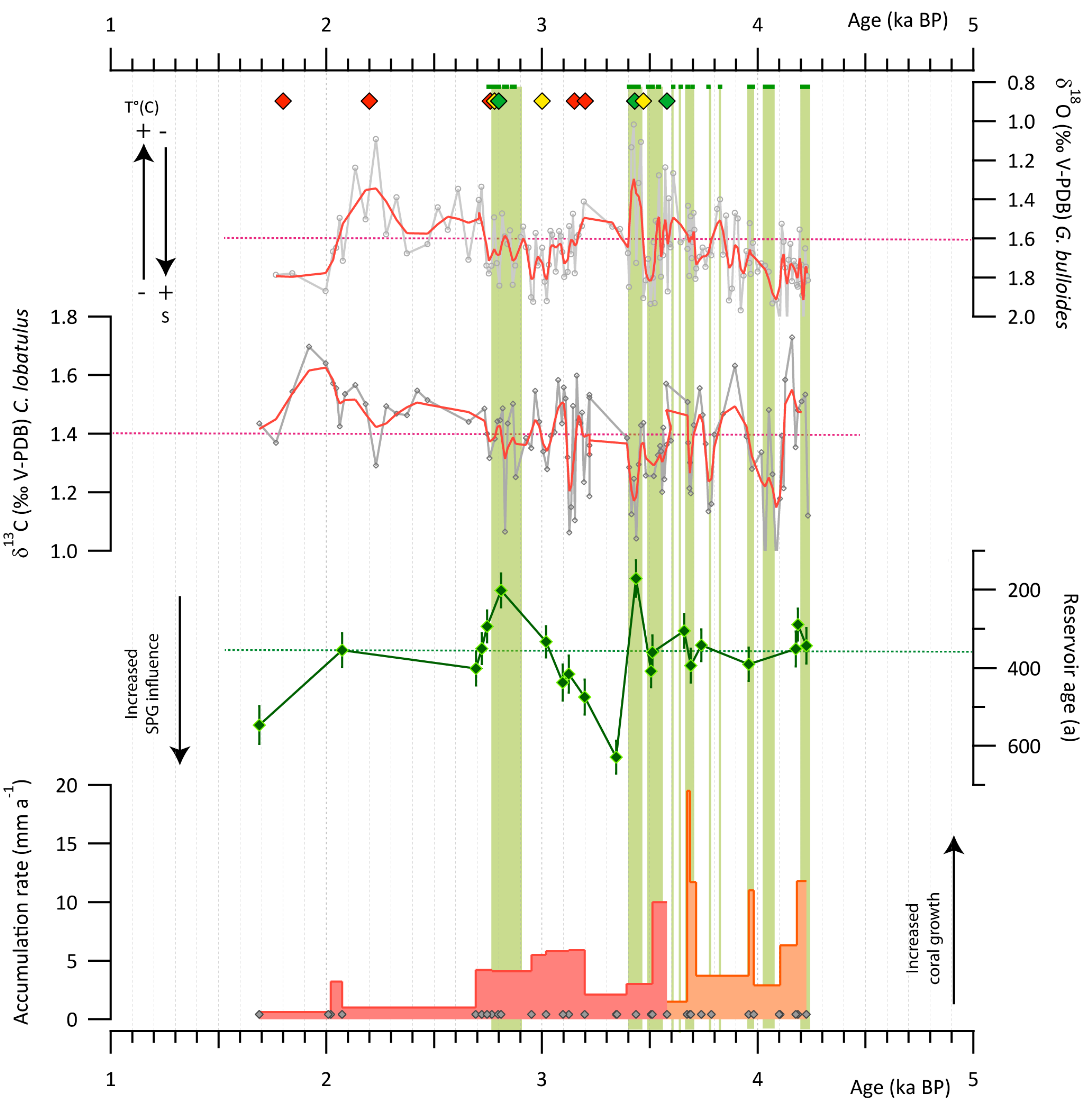

Figure 7- 7: Mingulay Reef Complex accumulation rates and environmental changes provided from reservoir age reconstruction derived from cold-water corals U-series and radiocarbon dating and foraminifera isotopic profiles from cores 929 and 930. Shelly-coral hash facies are represented by green bands. The sediment layers analysed for foraminifer assemblages are reported as red diamonds for coral-rich facies, yellow diamonds for sediment-rich layers and green diamonds for shelly-coral hash facies.

7.7 Conclusions

Changes in the depositional environment shaped cold-water coral reef internal structure (Chapter 5). The distinct layers defined as coral-rich layers, sediment-rich layers and shelly-coral hash layers are associated with different stages of cold-water coral reef framework development and subsequent sedimentological regimes, faunal biodiversity and processes of erosion (Chapter 5). In this chapter we show that the resulting depositional environments are not associated with changes in benthic foraminifer assemblages, suggesting that the different facies do not provide significantly different habitats for benthic foraminiferal communities. We thus conclude that at Mingulay, the benthic foraminifera community are not sensitive enough to small and short lived changes in hydrology.

Downcore benthic foraminifera *C. lobatulus* $\delta^{13}C$ records highlight a series of well defined short lived 0.2 – 0.4 ‰ shifts towards depleted values. Most of these events are associated with the occurrence of shelly coral hash layers. This suggests that the high macro-benthic diversity and resulting enhanced organic carbon decomposition rates characterizing the depositional environment have a significant impact on the *C. lobatulus* $\delta^{13}C$. However, shelly-coral hash layers results from the collapse of coral framework that may be provoked by oceanic shift. Thus depleted benthic $\delta^{13}C$ signal may indirectly highlight hydrological changes.

Downcore planktonic foraminifera *G. bulloides* $\delta^{18}O$ changes vary from 1 to 2.1 ‰ between 1.7 and 4.2 ka BP. We hypothesized that this range of $\delta^{18}O$ is attributable to combined shifts in SST associated with the relative influence of the SCC added to the NAC. Hence, periods of strengthened SPG would favour the surface inflow of colder SCC to the Mingulay area and would produce even more enriched *G. bulloides* $\delta^{18}O$ values. Conversely, during periods of weakened SPG, the enhanced STG water influx into the site added to a significantly reduced SCC inflow would imply depleted isotopic values.

The non-linear age offsets between cold-water coral fragments and the matrix sediment make the comparison between absolute radiocarbon dated reconstructions and foraminifer isotopic profiles challenging. It is therefore necessary to conduct additional radiocarbon dating on foraminifers before conducting any sediment matrix palaeo-environmental reconstruction.

Chapter 8: Conclusions and perspectives

8.1 Foreword

This work has focused on the study of two shallow water vibrocores collected in the Mingulay Reef Complex at around 130 m water depth. These cores contain mixed sediment and cold-water coral fragments and cover the late Holocene from 1.7 to 4.2 ka. This shallow inshore *Lophelia pertusa* reefs system off western Scotland in the Sea of Hebrides (56°50'N; 7°20'W) is characterized by exceptionally high accumulation rates and is bathed by waters from the North Atlantic Current (NAC).

The aims of this study were to: 1) provide a better understanding of cold-water coral reef build-up, 2) document *Lophelia pertusa* temporal and spatial distribution to establish corals as a palaeo-indicator for environmental changes, 3) conduct a detailed reconstruction of hydrological reconstructions with high temporal resolution, 4) explore potential links between rapid oceanic shift and *Lophelia pertusa* performance and, 5) investigate cold-water coral skeleton trace elemental incorporation in view to develop their potential for palaeo-environmental reconstructions.

The following sections summarise the specific conclusions from these five major axes of research. The multi-disciplinary investigation conducted during this project has also shown the value to undertake further investigations. Suggestions and priorities for future research and investigations are therefore addressed.

8.2 Concluding remarks

8.2.1 Coral reef build-up

Successive reef framework-forming *Lophelia pertusa* growth shapes large topographic features such as cold-water coral reefs or coral carbonate mounds. As a result of *L. pertusa* areas being dominated by high current regimes, cold-water coral structure erosion and sedimentation is significantly influenced by the relative occurrence of coral trapping the vertical and lateral flux of sediment.

CT scan images and downcore faunal analysis were performed on the Mingulay Reef Complex sediment cores to reconstruct and quantify the relative contribution and preservation of coral fragments in the cores. Three distinct reef facies representative of singular depositional environments were identified: coral-rich layers, sediment-rich layers and shelly-coral hash layers. Coral rich layers represent extensive growth of a *Lophelia pertusa* framework under favorable environmental conditions followed by its collapse. Shelly-coral hash layers reflect a high benthic biodiversity and mechanical erosion due to the absence of coral framework acting as a physical barrier against the strong currents characterizing the area. Finally the sediment-rich layers indicate a depositional environment relatively protected from currents, likely due to the presence of coral framework and allowing the deposition of sediment. The successive sequences of these facies characterized by distinct biodiversity, sedimentological regimes and erosional processes suggests cyclic depositional environment driving cold-water coral reef build-up (Chapter 5).

Analyses of Mingulay Reef Complex downcore benthic foraminifer assemblages were performed to document environmental changes associated with the distinct cold-water coral reef facies. The Complex is defined by very high benthic foraminifer diversity with more than 100 species identified. The dominant species confirm strong bottom current, high food availability and patchwork substrates characterizing the area. However, the distinct coral/sediment core layers are not associated with statistically different foraminifer communities. The sensitivity of the benthic foraminifer assemblages reconstructed in this study is insufficient to confirm if hydrological changes are associated with the distinct cold-water coral reef facies (Chapter 8).

Downcore measurements of benthic foraminifer carbon ($\delta^{13}C$) isotopes were also performed to document hydrological changes associated with cold-water coral reef facies. Depleted $\delta^{13}C$ in the epibenthic *C. lobatulus* appears to be systematically associated with shelly coral-hash layers. It is suggested that the enhanced organic carbon decomposition rates associated with the high benthic community characterising such facies would be the predominant processes influencing *C. lobatulus* $\delta^{13}C$ composition. The comparison of the isotope data with absolute dated reservoir age reconstruction and reef accumulation rate estimation suggests that the occurrence of shelly coral-hash layers could be associated with some of the observed shift in ocean circulation (Chapter 8).

Mingulay Reef Complex sediment cores were intensively U-series dated to establish the chronology of the Complex reef build-up. The 39 analyses of *Lophelia pertusa* fragments highlights that the cycles of reef development, disturbance and recovery occur within about 100 yrs (Chapter 4 and Chapter 5).

8.2.2 *Lophelia sp.* spatial and temporal occurrence

The factors that may influence the growth, abundance and distribution of reef framework-forming scleractinian *Lophelia pertus*a are water mass properties, food supply, current strength, planula recruitment. As part of the efforts to document periods of active *Lophelia pertus*a framework expansion, researchers have begun to quantify cold-water coral structure accumulation rates.

High frequency (at least one date every 100 yrs) downcore U-series dating of *Lophelia pertusa* fragments were performed to examine variations in coral reef accumulation rates between 1.7 and 4.2 ka. The Mingulay Reef Complex accumulation rates averaged 3 – 4 mm a^{-1} and can reach up to 12 mm a^{-1}. The growth of the complex was punctuated by four phases of reduction/interruption at: 1.70 – 2.8 ka, 3.2 – 3.6 ka, 3.8 – 4 ka and 4.2 ka, indicative of unfavorable periods for coral growth and reef expansion. Additionally, surface *Lophelia pertusa* samples were radiocarbon dated to highlight their temporal occurrence within the entire reef. From the 60 dates acquired so far there is no evidence of coral growth from 1.4 ka until present (pre-bomb), when environmental conditions appear conductive for *Lophelia pertusa* growth (Chapter 4).

A review of all NE Atlantic *Lophelia pertusa* dated and cold-water coral structures accumulation rates were performed to test regional changes in *Lophelia pertusa* occurrence and growth. We observed that shallow cold-water coral reef systems, and the Mingluay Reef Complex in particular, present significantly higher accumulation rates than coral carbonate mounds. Our study highlights that the Holocene, and especially at 2 – 5 ka and 8 – 11 ka, was a remarkable period for *Lophelia pertusa* growth in this region. Holocene coral structure accumulation rates seem to respond synchronously over a wide region and therefore could respond to large-scale shifts in palaeo-environmental regimes (Chapter 4).

8.2.3 Holocene climate reconstructions

The documentation of short-millennial time scale and small amplitude oceanic circulation changes such as those occurring during the Holocene are limited by the accuracy, time resolution and chronology of sediment cores archives. In the North Atlantic, the surface limb of the AMOC, the NAC, composition, strength and location has varied in response to the relative influence of Sub-Polar Gyre waters (SPG; radiocarbon depleted, fresher and cooler) influence to the NAC relative to the Sub-Tropical Gyre (STG; radiocarbon enriched, saltier and warmer).

Centennially resolved marine radiocarbon ($\Delta^{14}C$) variability and associated reservoir ages changes between 1.7 and 4.2 ka BP were reconstructed from downcore paired U-series and ^{14}C dating preformed on cold-water coral fragments. Mingulay Reef Complex sub-surface water exhibits high amplitude $\Delta^{14}C$ changes over the period considered. From 2.1 to 2.7 ka BP and 3.5 to 4.2 ka BP, the $\Delta^{14}C$ values recorded at Mingulay follow the marine international average (Reimer et al., 2009) indicative of modern-like and relative stable AMOC. The corresponding reservoir ages centred at 350 yrs confirmed a major influence of the NAC in the region. The $\Delta^{14}C$ values recorded in Mingulay deviate however, significantly from the marine international standard (Reimer et al., 2009) at 1.7 ka BP, and between 2.7 and 3.5 ka BP. For the last period our results suggest significant AMOC changes over 800 years following a perturbation occurring 3.5 ka BP. Thus, our study highlights that substantial, abrupt modification of the NAC composition in response to the SPG influence changes has occurred during the Holocene. The corresponding reservoir age changes from 170 to 630 yrs between 2.7 and 3.5 ka BP highlight the need to better define Holocene short term reservoir age changes associated with abrupt oceanic shifts for better temporal resolution for marine records relying on radiocarbon ages.

In this study it is proposed a "$\Delta\Delta^{14}C$" index generated from the existing $\Delta^{14}C$ residual and ΔTotal Solar Irradiance (TSI) based on the cosmogenic ^{10}Be measured in ice core datasets (Reimer et al., 2004; Steinhilber et al., 2009). Both proxies are usually seen as solar output indicators as they simulate the cosmic radiation. However, the $\Delta^{14}C$ residual reflect also the relative $\Delta^{14}C_{atm}$ up-taken throughout deep-water formation. Thus, to highlight the relative proportion of deep-water formation changes the $\Delta^{14}C$ residual dataset was normalized and subtracted from the ΔTSI. Over the period from 1.7 to 4.2 ka BP, the sub-surface NAC composition variability recorded from *Lophelia pertusa* $\Delta^{14}C$ correlates with the relative changes in the "$\Delta\Delta^{14}C$" index suggesting that changes in the NAC composition have influenced the deep-water formation. Thus, such a proxy could be used as a palaeo-indicator of AMOC variability and thus global abrupt climate changes during the Holocene.

Downcore planktonic foraminifer oxygen isotopic profiles were reconstructed in this study to reveal short-time scale and low amplitude hydrological changes from 1.7 to 4.2 ka BP. *G. bulloides* $\delta^{18}O$ exhibits a wide range of variability highlighting significant hydrological changes over the period considered. It is hypothesised that enhanced $\delta^{18}O$ signal induced by the increased influence of the cold SCC water during strengthened SPG makes the Mingulay Reef Complex an unique area to document Holocene low amplitude and short time scale hydrological changes from foraminifer isotopes. However, significant age offsets between the cold-water fragments and the matrix sediments seem to bias the foraminifer isotopic signal toward younger ages relative to the absolute dated cold-water coral fragments (Chapter 8).

8.2.4 *L. pertusa* responses to oceanic shifts

Cold-water corals have a worldwide distribution and are presently found across a wide range of environment settings. Thus, cold-water corals should be able to adapt to relatively slow environmental changes. However, the performance of such long-lived and immobile ecosystems would be significantly affected by abrupt climatic changes causing local reduction of cold-water coral occurrence and their potential disappearance.

Accumulation rates changes and centennially resolved marine radiocarbon ($\Delta^{14}C$) reconstruction acquired from Mingulay Reef Complex sediment cores were compared to test if abrupt oceanic shift occurring during the Holocene would have caused *Lophelia pertusa* decline within the area. The reduced expansion of the Mingulay Reef Complex centred at 3.5, 2.8 and 1.6 ka BP appears directly associated with abrupt shifts in the NAC and AMOC. The sub-surface circulation regime shifts have repeatedly weakened Mingulay Reef Complex cold-water coral growth till the total disappearance of the ecosystem 1.4 ka BP, but also likely across the wider northern European margin. A synthesis of all *Lophelia pertusa* ages in the North Atlantic suggest that factors responsible for the reduction in growth in Mingulay also affected reef growth in other localities. Therefore, *Lophelia pertusa* temporal and spatial distribution can be established as a palaeo-indicator for environmental changes. *Lophelia pertusa* occurrence has resumed in Mingulay recently sometime during the past 400 years. Results from this study raise a fundamental question: With the increasing probability of abrupt changes in the AMOC strength could this lead to significant damage or cause a mortality event in Mingualy similar to those recorded in the past?

8.3 Future projects

8.3.1 Palaeo-environmental reconstructions

The Mingulay Reef Complex is bathed by the surface limb of the AMOC, the NAC. The high accumulation rates of this shallow (72 - 215 m) reef system are ideally suitable to document small amplitude and rapid changes of North Atlantic surface circulation. The coral/sediment cores analyzed during this study have allowed high temporal resolution palaeo-environmental reconstructions from 1.7 to 4.2 ka BP. Collecting other coral/sediment cores extending further back in time but also off-reef would be of significant interest for the following reason:

1) Providing a continuous and absolute dated short-time scale and amplitude marine radiocarbon reconstructions from *Lophelia pertusa* to document Holocene ocean circulation changes directly comparable with ice-cores atmospheric datasets.

2) Documenting *Lophelia pertusa* response to oceanic changes and establishing corals as a palaeo-indicator for environmental changes toward the Holocene from downcores and surface *Lophelia pertusa* dating. Off-mound sediment cores, which will have received downslope deposits containing fragments of corals

transported from the living reef, could also be collected to provide further indication of the temporal occurrence of the species within the Mingulay Reef Area.

3) Obtaining complementary information on what would have affected cold-water coral reef expansion from off-reef sediment core analyses.

For the future, projects have already been proposed to further investigate the area and extend back in time some of the axes of research conducted during this PhD project.

This multi-disciplinary study also raises a certain number of questions that need to be address:

1) What would be the main causes of *Lophelia pertusa* weakening and/or disappearance: water mass properties, food supply, current strength, planula recruitment?

2) What are the mechanisms allowing *Lophelia pertusa* to re-colonise an area after disturbance?

8.3.2 Proxy development

Coral-water corals have great potential for high-resolution ocean chemistry reconstructions. However, limited understanding of corals processes of bio-mineralization makes their use for palaeo-environmental reconstructions challenging.

During this project high-resolution profiles were conducted using Secondary Ion Mass Spectrometer (SIMS) to document trace elements variability and reproducibility within *Lophelia perstua* skeleton and to make accurate correspondence between coral's microstructures and trace/minor ratios composition. The results presented in Appendix 3 show that Li/Ca and Mg/Ca ratios present significantly different elementary characteristics, which do not seem to be the case of Sr/Ca and B/Ca ratio. Within the sclerodermites, a good reproducibility between the 4 profiles is observed for Li/Ca, Mg/Ca, B/Ca and the "EMZ-like" present often relatively high values comparing to the band zones within the sclerodermites but to necessary the highest values. Trace elements variability within coral skeleton could be affected by several factors such as: temperature, salinity, vital effects, growth rate, productivity, for example. It has been suggested that the Li/Mg ratio would be temperature dependant, for now our study do not concur this hypothesis for *Lophelia pertusa*, but further work need to be conducted.

However, in the restricted period allocated to this project I did not manage complete my investigation. Further works involving additional laser ablation trace element profiles performed in the same coral sample SIMS's analysed have already been implemented, but by the time I was writing my thesis the data was not available.

References

A

Adkins, J.F., 2001. Dating-Vive la difference. Science, 294: 1844-1845.

Adkins, J.F. and Boyle, E.A., 1997. Changing Atmospheric $\Delta^{14}C$ and the Record of Deep Water Paleoventilation Ages. Paleoceanography, 12(3): 337-344.

Adkins, J.F., Boyle, E.A., Curry, W.B. and Lutringer, A., 2003. Stable isotopes in deep-sea corals and a new mechanism for "vital effects". Geochim. Cosmochim, Acta 67: 1129–1143.

Adkins, J.F., Cheng, H., Boyle, E.A., Druffel, E.R.M. and Lawrence Edwards, R., 1998. Deep-Sea Coral Evidence for Rapid Change in Ventilation of the Deep North Atlantic 15,400 Years Ago. Science, 280(N 5364): 725-728.

Alley, R.B., 2000. The Younger Dryas cold interval as viewed from central Greenland. Quaternary Science Reviews, 19(1-5): 213-226.

Alley, R.B. et al., 2003. Abrupt Climate Change. Science, 299(5615): 2005-2010.

Altenbach, A.V., Heeger, T., Linke, P., Spindler, M. and Thies, A., 1993. Miliolinella subrotunda (Montagu), a miliolid foraminifer building large detritic tubes for a temporary epibenthic lifestyle. Marine Micropaleontology, 20(3-4): 293-301.

Altenbach, A.V. et al., 1999. Scaling percentages and distributional patterns of benthic Foraminifera with flux rates of organic carbon. The Journal of Foraminiferal Research, 29(3): 173-185.

Andersen, M.B. et al., 2008. High-precision U-series measurements of more than 500,000 year old fossil corals. Earth and Planetary Science Letters, 265(1-2): 229-245.

Ascough, P.L., Cook, G.T. and Dugmore, A.J., 2009. North Atlantic marine 14C reservoir effects: Implications for late-Holocene chronological studies. Quaternary Geochronology, 4: 171-180.

Ascough, P.L., Cook, G.T., Dugmore, A.J., Scott, E.M., 2007. The North Atlantic marine reservoir effect in the Early Holocene: implications for defining and understanding MRE values. Nuclear Instruments and Methods in Physics Research, Section B 259 (1), 438–447.

Ascough, P.L., Cook, G.T., Church, M.J., Dugmore, A.J., Arge, S.V., McGovern, T.H., 2006. Variability in North Atlantic marine radiocarbon reservoir effects at c.1000 AD. The Holocene 16 (1), 131–136

Ascough, P.L., Cook, G.T., Dugmore, A.J., Scott, E.M., Freeman, S.P.H.T., 2005. Influence of mollusc species on marine DR determinations. Radiocarbon 47 (3), 433–440.

Ascough, P.L. et al., 2004. Holocene variations in the Scottish marine radiocarbon reservoir effect. Radiocarbon, 46(2): 611-620.

Austin, W.E.N., Cage, A.G. and Scourse, J.D., 2006. Mid-latitude shelf seas: a NW European perspective on the seasonal dynamics of temperature, salinity and oxygen isotopes. The Holocene, 16(7): 937-947.

Austin, W.E.N. and Kroon, D., 1996. Late glacial sedimentology, foraminifera and stable isotope stratigraphy of the Hebridean Continental Shelf, northwest Scotland. Geological Society, London, Special Publications, 111(1): 187-213.

B

Bemis, B.E., Spero, H.J., Bijma, J. and Lea, D.W., 1998. Reevaluation of the oxygen isotopic composition of planktonic foraminifera: experimental results and revised paleotemperature equations. Paleoceanography, 13(150-160).

Berger, A.L., 1978. Long-Term Variations of Daily Insolation and Quaternary Climatic Changes. Journal of the Atmospheric Sciences, 35(12): 2362-2367.

Berger, A., Loutre, M.F., 1991. Insolation values for the climate of the last 10 million years. Quaternary Science Reviews 10, 297–317.

Blamart, D., Cuif, J.-P. and Juillet-Leclerc, A., 2002. O-stable isotopes distribution in deep-sea corals from SIMS measurements. Abstract EGS02-A-01713 presented at 27th General Assembly of the European Geophysical Society, Nice, France, 21 –26 April.

Blamart, D., Rollion-Bard, C., Cuif, J.-P., Juillet-Leclerc, A. and Dauphin, Y., 2007. Correlation of boron isotopic composition with ultrastructure in the deep-sea coral Lophelia pertusa: Implications for biomineralization and paleo-pH Geochemistry Geophysics Geosystems, 8(12): 1-11.

Blamart, D. et al., 2005. C and O Isotopes in a Deep-Sea Scleractinian Coral (Lophelia Pertusa) Related to Skeletal Microstructure. In: A. Freiwald and J.M. Roberts (Editors), Cold-water Corals and Ecosystems. Springer, Berlin-Heidelberg, pp. 1005-1020.

Bond, G. et al., 2001. Persistent Solar Influence on North Atlantic Climate During the Holocene. Science, 294(5549): 2130-2136.

Bond, G. et al., 1997. A Pervasive Millennial-Scale Cycle in North Atlantic Holocene and Glacial Climates Science, 278: 1256-1266.

Broecker, W.S., 1987. Unpleasant surprises in the greenhouse? Nature, 328(6126): 123-126.

Broecker, W.S., Gerard, R., Ewing, M. and Heezen, B.C., 1960. Natural Radiocarbon in the Atlantic Ocean. J. Geophys. Res., 65(9): 2903-2931.

Bronk Ramsey, C., 2009. Bayesian analysis of radiocarbon dates. Radiocarbon, 51(N1): 337-360.

Burke, A. and Robinson, L.F., 2012. The Southern Ocean's Role in Carbon Exchange During the Last Deglaciation. Science, 335(6068): 557-561.

Butzin, M., Prange, M. and Lohmann, G., 2005. Radiocarbon simulations for the glacial ocean: The effects of wind stress, Southern Ocean sea ice and Heinrich events. Earth and Planetary Science Letters, 235(1-2): 45-61.

C

Cairns, S., 1984. New records of ahermatypic corals (Scleractinia) from Hawaiian and Line Island. Occas. Pap. Bishop Mus., 25 (10): 1-30.

Cairns, S., 2007. Deep-water corals: an overview with special reference to diversity and distribution of deep-water scleractinian corlas. Bulletin of Marine Science, 81(3): 311-322.

Cairns, S. and Stanley, J.D., 1981. Ahermatypic coral banks: living and fossil counterparts. Proceedings of the Fourth International Coral Reef Symposium, Manila, 1: 611-618.

Cairns, S.D., 1981. Marine Flora and Fauna of the Northeastern United States. Scleractinia. NOAA Technical Report NMFS Circular 438.

Case, D.H., Robinson, L.F., Auro, M.E. and Gagnon, A.C., 2010. Environmental and biological controls on Mg and Li in deep-sea scleractinian corals. Earth and Planetary Science Letters, 300(3-4): 215-225.

Chen, J.H., Edwards, R.L. and Wasserburg, G.J., 1986. 238U, 234U and 232Th in seawater. Earth Planet. Sci. Lett, 80: 241-251.

Cheng, H., Adkins, J.F., Lawrence Edwards, R. and Boyle, E.A., 2000a. U-Th dating of deep-sea corals. Geochimica et Cosmochimica Acta, 64(N14): 2401-2416.

Cheng, H. et al., 2000b. The half-lives of uranium-234 and thorium-230. Chemical Geology, 169: 17-33.

Clark, P.U., Pisias, N.G., Stocker, T.F. and Weaver, A.J., 2002. The role of the thermohaline circulation in abrupt climate change. Nature, 415(6874): 863-869.

Cohen, A.L., and Gaetani, G.A., Lundälv, T., B.H., C. and George, R.Y., 2006. Compositional variability in a cold-water scleractinian, Lophelia pertusa: New insights into ''vital effects''. Geochemistry Geophysics Geosystems, 7: 1525-2027.

Colin, C., Frank, N., Copard, K. and Douville, E., 2010. Neodymium isotopic composition of deep-sea corals from the NE Atlantic: implications for past hydrological changes during the Holocene. Quaternary Science Reviews, 29(19-20): 2509-2517.

Copard, K. et al., 2010. Nd isotopes in deep-sea corals in the North-eastern Atlantic. Quaternary Science Reviews, 29(19-20): 2499-2508.

Copard, K. et al., 2012. Late Holocene intermediate water variability in the northeastern Atlantic as recorded by deep-sea corals. Earth and Planetary Science Letters, 313-314(0): 34-44.

Craig, R.E., 1959. Hydrography of Scottish coastal waters. Marine Research 1958, 2: 33.

Cuif, J.-P. and Dauphin, Y., 2005. The two-step mode of growth in the scleractinian coral skeletons from the micrometre to the overall scale. Journal of Structural Biology, 150: 319-331.

Cuif, J.-P., Dauphin, Y. and 1998. Microstructural and physico-chemical characterization of "centres of calcification" in septa of some recent Scleractinian corals. Paläont. Zeit., 72: 257–270.

Cuif, J.-P., Dauphin, Y., Doucet, J., Salome, M. and Susini, J., 2003. XANES mapping of organic sulfate in three scleractinian coral skeletons. Geochimica et Cosmochimica Acta, 67: 75-83.

Curry, W.B. and Oppo, D.W., 2005. Glacial water mass geometry and the distribution of $\delta 13C$ of $\Sigma CO2$ in the western Atlantic Ocean. Paleoceanography, 20(1): PA1017.

D

Davies, A.J. et al., 2009. Downwelling and deep-water bottom currents as food supply mechanisms to the cold-water coral Lophelia pertusa (Scleractinia) at the Mingulay Reef complex. Limnology and Oceanography, 54(2): 620-629.

Davies, A.J., Wisshak, M., Orr, J.C. and Murray Roberts, J., 2008. Predicting suitable habitat for the cold-water coral Lophelia pertusa (Scleractinia). Deep Sea Research Part I: Oceanographic Research Papers, 55(8): 1048-1062.

De Haas, H. et al., 2009. Morphology and sedimentology of (clustered) cold-water coral mounds at the south Rockall Trough margins, NE Atlantic Ocean. Facies, 55(1): 1-26.

De Mol, B., Henriet, J.-P., Canals, M., Freiwald, A. and Roberts, J.M., 2005. Development of coral banks in Porcupine Seabight: do they have Mediterranean ancestors?

De Mol, B. et al., 2002. Large deep-water coral banks in the Porcupine Basin, southwest of Ireland. Marine Geology, 188: 193-231.

Delanghe, D., Bard, E. and Hamelin, B., 2002. New TIMS constraints on the uranium-238 and uranium-234 in seawaters from the main ocean basins and the Mediterranean Sea. Marine Chemistry, 80: 79-93.

deMenocal, P.B., 2001. Cultural Responses to Climate Change During the Late Holocene. Science, 292(5517): 667-673.

Denton, G.H. and Karlén, W., 1973. Holocene climatic variationsion: Their pattern and possible cause. Quaternary Research, 3(2): 155-205.

Dodds, L.A., 2007. The ecophysiology of the cold-water coral Lophelia pertusa (Scleractinia), University of Aberdeen, 195 pp.

Dodds, L.A., Roberts, J.M., A.C., T. and Marubini, F., 2007. Metabolic tolerance of the cold-water coral Lophelia pertusa (Scleractinia) to temperature and dissolved oxygen change. Journal of Experimental Marine Biology and Ecology, 349: 205-214.

Dorschel, B., 2003. Late Quaternary Development of a deep-water Carbonate Mound in the northeast Atlantic, der Universitat Bremen, Bremen, 87 pp.

Dorschel, B., Hebbeln, D., Foubert, A., White, M. and Wheeler, A.J., 2007a. Hydrodynamics and cold-water coral facies distribution related to recent sedimentary processes at Galway Mound west of Ireland. Marine Geology, 244(1-4): 184-195.

Dorschel, B., Hebbeln, D., Rüggeberg, A. and Dullo, C., 2007b. Carbonate budget of a cold-water coral carbonate mound: Propeller Mound, Porcupine Seabight. Int J Earth Sci 73-83.

Dorschel, B., Hebbeln, D., Rüggeberg, A., Dullo, W.-C. and Freiwald, A., 2005. Growth and erosion of a cold-water coral covered carbonate mound in the

Northeast Atlantic during the Late Pleistocene and Holocene Earth and Planetary Science Letters, 233(1-2): 33-44.

Douville, E. et al., 2010. Rapid and Accurate U-Th Dating of Ancient Carbonates using Inductively Coupled Plasma-Quadrupole Mass Spectrometry. Chemical Geology, 272(1-4): 1-11.

Duplessy, J.-C. et al., 1984. ^{13}C Record of Benthic Foraminifera in the Last Interglacial Ocean: Implication for the Carbon Cycle and the Global Deep Water Circulation. Quaternry Research, 21: 225-243.

Duplessy, J.C. et al., 1992. Changes in surface salinity of the North Atlantic Ocean during the last deglaciation. Nature, 358(6386): 485-488.

E

Edwards, R.L., Chen, J.H., Ku, T.-L. and Wasserburg, G.J., 1987. Precise timing of the Last Interglacial period from mass spectrometric analysis of 230Th in corals. Science, 236: 1547–1553.

Edwards, R.L., Chen, J.H. and Wasserburg, G.J., 1988. ^{238}U-^{234}U-^{230}Th-^{232}Th systematics and the precise measurement of time over the past 500,000 years. Earth and Planetary Science Letters, 81: 175-192.

Eisele, M. et al., 2011. Productivity controlled cold-water coral growth periods during the last glacial off Mauritania. Marine Geology, 280(1-4): 143-149.

Eisele, M., Hebbeln, D. and Wienberg, C., 2008. Growth history of a cold-water coral covered carbonate mound — Galway Mound, Porcupine Seabight, NE-Atlantic. Marine Geology, 253: 160-169.

Emiliani, C., 1955. Pleistocene Temperatures. The Journal of Geology, 63: 538-578.

F

Frank, N. et al., 2011. Northeastern Atlantic cold-water coral reefs and climate. Geology, 39(8): 743-746.

Frank, N. et al., 2005. Deep-water corals of the notheastern Atlantic margin: carbonate mound evolution and upper intermediate ventilation during the Holocene. Cold-water Corals and Ecosystems, Springer-Verlag Berlin Heidelberg: 113-133.

Frank, N. et al., 2004. Eastern North Atlantic deep-sea corals: tracing upper intermediate water Δ^{14}C during the Holocene. Earth and Planetary Science Letters 219: 297-309.

Frank, N. et al., 2009. The Holocene occurrence of cold water corals in the NE Atlantic: Implications for coral carbonate mound evolution. Marine Geology, 266: 129-142.

Franke, J., Paul, A. and Schulz, M., 2008. Modeling variations of marine reservoir ages during the last 45 000 years. Climate of the Past, 4(2): 125-136.

Frederiksen, R., Jensen, A. and Westerberg, H., 1992a. The distribution of the scleractinian coral Lophelia pertusa around Faroe Islands and the relation to internal tidal mixing. Sarsia, 77: 157-171.

Frederiksen, R., Jensen, A. and Westerberg, H.k., 1992b. The distribution of the scleractinian coral Lophelia pertusa around the Faroe islands and the relation to internal tidal mixing. SARSIA, 77(2): 157-171.

Freiwald, A., 2002. Reef-Forming Cold-Water Corals. Wefer, G. et al. (Ed.) (2002). Ocean margin systems. Springer-Verlag Berlin Heidelberg: 365-385.

Freiwald, A., Fosså, J.H., Grehan, A., Koslow, T. and Roberts, J.M., 2004. Cold-water coral reefs. UNEP-WCMC, Cambridge,.

Freiwald, A. et al., 2005. High-resolution trace and minor element compositions in deep-water scleractinian corals (*Desmophyllum dianthus*) from the Mediterranean Sea and the Great Australian Bight. In: A. Freiwald (Editor), Cold-Water Corals and Ecosystems. Erlangen Earth Conference Series. Springer Berlin Heidelberg, pp. 1109-1126.

Freiwald, A., Wilson, J.B. and Henrich, R., 1999. Grounding Pleistocene icebergs shape recent deep-water coral reefs. Sedimentary Geology, 125(1-2): 1-8.

G

Gass, S.E and Roberts, J.M. The occurrence of the cold-water coral Lophelia pertusa (Scleractinia) on oil and gas platforms in the North Sea: Colony growth, recruitment and environmental controls on distribution, Marine Pollution Bulletin, Volume 52, Issue 5, May 2006, Pages 549-559, ISSN 0025-326X, 10.1016/j.marpolbul.2005.10.002.

Gaetani, G.A. and Cohen, A.L., 2006. Element partitioning during precipitation of aragonite from seawater: A framework for understanding paleoproxies. Geochimica et Cosmochimica Acta, 70(18): 4617-4634.

Gaetani, G.A., Cohen, A.L., Wang, Z. and Crusius, J., 2011. Rayleigh-based, multi-element coral thermometry: A biomineralization approach to developing climate proxies. Geochimica et Cosmochimica Acta, 75(7): 1920-1932.

Gagnon, A.C., Adkins, J.F. and Erez, J., 2012. Seawater transport during coral biomineralization. Earth and Planetary Science Letters, 329-330(0): 150-161.

Gagnon, A.C., Adkins, J.F., Fernandez, D.P. and Robinson, L.F., 2007. Sr/Ca and Mg/Ca vital effects correlated with skeletal architecture in a scleractinian deep-sea coral and the role of Rayleigh fractionation. Earth and Planetary Science Letters, 261: 280-295.

Ganssen, G.M. and Kroon, D., 2000. The isotopic signature of planktonic foraminifera from NE Atlantic surface sediments: implications for the reconstruction of past oceanic conditions. Journal of the Geological Society, 157(3): 693-699.

Genin, A., Dayton, P.K., Lonsdale, P.F. and Spiess, F.N., 1986. Corals on seamount peaks provide evidence of current acceleration over deep-sea topography. Nature, 322(59-61).

Godwin, H., 1962. Half-life of Radiocarbon. Nature, 195(4845): 984-984.

Guinotte, J.M. et al., 2006. Will human-induced changes in seawater chemistry alter the distribution of deep-sea scleractinian corals? Frontiers in Ecology and the Environment, 4(3): 141-146.

H

Häkkinen, S. and Rhines, P.B., 2004. Decline of Subpolar North Atlantic Circulation During the 1990s. Science, 304(5670): 555-559.

Harkness, D.D., 1983. The extent of natural 14C deficiency in the coastal environment of the United Kingdom, Council of Europe.

Harloff, J. and Mackensen, A., 1997. Recent benthic foraminiferal associations and ecology of the Scotia Sea and Argentine Basin. Marine Micropaleontology, 31(1-2): 1-29.

Hátún, H., Sandø, A.B., Drange, H., Hansen, B. and Valdimarsson, H., 2005. Influence of the Atlantic Subpolar Gyre on the Thermohaline Circulation. Science, 309(5742): 1841-1844.

Heikkilä, M. and Seppä, H., 2003. A 11,000 yr palaeotemperature reconstruction from the southern boreal zone in Finland. Quaternary Science Reviews, 22(5-7): 541-554.

Hemming, N.G. and Hanson, G.N., 1992. Boron isotopic composition and concentration in modern marine carbonates. Geochimica et Cosmochimica Acta, 56(1): 537-543.

Henriet, J.-P. et al., 1998. Gas hydrate crystals may help build reefs. Nature, 391: 648-649.

Henriet, J.-P., De Mol, B., Vanneste, M., Huvenne, V.A.I. and Van Rooij, D., 2001. Carbonate mounds and slope failures in the Porcupine Basin: a development model involving fluid venting. Geological Society, London, Special Publications, 188: 375-383.

Henriet, J.-P. and Guidard, S. (Editors), 2002. ODP "Proposal 573" Team Carbonate mounds as a possible example for microbial activity in geological processes. Ocean Margin Systems. Springer-Verlag, Berlin, 439-455 pp.

Henry, L.-A., Davies, A. and Murray Roberts, J., 2010. Beta diversity of cold-water coral reef communities off western Scotland. Coral Reefs, 29(2): 427-436.

Henry, L.-A. and Roberts, J.M., 2007. Biodiversity and ecological composition of macrobenthos on cold-water coral mounds and adjacent off-mound habitat in the bathyal Porcupine Seabight, NE Atlantic. Deep-Sea Research I, 54: 654-672.

Hiess, J., Condon, D.J., McLean, N, Noble, S.R., 2012. $^{238}U/^{235}U$ systematics in terrestrial uranium-bearing minerals. Science 335, 1610-1614.

Hill, A.E. et al., 1997. Observations of a Density-driven Recirculation of the Scottish Coastal Current in the Minch. Estuarine, Coastal and Shelf Science, 45: 473-484.

Holliday, N.P., 2003. Air-sea interaction and circulation changes in the northeast Atlantic. J. Geophys. Res., 108(C8): 32-59.

Hovland, M., 1990. Do carbonate reefs form due to fluid seepage? Terra Nova, 2: 8-18.

Hovland, M., Croker, P.F. and Martin, M., 1994. Fault-associated seabed mounds (carbonate knolls?) off western Ireland and north-west Australia. Marine and Petroleum Geology, 11(2): 232-246.

Hovland, M., Mortensen, P.B., Brattegard, T., Strass, P. and Rokengen, K., 1998a. Ahermatypic coral banks off mid-Norway; evidence for a link with seepage of light hydrocarbons. PALAIOS, 13(2): 189-200.

Hovland, M., Mortensen, P.B., Brattegard, T., Strass, P. and Rokoengen, K., 1998b. Ahermatypic Coral Banks off Mid-Norway: Evidence for a Link with Seepage of Light Hydrocarbons. PALAIOS, 13: 189-200.

Hovland, M. and Risk, M.J., 2003. Do Norwegian deep-water coral reefs rely on seeping fluids? Marine Geology, 198: 83-96.

Howell, K.L., Holt, R., Endrino, I.s.P. and Stewart, H., 2011. When the species is also a habitat: Comparing the predictively modelled distributions of Lophelia pertusa and the reef habitat it forms. Biological Conservation, 144(11): 2656-2665.

Huvenne, V. et al., 2007. The Magellan mound province in the Porcupine Basin. International Journal of Earth Sciences, 96(1): 85-101.

I

Inall, M., Gillibrand, P., Griffiths, C., MacDougal, N. and Blackwell, K., 2009. On the oceanographic variability of the North-West European Shelf to the West of Scotland. Journal of Marine Systems, 77(3): 210-226.

Ivanovitch, M. and Harmon, R.S. (Editors), 1992. Uranium-series Desequilibrium, and Environmental Sciences, application to earth, marine and environmental Sciences. Oxford University Press.

J

Jansen, E., J. Overpeck, K.R. Briffa, J.-C. Duplessy, F. Joos, V. Masson-Delmotte, D. Olago, B. Otto-Bliesner, W.R. Peltier, S. Rahmstorf, R. Ramesh, D. Raynaud, D. Rind, O. Solomina, R. Villalba and D. Zhang, 2007: Palaeoclimate. In: *Climate Change 2007: The Physical Science Basis. Contribution of Working Group I to the Fourth Assessment Report of the Intergovernmental Panel on Climate Change* [Solomon, S., D. Qin, M. Manning, Z. Chen, M. Marquis, K.B. Averyt, M. Tignor and H.L. Miller (eds.)]. Cambridge University Press, Cambridge, United Kingdom and New York, NY, USA.

Johnsen, S.J., Clausen, H.B., Dansgaard, W., Gundestrup, N.S., Hammer, C.U., Andersen, U., Andersen, K.K., Hvidberg, C.S., Dahl-Jensen, D., Steffensen, J.P. Shoji, H., White, J., Jouzel, J., Fishe, D., 1997. The δ18O record along the Greenland Ice Core Project deep ice core and the problem of possible Eemian climatic instability. J. Geophys. Res. 102, 26,397- 26,410.

Jones, C.G., Lawton, J.H. and Shachak, M., 1994. Organisms as Ecosystem Engineers. Oikos, 69(3): 373-386.

Jorissen, F.J., Barmawidjaja, D.M., Puskaric, S. and van der Zwaan, G.J., 1992. Vertical distribution of benthic foraminifera in the northern Adriatic Sea: The relation with the organic flux. Marine Micropaleontology, 19(1-2): 131-146.

Jorissen, F.J., de Stigter, H.C. and Widmark, J.G.V., 1995. A conceptual model explaining benthic foraminiferal microhabitats. Marine Micropaleontology, 26(1-4): 3-15.

Jorissen, F.J., Fontanier, C., Thomas, E., Claude, H.M. and Anne De, V., 2007. Chapter Seven Paleoceanographical Proxies Based on Deep-Sea Benthic

Foraminiferal Assemblage Characteristics, Developments in Marine Geology. Elsevier, pp. 263-325.

Joseph, N., López Correa, M., Schönfeld, J., Rüggeberg, A. & Freiwald, A. 2012: Sub-arctic Holocene climatic and oceanographic variability in Stjernsund, northern Norway: evidence from benthic foraminifera and stable isotopes. Boreas, 10.1111/j.1502-3885.2012.00303.x. ISSN 0300-9483.

K

Kaufman, D.S. et al., 2004. Holocene thermal maximum in the western Arctic (0 - 180 W). Quaternary Science Reviews, 23(5-6): 529-560.

Kenyon, N.H. et al., 2003. Giant carbonate mud mounds in the southern Rockall Trough. Marine Geology, 195: 5-30.

Kiriakoulakis, K., Freiwald, A., Fischer, E. and Wolff, G.A., 2007. Organic matter quality and supply to deep-water coral/mound systems of the NW European Continental Margin. Int J Earth Sci (Geol Rundsch), 96: 159-170.

Koç, N., Jansen, E., Haflidason, H., 1993. Paleoceanographic reconstructions of surface ocean conditions in the Greenland, Iceland and Norwegian seas through the last 14 ka based on diatoms. Quaternary Science Reviews 12, 115e140.

Kuhlbrodt, T. et al., 2007. On the driving processes of the Atlantic meridional overturning circulation. Rev. Geophys., 45(2): RG2001.

L

Lazier, A.V., Smith, J.E., Risk, M.J. and Schwarcz, H.P., 1999. The skeletal structure of Desmophyllum cristugulli: the use of deepwater corals in sclerochronology. Lethaia, 32: 119-130.

Levitus, S. and Boyer, T., 1994. World Ocean Atlas, Volume 4: Temperature., U.S. Department of Commerce. D.C., Washington, .

Lindberg, B., Bernt, C. and Mienert, J., 2007. The Fugløy Reef at 70N; acoustic signature, geologic, geomorphologicand oceanographic setting. Int J Earth Sci, 96: 201-213.

Lindberg, B. and Mienert, J., 2005. Postglacial carbonate production by cold-water corals on the Norwegian Shelf and their role in the global carbonate budget. Geology, 33: 537-540.

Linnaeus, C., 1958. Systema naturae. 10th edition, I.

Lomitschka, M. and Mangini, A., 1999. Precise Th/U-dating of small and heavily coated samples of deep sea corals. Earth and Planetary Science Letters, 170: 391-401.

Long, D. and Wilson, C.K., 2003. Geological background to cold-water coral occurences in the Minch. Internal report IR/03/149.

López Correa, M. et al., 2012. Preboreal onset of cold-water coral growth beyond the Arctic Circle revealed by coupled radiocarbon and U-series dating and neodymium isotopes. Quaternary Science Reviews(0).

López Correa, M., Montagna, P., Vendrell-Simon, B., McCulloch, M. and Taviani, M., 2010. Stable isotopes (δ18O and δ13C), trace and minor element compositions of Recent scleractinians and Last Glacial bivalves at the Santa Maria di Leuca deep-water coral province, Ionian Sea Deep Sea Research Part II: Topical Studies in Oceanography, 57(5-6): 471-486.

Lozier, M.S. and Stewart, N.M., 2008. On the temporally varying northward penetration of mediterranean overflow water and eastward penetration of Labrador sea water. Journal of Physical Oceanography, 38(9): 2097-2103.

Ludwig, K.R., 2003a. ISOPLOT 3.00: a geochronology toolkit for Microsoft Excel, Berkeley Geochronological Center Special Publication, Berkeley.

Ludwig, K.R., 2003b. Mathematical-Statistical Treatment of Data and Errors for 230Th/U Geochronology. Reviews in Mineralogy and Geochemistry, 52(1): 631-656.

Lutringer-Paquet, A., 2005. Reconstruction de la variabilite des eaux intermediaires par l'etude geochimique des coraux profonds, Universite Paris XI Orsay, Paris, 280 pp.

M

Mangerud, J.A.N., 1972. Radiocarbon dating of marine shells, including a discussion of apparent age of Recent shells from Norway. Boreas, 1(2): 143-172.

Mangini, A., Lomitschka, M., Eichstadter, R., Frank, N. and Vogler, S., 1998. Coral provides way to age deep water. Nature, 392: 347-348.

Margreth, S., Rüggeberg, A. and Spezzaferri, S., 2009. Benthic foraminifera as bioindicator for cold-water coral reef ecosystems along the Irish margin. Deep Sea Research Part I: Oceanographic Research Papers, 56(12): 2216-2234.

Marshall, J. and Schott, F., 1999. Open-ocean convection: Observations, theory, and models. Reviews of Geophysics, 37(1): 1-64.

Mayewski, P.A. et al., 2004. Holocene climate variability. Quaternary Research, 62(3): 243-255.

McConnaughey, T.A., 1989a. 13 C and 18 O isotopic disequilibrium in biological carbonates: I. Patterns. Geochimica et Cosmochimica Acta, 53: 151-162.

McConnaughey, T.A., 1989b. 13C and 18O isotopic disequilibrium in biological carbonates: II. In vitro simulation of kinetic isotope effects. Geochimica et Cosmochimica Acta, 53: 163-171.

McCorkle, D.C., Corliss, B.H. and Farnham, C.A., 1997. Vertical distributions and stable isotopic compositions of live (stained) benthic foraminifera from the North Carolina and California continental margins. Deep Sea Research Part I: Oceanographic Research Papers, 44(6): 983-1024.

McCulloch, M. et al., 2010. Proliferation and demise of deep-sea corals in the Mediterranean during the Younger Dryas. Earth and Planetary Science Letters, 298(1-2): 143-152.

Meeker, L.D. and Mayewski, P.A., 2002. A 1400-year high-resolution record of atmospheric circulation over the North Atlantic and Asia. The Holocene, 12(3): 257-266.

Meibom, A. et al., 2008. Compositional variations at ultra-structure length scales in coral skeleton. Geochimica et Cosmochimica Acta, 72(6): 1555-1569.

Mienis, F., de Stigter, H.C., De Haas, H. and Van Weering, T.C.E., 2009a. Near-bed particle deposition and resuspension in a cold-watercoral mound area at the Southwest Rockall Trough margin, NEAtlantic. Deep-Sea Research I.

Mienis, F. et al., 2007. Hydrodynamic controls on cold-water coral growth and carbonate-mound development at the SW and SE Rockall Trough Margin, NE Atlantic Ocean. Deep-Sea Research I, 54: 1655-1674.

Mienis, F. et al., 2009b. Sediment accumulation on a cold-water carbonate mound at the Southwest Rockall Trough margin. Marine Geology, 265: 40-50.

Mikkelsen, N., Erlenkeuser, H., Killingley, J.S. and Berger, W.H., 1982. Norwegian corals: radiocarbon and stable isotopes in Lophelia pertusa. Boreas, 11(2): 163-171.

Montagna, P. et al., 2008. Coral Li/Ca in micro-structural domains as a temperature proxy, Goldschmidt, Vancouver, Canada.

Montagna, P., McCulloch, M., Taviani, M., Remia, A. and Rouse, G., 2005. High-resolution trace and minor element compositions in deep-water scleractinian corals (Desmophyllum dianthus) from the Mediterranean Sea and the Great

Australian Bright. In: A. Freiwald and J.M. Roberts (Editors), Cold-water Corals and Ecosystems. Springer-Verlag, Berlin Heidelberg, pp. 1109-1126.

Moran, S.B., Hoff, J., Buesseler, K.O. and Edwards, R.L., 1995. High precision 230Th and 232Th in the Norwegian Sea and Denmark by thermal ionization mass spectrometry. Geophys. Res. Lett., 22: 2589-2589.

Mortensen, P. and Rapp, H.T., 1998. Oxygen and carbon isotope ratios related to growth line patterns in skeletons of Lophelia pertusa (L) (Anthozoa, Scleractinia): implications for determination of linear extension rates. SARSIA, 83: 433-446.

Mortensen, P.B., 2001. Aquarium observations on the deep-water coral Lophelia pertusa (L.,1758) (Scleractinia) and selected associated invertebrates. Ophelia, 54(2): 83-104.

Mortensen, P.B., Hovland, M., Brattegard, T. and Farestveit, R., 1995. Deep water bioherms of the scleractinian coral Lophelia pertusa (L.) at 64Â° n on the Norwegian shelf: Structure and associated megafauna. SARSIA, 80(2): 145-158.

Murray, J.W., 1985. Recent Foraminifera from the North Sea (Forties and Ekofisk areas) and the continental shelf west of Scotland J.micropalaeontol., 4(2): 117-125.

Murray, J.W. (Editor), 1991a. Ecology and palaeoecology of benthic foraminifera Longman Scientific & Technical, New York

Murray, J.W. (Editor), 1991b. Ecology and palaeoecology of benthic foraminifera, Harlow.

Murray, J.W., 2000. Revised taxonomy, An Atlas of British Recent Foraminiferids. Journal of Micropalaeontology, 19(1): 44.

Murray, J.W., 2003. FORAMINIFERAL ASSEMBLAGE FORMATION IN DEPOSITIONAL SINKS ON THE CONTINENTAL SHELF WEST OF SCOTLAND. The Journal of Foraminiferal Research, 33(2): 101-121.

Murray, J.W., 2004a. The Holocene palaeoceanographic history of Muck Deep, Hebridean shelf, Scotland: has there been a change of wave climate in the past 12 000 years? Journal of Micropalaeontology 23: 153-161.

Murray, J.W., 2004b. The Holocene palaeoceanographic history of Muck Deep, Hebridean shelf, Scotland: has there been a change of wave climate in the past 12 000 years?

Murray, J.W., 2006. Ecology and Applications of Benthic Foraminifera, New York New, A.L., Barnard, S., Herrmann, P. and Molines, J.M., 2001. On the origin and pathway of the saline inflow to the Nordic Seas: insights from models. Progress In Oceanography, 48(2-3): 255-287.

O

Ogilvie, M.M., 1896. Microscopic and Systematic Study of Madreporarian Types of Corals. Philosophical Transactions of the Royal Society of London. Series B, Containing Papers of a Biological Character, 187: 83-345.

Orejas, C., Gori, A. and Gili, J., 2008. Growth rates of live *Lophelia pertusa* and *Madrepora oculata* from the Mediterranean Sea maintained in aquaria. Coral Reefs, 27(2): 255-255.

Orr, J.C. et al., 2005. Anthropogenic ocean acidification over the twenty-first century and its impact on calcifying organisms. Nature, 437: 681-686.

P

Paillard, D., Labeyrie, L. and Yiou, P., 1996. Macintosh Program performs time-series analysis. Eos Trans. AGU, 77(39): 379-379.

Piepgras, D.J. and Wasserburg, G.J., 1987. Rare earth element transport in the western North Atlantic inferred from Nd isotopic observations. Geochimica et Cosmochimica Acta, 51(5): 1257-1271.

Pirlet, H., Colin, C., Thierens, M., Latruwe, K., Van Rooij, D., Foubert, A., Frank, N., Blamart, D., Huvenne, V.A.I., Swennen, R., Vanhaecke,F.,Henriet, J.-P., 2011. The importance of the terrigenous fraction within a cold-water coral mound: A case study. Marine Geology 282, 13-25.

Pons-Branchu, E., Hillaire-Marcel, C., Deschamps, P., Ghaleb, B. and Sinclair, D.J., 2005. Early diagenesis impact on precise U-series dating of deep-sea corals: Example of a 100–200-year old Lophelia pertusa sample from the northeast Atlantic. Geochimica et Cosmochimica Acta, 69: 4865-4879.

R

Rahmstorf, S., 2002. Ocean circulation and climate during the past 120,000 years. Nature, 419(6903): 207-214.

Reid, J.L., 1979. On the contribution of the Mediterranean Sea outflow to the Norwegian-Greenland Sea. Deep Sea Research Part A. Oceanographic Research Papers, 26(11): 1199-1223.

Reimer, P.J. et al., 2002. Marine radiocarbon reservoir corrections for the mid-to late Holocene in the eastern subpolar North Atlantic. Holocene 12 (2) 129-135.

Reimer, P.J. et al., 2004. Residual delta 14C around 1000 year moving average of IntCal04. Radiocarbon, 46: 1029-1058.

Reimer, P.J. and Reimer, R., 2005 Marine Reservoir Correction database. <radiocarbon.pa.qub.ac.uk>.

Reimer, P.J. et al., 2009. IntCal09 and Marine09 radiocarbon age calibration curves, 0–50,000 years cal BP. Radiocarbon, 5 (4): 1111-1150.

Renssen, H. et al., 2009. The spatial and temporal complexity of the Holocene thermal maximum. Nature Geosci, 2(6): 411-414.

Roberts, J.M., 2005. Reef-aggregating behaviour by symbiotic eunicid polychaetes from cold-water corals:do worms assemble reef? Journal of the Marine Biological Association of he United Kingdom, 85: 813-819.

Roberts, J.M., Brown, C.J., Long, D. and Bates, C.R., 2005. Acoustic mapping using a multibeam echosounder reveals cold-water coral reefs and surrounding habitats. Coral Reefs, 24: 654-669.

Roberts, J.M., Brown, C.J., Long, D., Wilson, C.K. and Bates, C.R., 2004. Final Report: Mapping INshore Coral Habitats the MINCH project.

Roberts, J.M. et al., 2009a. The Mingulay Reef Complex: an interdisciplinary study of cold-water coral habitat, hydrography and biodiversity. Marine Ecology Progress Series, 397: 139-151.

Roberts, J.M., Wheeler, A.J. and Freiwald, A., 2006. Reefs of the Deep: The Biology and Geology of Cold-Water Coral Ecosystems. Science, 312: 543-546.

Roberts, J.M., Wheeler, A.J., Freiwald, A. and Cairns, S. (Editors), 2009b. Cold-Water Corals The Biology and Geology of Deep-sea Coral Habitats. Cambridge Univeristy Press.

Roberts, S. and Hirshfield, M., 2004. Deep-Sea Corals: Out of Sight, but No Longer out of Mind. Frontiers in Ecology and the Environment, 2: 123-130.

Robinson, L.F. et al., 2005. Radiocarbon Variability in the Western North Atlantic During the Last Deglaciation. Science, 310: 1469-1473.

Robinson, L.F., Belshaw, N.S. and Henderson, G.M., 2004. U and Th concentrations and isotope ratios in modern carbonates and waters from the Bahamas. Geochim. Cosmochim, Acta 68: 1777–1789.

Rogers, A.D., 1999. The Biology of Lophelia pertusa (Linnaeus 1758) and Other Deep-Water Reef-Forming Corals and Impacts from Human Activities. Interational Review of Hydrobiology, 84.

Rollion-Bard, C., Blamart, D., Cuif, J.-P. and Dauphin, Y., 2010. In situ measurements of oxygen isotopic composition in deep-sea coral, Lophelia pertusa: Re-examination of the current geochemical models of biomineralisation. Geochimica et Cosmochimica, 74: 1338-1349.

Rollion-Bard, C., Chaussidon, M. and France-Lanord, C., 2003. pH control on oxygen isotopic composition of symbiotic corals. Earth and Planetary Science Letters, 215(1-2): 275-288.

Rollion-Bard, C. et al., 2009. Effect of environmental conditions and skeletal ultrastructure on the Li isotopic composition of scleractinian corals. Earth and Planetary Science Letters, 286(1-2): 63-70.

Rothwell, R.G. and Rack, F.R., 2006. New techniques in sediment core analysis: an introduction. The Geological Society of London 267: 1-29.

Rüggeberg, A., Dullo, C., Dorschel, B. and Hebbeln, D., 2007. Environmental changes and growth history of a cold-water carbonate mound (Propeller Mound, Porcupine Seabight). Int J Earth Sci 96(1): 57-72.

S

Sadvidge, G. and Lennon, H.J., 1987. Hydrography and phytoplancton distributions in Northwest Scottish Waters. Continental shelf research, 7: 45-66.

Schönfeld, J., 2002a. A new benthic foraminiferal proxy for near-bottom current velocities in the Gulf of Cadiz, northeastern Atlantic Ocean. Deep Sea Research Part I: Oceanographic Research Papers, 49(10): 1853-1875.

Schönfeld, J., 2002b. Recent benthic foraminiferal assemblages in deep high-energy environments from the Gulf of Cadiz (Spain). Marine Micropaleontology, 44(3-4): 141-162.

Schönfeld, J. et al., 2011. Recent benthic foraminiferal assemblages from cold-water coral mounds in the Porcupine Seabight. Facies, 57(2): 187-213.

Schröder-Ritzrau, A., Freiwald, A. and Mangini, A., 2005. U/Th-dating of deep-water corals from the estern North Atlantic and the western Mediterranean Sea. Cold-water Corals and Ecosystems, Springer-Verlag Berlin Heidelberg: 157-172.

Schröder-Ritzrau, A., Mangini, A. and Lomitschka, M., 2003. Deep-sea corals evidence periodic reduced ventilation in the North Atlantic during the LGM/Holocene transition. Earth and Planetary Science Letters, 216(3): 399-410.

Shackleton, N.J. et al., 1977. The Oxygen Isotope Stratigraphic Record of the Late Pleistocene [and Discussion]. Philosophical Transactions of the Royal Society of London. B, Biological Sciences, 280(972): 169-182.

Shennan, I., Hamilton, S., Hillier, C. and Woodroffe, S., 2005. A 16 000-year record of near-field relative sea-level changes, northwest Scotland, United Kingdom. Quaternary International 133-134: 95-106.

Shennan, I. and Horton, B., 2002. Holocene land- and sea-level changes in Great Britain. Journal of Quaternary Science 17(5-6): 511-526.

Sinclair, D.J., Williams, B. and Risk, M.J., 2006. A biological origin for climate signals in corals—Trace element ''vital effects'' are ubiquitous in Scleractinian coral skeletons. Geophys. Res. Lett., 33.

Slota, P., Jull, A., Linick, T. and Toolin, L., 1987. Preparation of small samples for 14C accelerator targets by catalytic reduction of CO. Radiocarbon, 29: 303-306.

Smith, J.E., Schwarcz, H.P., Risk, M.J., McConnaughey, T.A. and Keller, N., 2000. Paleotemperatures From Deep-Sea Corals: Overcoming 'Vital Effects'. PALAIOS, 15: 25-32.

Spiro, B., Roberts, J.M., Gage, J. and Chenery, S., 2000. 18O/16O and 13C/12C in an Ahermatypic Deep-Water Coral Lophelia Pertusa from the North Atlantic: A Case of Disequilibrium Isotope Fractionation. Rapid Communications in Mass Spectrometry 14: 1132-1336.

Squires, D.F., 1964. Fossil Coral Thickets in Wairarapa, New Zealand. Journal of Paleontology, 38(5): 904-915.

Steinhilber, F., Beer, J. and Fröhlich, C., 2009. Total solar irradiance during the Holocene. Geophys. Res. Lett., 36(19): L19704.

Stenseth, N.C. et al., 2003. Review article. Studying climate effects on ecology through the use of climate indices: the North Atlantic Oscillation, El Nino Southern Oscillation and beyond. Proceedings of the Royal Society of London. Series B: Biological Sciences, 270(1529): 2087-2096.

Stewart, H.A. and Gatliff, R.W., 2008. Preliminary geological results of sea-bed sampling in the Hebrides area from the RRS James Cook in 2007. Internal report, IR/08/004.

Stuiver, M., Pearson, G.W. and Braziunas, T., 1986. Radiocarbon age calibration of marine samples back to 9000 cal yr BP. Radiocarbon, 28(2): 980-1021.

T

Talley, L.D., 2008. Freshwater transport estimates and the global overturning circulation: Shallow, deep and throughflow components. Progress In Oceanography, 78(4): 257-303.

Thornalley, D.J.R., Elderfield, H. and McCave, I.N., 2009. Holocene oscillations in temperature and salinity of the surface subpolar North Atlantic. Nature, 457(7230): 711-714.

Titschack, J. et al., 2009. Carbonate budget of a cold-water coral mound (Challenger Mound, IODP Exp. 307). Marine Geology, 259: 36-49.

Trenberth, K.E. and Solomon, A., 1994. The global heat balance: heat transports in the atmosphere and ocean. Climate Dynamics, 10(3): 107-134.

Turley, C.M., Roberts, J.M. and Guiotte, J.M., 2007. Corals in deep-water: will the unseen hand of ocean acidification destroy cold-water ecosystems? Coral Reefs, 26: 445-448.

V

Vogel, S., Scholten, J., Rutgers van der Loeff, M. and Mangini, A., 1998. 230Th in the eastern North Atlantic: the importance of water mass ventilation in the balance of 230Th. Earth and Planetary Science Letters, 156: 61-74.

W

Wanner, H. et al., 2008. Mid- to Late Holocene climate change: an overview. Quaternary Science Reviews, 27(19-20): 1791-1828.

Wanner, H., Solomina, O., Grosjean, M., Ritz, S.P. and Jetel, M., 2011. Structure and origin of Holocene cold events. Quaternary Science Reviews, 30(21-22): 3109-3123.

Weber, J.N., 1973. Deep-sea ahermatypic scleractinian corals: isotopic composition of the skeleton. Deep Sea Research and Oceanographic Abstracts, 20(10): 901-909.

Weber, J.N. and Woodhead, P.M., 1970. CARBON AND OXYGEN ISOTOPE FRACTIONATION IN SKELETAL CARBONATE OF REEF-BUILDING CORALS. Chemical Geology, 6(2): 93-&.

Wells, J.W., 1956. Scleractinia. Univ. Kansas Press.

Wheeler, A.J. et al., 2007. Morphology and environment of cold-water coral carbonate mounds on the NW European margin. Int J Earth Sci 96: 37-56.

Wheeler, A.J. et al., 2011. The Moira Mounds, small cold-water coral banks in the Porcupine Seabight, NE Atlantic: Part A - an early stage growth phase for future coral carbonate mounds? Marine Geology, 282(1-2): 53-64.

White, M., 2007. Benthic dynamics at the carbonate mound regions of the Porcupine Sea Bight continental margin. Int. J. Earth Sci (Geol Rundsch), 96: 1-9.

White, M., Mohm, C., De Stigter, H.C. and Mottram, G., 2005. Deep-water coral development as a function of hydrodynamics and surface productivity around the submarine banks of the Rockall Trough, NE Atlantic. Cold-water Corals and Ecosystems. Spinger-Verlag Berlin Heidelberg: 503-514.

Wienberg, C. et al., 2010. Glacial cold-water coral growth in the Gulf of Cádiz: Implications of increased palaeo-productivity. Earth and Planetary Science Letters, 298(3-4): 405-416.

Wienberg, C. et al., 2009. Scleractinian cold-water corals in the Gulf of Cádiz: First clues about their spatial and temporal distribution. Deep Sea Research Part I: Oceanographic Research Papers, 56(10): 1873-1893.

Wilson, J.B., 1979. 'Patch' development of the deep-water coral Lophelia pertusa (L.) on Rockall Bank. Journal of the Marine Biological Association of he United Kingdom, 59(165-177).

Wright, J.P. and Jones, C.G., 2006. The Concept of Organisms as Ecosystem Engineers Ten Years On: Progress, Limitations, and Challenges. BioScience, 56(3): 203-209.

Z

Zahn, R., Winn, K. and Sarnthein, M., 1986. Benthic Foraminiferal $\delta^{13}C$ and Accumulation Rates of Organic Carbon: Uvigerina Peregrina Group and Cibicidoides Wuellerstorfi. Paleoceanography, 1(1): 27-42.

Zibrowius, H., 1980. Les Scleractiniaries de la Mediterranee et de l'atlantic nord-oriental. Memoire Institute Oceanographique, Monaco, 11(1-284).

Appendix 1: Methods of coral dating

A1.1 Sample Preparation

Cleaning steps are essential to remove added uranium, thorium mostly from continental derived detrital particles, and from coating with iron and manganese oxides/hydroxides and thus to reduce errors in ^{230}Th/U ages of fossil corals.

A1.1.1 Sample Selection and Preparation

Cold-water coral fragments removed from sediment cores or taken from their natural environment are typically filled with sediment (e.g. carbonate, aluminosilicates and quartz). The sediment has its own ^{230}Th/^{232}Th signature. Therefore, prior to further investigation the sediment particles had to be removed from the coral fragments, to avoid any potential contamination. To do this, samples were ultrasonically cleaned in a beaker of distilled water. Every 15 minutes, the distilled water from the beaker was changed and samples were rinsed and brushed under a stream of distilled water. This procedure was then repeated several times until the coral samples looked to be free of sediment particles.

A 5g piece of each sample was then cut. This was enough for 3 sub-samples: (1) for X-ray diffraction (XRD) analysis to make sure the samples have not been re-crystallised into calcite (50 mg); (2) for ^{230}Th/U dating (250 mg before the cleaning procedure (Frank et al., 2004)) and (3) for radiocarbon dating (50 mg). The amount of each coral cut was larger than required from the subsamples in order to accommodate the quantity of material, which would be lost during the cleaning procedure (see below).

A1.1.2 Mechanical Cleaning

It is not rare to observe cold-water coral samples coated with iron and manganese oxides/ hydroxides. These iron/manganese crusts may absorb additional thorium and uranium from the seawater and thus may result an erroneous ^{230}Th/U age (Lomitschka and Mangini, 1999). Such contamination has been generally observed both on the outer and inner surfaces of the coral aragonite (Frank et al., 2004). With this in mind, the next cleaning step was a mechanical removal of the inner and the outer surface of the samples using a DREMEL tool. During this procedure, regular ultrasonic cleaning steps were undertaken followed by visual inspections under a binocular microscope until samples appeared completely clean.

A1.1.3 Chemical Cleaning

Most of the chemical cleaning procedures published are based upon the methods of Lomitschka and Mangini (1999) which requires an extensive set of chemical leaching steps including ascorbic acid and chelating agent (Na_2EDTA) treatments. However, this method results in significant loss of sample. For this reason, some authors have adopted methods balancing the objective of minimizing the loss of sample with the necessity of removing contaminants to minimize errors in $^{230}Th/U$ dating of fossil corals (Frank et al., 2005; Frank et al., 2004; Frank et al., 2009; Schröder-Ritzrau et al., 2003). These abbreviated cleaning procedures mostly focus on removing contaminant coatings of the sample. Adopting a similar approach, only relatively pristine corals have been selected, and following physical removal of the surface (see above), the samples were leached for one minute with hydrochloric acid (0.1N) and rinsed three times with MilliQ water.

A1.1.3 X-Ray Diffraction (XRD) Analyses

After this cleaning procedure a piece of each sample was powered using a mortar and pestle and analyzed by XRD at the University of Edinburgh. These analyses confirmed that all coral fragments are made of more than 99 % aragonite, which means that they have not been re-crystallized into calcite since the mineralization of the bio-carbonate. We are therefore confident that the U/Th dates will give us the real age of formation of the cold-water corals picked all along the cores.

A1.2 Sample Preparation

Cold-water corals have recently been used to obtain precise absolute dates via U-series dating (Cheng et al., 2000a; Cheng et al., 2000b; Douville et al., 2010; Frank et al., 2005; Frank et al., 2004; Frank et al., 2009; Lomitschka and Mangini, 1999; Pons-Branchu et al., 2005). The aragonitic skeleton of cold-water corals has high uranium content (between 3 100 and 5 500 ppb (Cheng et al., 2000a; Frank et al., 2005; Lomitschka and Mangini, 1999) which is higher than other (bio)carbonates that are currently used for ^{230}Th/U dating). Corals therefore constitute an ideal candidate for U-series dating (Cheng et al., 2000a).

A1.2.1 Theory

Assuming closed-system behaviour of the coral's aragonite, the ^{230}Th/U dating method is based on the radioactive decay series of the ^{238}U in the sample itself. The first steps of the ^{238}U decay series being:

$$^{238}U \underset{\alpha}{\rightarrow} {}^{234}Th \underset{\beta-}{\rightarrow} {}^{234}Pa \underset{\beta-}{\rightarrow} {}^{234}U \underset{\alpha}{\rightarrow} {}^{230}Th$$

^{234}Th (24 days) and ^{234}Pa (1 day) have very short half-lives, thus the only isotopes of interest for the U-series dating will be ^{238}U, ^{234}U and ^{230}Th.

The age of the aragonite mineralisation can be calculated by measuring the present-day activity ratios of ^{230}Th/^{238}U and ^{234}U/^{238}U (Ivanovitch and Harmon, 1992) according to this equation (1).

$$\left[{}^{230}Th/{}^{238}U\right] = \left(1 - e^{-\lambda_{230}t}\right) + \left(\frac{\lambda_{230}}{\left(\lambda_{230} - \lambda_{234}\right)} \frac{\delta^{234}U_t}{1000}\left(1 - e^{-(\lambda_{230} - \lambda_{234}t)}\right)\right) \quad (1)$$

Equation (1) can be solved iteratively by using the program ISOPLOT provided by Ludwig (2001).

Here the decay constant of ^{230}Th and ^{234}U are respectively λ_{230}= $(9.158\pm0.028)\times10^{-6}$ yr^{-1} and λ_{234}= $(2.8263\pm0.0056)\times10^{-6}$ yr^{-1} (Cheng et al., 2000b), t is the time since aragonite mineralisation and δ^{234}U represents the deviation of the measured ^{234}U/^{238}U atomic ratio from the atomic ratio at secular equilibrium calculated according to the following equation (2):

$$\delta^{234}U = \left[\frac{\left({}^{234}U/{}^{238}U\right)_{measured}}{\left({}^{234}U/{}^{238}U\right)_{equilibrium}} - 1\right] \times 1000 \quad (2)$$

Under equilibrium conditions the atomic ratio $({}^{234}U/{}^{238}U)_{equilibrium} = \lambda_{238}/\lambda_{234}$= 54.89×10^{-6}, the ratio of the two decay constants λ_{238}=1.5513×10^{-10} yr^{-1} (Jaffey et al.,

1971) and λ_{234}= (2.8263±0.0056)×10^{-6} yr^{-1} (Cheng et al., 2000b). Therefore, if we consider the activity ratio, ($^{234}U/^{238}U)_{equilibrium}$ is equal to 1 (Cheng et al., 2000b).

The initial $^{234}U/^{238}U$ activity ratio ($\delta^{234}U_0$), which should be constant for samples of equal age, can be estimated using the equation (3):

$$\delta^{234}U_t = \delta^{234}U_0 \times e^{-\lambda_{234}t} \tag{3}$$

Since the mean ocean mixing time is much shorter than the uranium residence time, uranium is expected to behave conservatively in the seawater. Thus, assuming a $\delta^{234}U$ of seawater temporally and spatially constant and that marine carbonates incorporate the same $\delta^{234}U$ value as seawater, the $\delta^{234}U_0$ can be used to test whether diagenesis has occurred and the system has had a closed behavior since its formation (Edwards et al., 1987). Closed system behaviour was partly confirmed by Cheng et al. (2000a) as they measured a $\delta^{234}U$ mean of 145.5±2.3‰ (2 σ, n=20 modern cold-water corals from 9 different depths across the Pacific, Atlantic, Indian and southern ocean the upper 2000m) which is very close to the first seawater U isotopes values measured (Chen et al., 1986). Two more recent studies gave us a more precise measure of a mean seawater $\delta^{234}U$ of 149.6% (1SD of 3‰, n=23) (Delanghe et al., 2002) and of 146.6% (1se of less than 2.5‰) (Robinson et al., 2004). These two studies considered seawater samples from different depth and locations.

On the other hand, thorium has a non-conservative behaviour and several ^{230}Th sources are suspected to increase errors in $^{230}Th/U$ dating:

(1) ^{230}Th concentration and $^{230}Th/^{232}Th$ ratio increase with depth. Therefore, cold-water corals are expected to incorporate more unsupported initial ^{230}Th (Cheng et al., 2000a) than species living in surface water.

(2) Continental derived detrital particles, which have their own $^{230}Th/^{232}Th$ signature (much lower ratio than found in the carbonates and water), might contaminate samples. Nevertheless, since all sediment is supposed to be removed at the time of the mechanical cleaning (see below), this source is not included in the thorium correction (Cheng et al., 2000a; Schröder-Ritzrau et al., 2003).

(3) It is assumed that the largest portion of potential contamination in thorium comes from the coating with iron and manganese oxides/hydroxides (Lomitschka and Mangini, 1999). Consequently, most of the cleaning procedure is focused on removing this fraction (see above).

(4) Even if the initial thorium incorporated into the aragonite during the lifetime of the coral is assumed to be very small (e.g. Schröder-Ritzrau et al., 2003) compared to the concentration added by the coating, a correction will have to be applied based on actual seawater data. Usually the initial ^{230}Th is calculated using the ^{232}Th content in the coral skeleton. However, the ^{230}Th/^{232}Th ratio incorporated in the coral skeleton is often assumed identical to the one measured in modern seawater (Moran et al., 1995; Vogel et al., 1998). Therefore most authors use these data to correct the initial ^{230}Th (Frank et al., 2005; Frank et al., 2004; Frank et al., 2009; Schröder-Ritzrau et al., 2003).

A1.2.2 ^{230}Th/U Analyses

U and Th chemical separation and mass spectrometry were carried out at the NERC Isotope Geosciences Laboratory (NIGL), British Geological Survey, Keyworth. Samples were ultrasonicated in dilute HNO_3 and MilliQ water before dissolution in 15 M HNO_3. Dissolved samples were spiked with a mixed ^{229}Th-^{236}U tracer calibrated against gravimetric solutions prepared from CRM 112a U metal and Ames Laboratory high purity Th metal. All acids were prepared by double sub-boiling-distillation starting with Romil SpA grade stock. Pre-concentration by Fe co-precipitation prior to U-Th separation used a Fe in 1M HCl solution prepared from Puratronic Fe nitrate and the initial chemical separation of U and Th on 0.6 ml columns using AG-1 x 8 anion resin followed procedures established by Edwards et al. (1988). Separated Th aliquots were further purified using a second pass through AG-1 x 8 columns, while separated U was purified on UTEVA columns following Andersen et al. (2008). Pilot U isotope data were obtained on a Thermo Triton thermal ionization mass spectrometer (TIMS) employing a Mascom SEM and RPQ. U was loaded as a nitrate on double zone-refined Re filament assemblies. Mass bias was monitored via replicate CRM 112a analyses, and SEM gain was corrected during sample analysis using ^{235}U/^{236}U measured sequentially on static SEM/Faraday and

Faraday/Faraday detectors. Corresponding Th data were obtained on a Nu instruments NuHRmulticollector inductively coupled mass spectrometer (MC-ICP-MS). The bulk of the U and Th data for this study, however, were obtained on a latterly acquired Thermo Neptune Plus MC-ICP-MS. Samples were introduced with an Aridus II desolvating nebulizer in 0.2 M HCl - 0.05 M HF, while sample washout used sequential 0.25 M HCl – 0.1 M HF and 0.2 M HCl – 0.05 M HF following Andersen et al. (2008). U mass bias and SEM/Faraday gain correction of unknowns was based on standard bracketing; exponential correction for U mass bias was determined by analysis of CRM 112a spiked with a $^{233}U/^{236}U$ tracer (IRMM 3636), while SEM gain was monitored using the static SEM/Faraday measurement of $^{234}U/^{235}U$ on mass bias-corrected unspiked CRM 112a data. On peak zero, hydride and tailing corrections followed Heiss et al. (2013). Accuracy (within 0.1%) and reproducibility (within 0.2%) were monitored by replicate $^{234}U/^{238}U$ analyses of Harwell uraninite HU-1. Mass bias and SEM gain for Th measurements were corrected using an in-house ^{229}Th-^{230}Th-^{232}Th reference solution calibrated by ICP-MS against CRM 112a. Total ^{238}U and ^{232}Th blanks were <10 pg and <4 pg, respectively, during this study and were negligible relative to the sample U and Th. Data were reduced using an in-house Excel spreadsheet and ages calculated with Isoplot version 3 add-in (Ludwig, 2003a) following Ludwig (2003b) using the decay constants of Cheng et al. (2000). Correction for ^{230}Th from seawater followed Frank et al. (2005) ([$^{230}Th/^{232}Th$] = 10 ± 4). Quoted uncertainties for activity ratios, initial $^{234}U/^{238}U$, and ages are given at the 2 sigma level. These include a c. 0.2% uncertainty calculated from the combined $^{236}U/^{229}Th$ tracer calibration uncertainty and measurement reproducibility of reference materials (HU-1, CRM 112a, in-house Th reference solution) as well as the propagated uncertainties from the seawater Th correction and measured isotope ratio uncertainty.

A1.3 Radiocarbon dating

A1.3.1 Theory

The radiocarbon dating method is based on the ^{14}C decay to ^{14}N. The half life of ^{14}C is of 5730 ± 40 a (Godwin, 1962) and can therefore be used to date carbonate of up to 40 ka. The ^{14}C atoms created in the upper atmosphere by cosmic rays are rapidly oxidized to $^{14}CO_2$ and exchanged between the different active carbon reservoirs (Adkins, 2001). The radiocarbon activity in the atmosphere is not constant in time and has varied due to the variations in the incoming cosmic radiation, and its partitioning between the different carbon reservoirs. Therefore, radiocarbon ages have to be calibrated to calendar age using reference atmospheric records (Reimer et al., 2009). Atmospheric radiocarbon is transferred to the ocean primarily by air-sea gas exchange of $^{14}CO_2$. Surface waters are equilibrated with the atmosphere but as they also exchange ^{14}C by mixing across the thermocline, their marine radiocarbon composition is depleted regarding to the atmospheric ^{14}C. The global average offset between the ^{14}C activity of the atmosphere and the surface water radiocarbon values is known as Marine Reservoir Effect (MRE) (Stuiver et al., 1986). When radiocarbon dating marine carbonates, this time-dependant offset can be corrected from the MARINE09 calibration curve (Reimer et al., 2009). However, for a given location the atmosphere/surface ocean ^{14}C offset may deviate from this modeled marine curve (Stuiver et al., 1986). Thus, this offset known as ΔR needs to be known, when dating marine carbonates.

Radiocarbon decay can therefore be used to either date carbonate fossils using the time-dependant calibration curves and when available the spatially and temporally variable ΔR, or when the radiocarbon age can be placed on an absolute age scale, to estimate ^{14}C spatial and temporal deviation from the modeled curve to reflects ocean circulations changes.

A1.3.2 Radiocarbon dating

The *Lophelia pertusa* fragments were prepared to graphite at the NERC Radiocarbon Facility (East Kilbride). The samples were chemically etched to remove the outer 20% (by weight) of each coral fragment by controlled hydrolysis using 0.02M HCl. The samples were rinsed, dried and homogenised. A known weight of the pretreated sample was hydrolysed to CO_2 using 85% orthophosphoric acid (H_3PO_4) at room temperature. An aliquot of CO_2 from each sample was taken to measure $\delta^{13}C$ on a dual inlet stable isotope mass spectrometer (VG OPTIMA) and is representative of $\delta^{13}C$ in the original, pre-treated sample material. The remaining

CO_2 was converted to graphite by a two-stage reduction over heated Fe and Zn (Slota et al., 1987).

The ^{14}C in the samples was measured at the SUERC AMS Laboratory in East Kilbride and the results corrected to $\delta^{13}C_{VPDB}$‰ -25 using $\delta^{13}C$ values provided in Table 3. Results are reported as conventional radiocarbon years BP (relative to AD 1950) at the ±1σ level for overall analytical confidence and as calibrated age-ranges using the OxCal 4.1 calibration software (Bronk Ramsey, 2009) with the Marine 09 dataset (Reimer et al., 2009).

A1.3.3 Calculation of the $\Delta^{14}C_{SW}$

The $\Delta^{14}C_{SW}$ (‰) is the difference relative between the modeled global marine radiocarbon curve and the radiocarbon measured in the marine sample (Stuiver et al., 1986). The $\Delta^{14}C_{SW}$ (‰) values of the water in which the corals grew can be calculated from the U-series and radiocarbon ages of the corals (Adkins and Boyle, 1997). The U-series ages were converted into years BP and the radiocarbon ages were expressed with a 2σ error to be consistent with the U-series ages.

$$\Delta^{14}C_{SW}(‰) = \left[\frac{e^{-{}^{14}C_{age}\times\lambda_L}}{e^{-cal.age\times\lambda_t}} - 1\right]\times 1000$$

With $\Delta^{14}C_{SW}$ being the $\Delta^{14}C$ of seawater, λ_L=1.2449*10^{-4} the Libby decay constant, λ_t=1.2097*10^{-4} the true decay constant, and $^{14}C_{age}$ (yr BP) the conventional radiocarbon age of the coral and cal age (yr BP) being the U-series age of the coral.

A1.3.4 Calculation of the reservoir ages

The reservoir age of a carbonate is the difference between the international atmospheric radiocarbon curve and the age of the marine sample (Stuiver et al., 1986). Two methods can be use to estimate the ventilation age of coral samples, the “foraminifers methods” which has been largely applied for ventilation age estimations using benthic and planktonic pairs, and the “backtrack” method (Adkins and Boyle, 1997).

To apply the “foraminifers” method to the corals, the U-series ages, “true” ages of the corals were converted to terrestrial ^{14}C age using the atmospheric radiocarbon calibration (INTCAL09) (Reimer et al., 2009). These "true $^{14}C_{atm}$" ages were then subtracted to the conventional ^{14}C age of the corals to obtain the ventilation ages of the water in which the corals grew.

By comparison with the "backtrack" method, the past atmosphere values are used as the reference point and are then corrected for surface reservoir contributions (Adkins and Boyle, 1997). The $^{14}C/^{12}C$ ratio of the seawater that had equilibrated with the past atmosphere $\Delta^{14}C_{SW\text{-}Atm}$ is therefore retrieved from the atmospheric radiocarbon calibration (INTCAL09) (Reimer et al., 2009). Then the reervoir ages R(yr) can be calculated using $\Delta^{14}C_{SW\text{-}Atm}$ and $\Delta^{14}C_{SW}$ determined before (Mangini et al., 1998). This method implies that the mixing factor of two water masses for the area-depth considered is known. In this study only the surface NAC is assumed to bath corals from Mingulay. Therefore, the equation to estimate the reservoir age of the study area is as following:

$$R(yr) = -\frac{1}{\lambda_L} \times \ln\left[\frac{\Delta^{14}C_{SW} + 1000}{\Delta^{14}C_{SW-Atm} + 1000}\right]$$

A1.3.1 Calculation of the ΔR

The ΔR is the difference between this modelled marine ^{14}C age and the measured ^{14}C age of the marine carbon sample (Stuiver et al., 1986).

Appendix 2: Supplementary material and data tables for Chapter 6

A2.1 Samples description

Lophelia pertusa coral fragments from two vibrocores from the Minguay Reef Complex were studied. The cores +56-08/929VE (from 127 m water depth) and +56-08/930VE (from 134 m water depth) were returned in October 2007 by the British Geological Survey during a survey on board the NERC vessel the *RRS James Cook* (Stewart and Gatliff, 2008). During the core sampling, real-time video footage was collected to ensure minimal damage to live corals. The total recovery of core +56-08/929VE (56°47’19’’N, 7°23’27’’W) and +56-08/930VE (56°49’20’’N, 7°23’47’’W) are 3.61 m and 5.25 m, respectively.

A2.2 Coral dating

A piece of about 5 g of each of the 20 *L. pertusa* fragments was then cut. This was enough for 3 sub-sampling: (1) for X-ray diffraction (XRD) analysis to make sure the samples have not been re-crystallized into calcite (~50 mg); (2) for $^{230}Th/U$ dating (~250 mg) and (3) for radiocarbon dating (~50 mg). The amount of each coral cut was larger than required from the sub-samples in order to accommodate the quantity of materiel, which would be lost during the cleaning procedure. The cleaning procedure of cold-water corals samples for U-series and radiocarbon dating was the same and follow precisely the method previously described in Chapter 4.

A2.2.1 U-series dating

U and Th chemical separation and mass spectrometry were carried out at the NERC Isotope Geosciences Laboratory (NIGL), British Geological Survey, Keyworth. Samples were ultrasonicated in dilute HNO_3 and MilliQ water before dissolution in 15 M HNO_3. Dissolved samples were spiked with a mixed ^{229}Th-^{236}U tracer calibrated against gravimetric solutions prepared from CRM 112a U metal and Ames Laboratory high purity Th metal. All acids were prepared by double sub-boiling-distillation starting with Romil SpA grade stock. Pre-concentration by Fe co-precipitation prior to U-Th separation used a Fe in 1M HCl solution prepared from Puratronic Fe nitrate and the initial chemical separation of U and Th on 0.6 ml columns using AG-1 x 8 anion resin followed procedures established by Edwards et al. (1988). Separated Th aliquots were further purified using a second pass through AG-1 x 8 columns, while separated U was purified on UTEVA columns following Andersen et al. (2008). Pilot U isotope data were obtained on a Thermo Triton thermal ionization mass spectrometer (TIMS) employing a Mascom SEM and RPQ. U was loaded as a nitrate on double zone-refined Re filament assemblies. Mass bias was monitored via replicate CRM 112a analyses, and SEM gain was corrected during sample analysis using $^{235}U/^{236}U$ measured sequentially on static SEM/Faraday and Faraday/Faraday detectors. Corresponding Th data were obtained on a Nu instruments NuHRmulticollector inductively coupled mass spectrometer (MC-ICP-MS). The bulk of the U and Th data for this study, however, were obtained on a latterly acquired Thermo Neptune Plus MC-ICP-MS. Samples were introduced with an Aridus II desolvating nebulizer in 0.2 M HCl - 0.05 M HF, while sample washout used sequential 0.25 M HCl – 0.1 M HF and 0.2 M HCl – 0.05 M HF following Andersen et al. (2008). U mass bias and SEM/Faraday gain correction of unknowns was based on standard bracketing; exponential correction for U mass bias was determined by analysis of CRM 112a spiked with a $^{233}U/^{236}U$ tracer (IRMM 3636), while SEM gain was monitored using the static SEM/Faraday measurement of $^{234}U/^{235}U$ on mass bias-corrected unspiked CRM 112a data. On peak zero, hydride and tailing corrections followed Heiss et al. (2013). Accuracy (within 0.1%) and reproducibility (within 0.2%) were monitored by replicate $^{234}U/^{238}U$ analyses of Harwell uraninite HU-1. Mass bias and SEM gain for Th measurements were corrected using an in-house ^{229}Th-^{230}Th-^{232}Th reference solution calibrated by ICP-MS against CRM 112a. Total ^{238}U and ^{232}Th blanks were <10 pg and <4 pg, respectively, during this study and were negligible relative to the sample U and Th. Data were reduced using an in-house Excel spreadsheet and ages calculated with Isoplot version 3 add-in (Ludwig, 2003a) following Ludwig (2003b) using the decay constants of Cheng et al. (2000). Correction for ^{230}Th from seawater followed Frank et al. (2005) ([$^{230}Th/^{232}Th$] = 10 ± 4). Quoted uncertainties (Table A2-1) for activity ratios, initial $^{234}U/^{238}U$, and ages are given at the 2 sigma level. These include a c. 0.2

% uncertainty calculated from the combined $^{236}U/^{229}Th$ tracer calibration uncertainty and measurement reproducibility of reference materials (HU-1, CRM 112a, in-house Th reference solution) as well as the propagated uncertainties from the seawater Th correction and measured isotope ratio uncertainty (Table A2 - 1).

Sample	^{238}U (ppm +/- 2σ)	^{232}Th (ppb +/- 2σ)	$\delta^{234}U$ (+/- 2σ)	$^{230}Th/^{238}U$ (AR +/- 2σ)	U-series age (yr BP +/- 2σ)
930 A/6 4-6 cm	3.474 ± 0.05	0.4740 ± 0.13	143.4 ± 2.3	0.01870 ± 0.29	1689 ± 27
930 A/6 42-45 cm	2.996 ± 0.07	0.2519 ± 0.07	147.4 ± 2.7	0.02256 ± 0.29	2073 ± 18
930 B/6 107-110 cm	3.230 ± 0.08	0.3177 ± 0.07	147.4 ± 2.5	0.02900 ± 0.27	2693 ± 22
930 B/6 142-146 cm	2.805 ± 0.05	0.1327 ± 0.07	146.6 ± 2.4	0.02910 ± 0.24	2721 ± 13
930 B/6 142-146 cm	2.824 ± 0.05	0.1503 ± 0.21	146.7 ± 2.4	0.02938 ± 0.42	2746 ± 17
930 B/6 134-137 cm	3.020 ± 0.05	0.2414 ± 0.26	147.6 ± 2.4	0.03015 ± 0.38	2810 ± 20
930 C/6 251-254 cm	3.025 ± 0.07	0.0999 ± 0.20	146.1 ± 2.4	0.03210 ± 0.28	3019 ± 13
930 D/6 388-392 cm	3.234 ± 0.05	0.3715 ± 0.09	146.0 ± 2.4	0.03316 ± 0.40	3097 ± 27
930 D/6 312-314 cm	2.747 ± 0.05	0.3625 ± 0.06	145.0 ± 2.4	0.03346 ± 0.24	3124 ± 28
930 D/6 356-358 cm	3.038 ± 0.05	0.2515 ± 0.07	147.8 ± 2.4	0.03414 ± 0.25	3198 ± 20
929 A/4 3-9 cm	3.356 ± 0.05	0.1409 ± 0.21	146.9 ± 2.4	0.03547 ± 0.43	3344 ± 19
930 D/6 377-379 cm	2.305 ± 0.05	0.3012 ± 0.07	146.4 ± 2.4	0.03668 ± 0.23	3436 ± 28
929 A/4 12-17 cm	3.748 ± 0.08	0.1361 ± 0.29	150.0 ± 3.5	0.03720 ± 0.32	3506 ± 18
930 E/6 438-440 cm	2.781 ± 0.05	0.2672 ± 0.06	142.9 ± 2.4	0.03723 ± 0.24	3512 ± 22
930 F/6 496-498 cm	2.714 ± 0.05	0.1785 ± 0.15	128.1 ± 2.3	0.03813 ± 0.27	3659 ± 18
929 B/4 106-108 cm	3.099 ± 0.05	0.1458 ± 0.21	146.7 ± 2.4	0.03901 ± 0.43	3690 ± 21
929 A/4 90-91cm	3.049 ± 0.05	0.1250 ± 0.07	147.8 ± 2.4	0.03952 ± 0.25	3739 ± 15
929 B/4 188-189 cm	3.124 ± 0.05	0.2477 ± 0.11	144.5 ± 2.4	0.04176 ± 0.23	3958 ± 20
929 D/4 310-312 cm	3.077 ± 0.05	0.2044 ± 0.21	146.3 ± 2.4	0.04400 ± 0.43	4177 ± 25
929 C14 284-290 cm	2.725 ± 0.05	0.1465 ± 0.11	147.2 ± 2.4	0.04409 ± 0.25	4187 ± 18
929 D/4 349-353 cm	2.981 ± 0.05	0.3327 ± 0.11	146.3 ± 2.4	0.04464 ± 0.23	4226 ± 26

Table A2 – 1: U-series ages from Mingulay Reef Complex cold-water corals.

Uncertainties are quoted at the ± 2s level, in % for activity ratios and absolute for other quantities.

A2.2.2 Radiocarbon dating

The *Lophelia pertusa* fragments were prepared to graphite at the NERC Radiocarbon Facility (East Kilbride). The samples were chemically etched to remove the outer 20 % (by weight) of each coral fragment by controlled hydrolysis using 0.02M HCl. The samples were rinsed, dried and homogenised. A known weight of the pretreated sample was hydrolysed to CO_2 using 85 % orthophosphoric acid (H_3PO_4) at room temperature. An aliquot of CO_2 from each sample was taken to measure $\delta^{13}C$ on a dual inlet stable isotope mass spectrometer (VG OPTIMA) and is representative of $\delta^{13}C$ in the original, pre-treated sample material. The remaining CO_2 was converted to graphite by a two-stage reduction over heated Fe and Zn (Slota et al., 1987).

The ^{14}C in the samples was measured at the SUERC AMS Laboratory in East Kilbride and the results corrected to $\delta^{13}C_{VPDB}$‰ -25 using $\delta^{13}C$ values provided in Table 3. Results are reported as conventional radiocarbon years BP (relative to AD 1950) at the ±1σ level for overall analytical confidence and as calibrated age-ranges using the OxCal 4.1 calibration software (Bronk Ramsey, 2009) with the Marine 09 dataset (Reimer et al., 2009) (Table A2 - 2).

Sample	$\delta^{13}C_{VPDB}$‰	Conventional Radiocarbon Age (yrs BP)	Δ14C (‰)	R (yrs)	ΔR (yrs)
930 A/6 4-6 cm	-5,4	2283 ± 37	-77 ± 4	547 ± 40	177 ± 39
930 A/6 42-45 cm	-7,7	2467 ± 37	-55 ± 4	355 ± 39	37 ± 38
930 B/6 107-110 cm	-6,0	2885 ± 35	-33 ± 4	402 ± 37	-7 ± 37
930 B/6 142-146 cm	-5,8	2894 ± 35	-31 ± 4	351 ± 37	-42 ± 36
930 B/6 142-146 cm	-5,8	2894 ± 35	-28 ± 4	294 ± 37	-91 ± 36
930 B/6 134-137 cm	-6,5	2937 ± 35	-25 ± 4	202 ± 39	-114 ± 36
930 C/6 251-254 cm	-7,8	3232 ± 35	-36 ± 4	333 ± 38	20 ± 36
930 D/6 388-392 cm	-5,4	3379 ± 35	-45 ± 4	438 ± 38	119 ± 37
930 D/6 312-314 cm	-7,2	3367 ± 35	-40 ± 4	416 ± 39	92 ± 38
930 D/6 356-358 cm	-6,8	3447 ± 37	-41 ± 4	475 ± 40	116 ± 38
929 A/4 3-9 cm	-5,2	3728 ± 35	-58 ± 4	629 ± 38	268 ± 36
930 D/6 377-379 cm	-7,5	3366 ± 35	-3 ± 4	171 ± 38	-185 ± 38
929 A/4 12-17 cm	-5,0	3706 ± 35	-37 ± 4	408 ± 37	93 ± 36
930 E/6 438-440 cm	-6,9	3664 ± 35	-31 ± 4	360 ± 38	49 ± 37
930 F/6 496-498 cm	-5,3	3723 ± 35	-21 ± 4	306 ± 39	-10 ± 36
929 B/4 106-108 cm	-4,8	3825 ± 35	-29 ± 4	394 ± 39	58 ± 36
929 A/4 90-91cm	-4,4	3850 ± 35	-27 ± 4	342 ± 38	49 ± 36
929 B/4 188-189 cm	-5,9	4015 ± 35	-21 ± 4	391 ± 38	49 ± 36
929 D/4 310-312 cm	-5,0	4156 ± 35	-12 ± 4	352 ± 37	15 ± 37
929 C14 284-290 cm	-6,5	4115 ± 35	-6 ± 4	289 ± 37	-14 ± 36
929 D/4 349-353 cm	-5,9	4151 ± 35	-6 ± 4	343 ± 37	-2 ± 37

Table A2 – 2: Radiocarbon dating results (AMS-14C), reconstructed past seawater $\Delta^{14}C$, Reservoir age (R) and local reservoir age ΔR.

Data presented in the table were calibrated using the program OxCal 4.1, Calibration curve: MARINE 09 (Bronk Ramsey, 2009), not corrected for local ΔR. Reservoir ages are relative to INTCAL 09 and DR are relative to MARINE 09.

A2.3 Calculation of $\Delta^{14}C_{SW}$

The $\Delta^{14}C_{SW}$ values of the water in which the corals grew was calculated from the U-series and radiocarbon ages of the corals (Adkins and Boyle, 1997). The U-series ages were converted into years BP and the radiocarbon ages were expressed with a 2σ error to be consistent with the U-series ages.

$$\Delta^{14}C_{SW}(‰) = \left[\frac{e^{-{}^{14}C_{age}\times\lambda_L}}{e^{-cal.age\times\lambda_t}} - 1\right]\times 1000$$

With $\Delta^{14}C_{SW}$ being the $\Delta^{14}C$ of seawater, λ_L=1.2449*10^{-4} the Libby decay constant, λ_t=1.2097*10^{-4} the true decay constant, and $^{14}C_{age}$ (yr BP) the conventional radiocarbon age of the coral and cal age (yr BP) being the U-series age of the coral.

A2.3 Calculation of the reservoir ages

Two methods can be use to estimate the ventilation age of coral samples, the "foraminifers methods" which has been largely applied for ventilation age estimations using benthic and planktonic pairs, and the "backtrack" method (Adkins and Boyle, 1997).

To apply the "foraminifers" method to the corals, the U-series ages, "true" ages of the corals were converted to terrestrial ^{14}C age using the atmospheric radiocarbon calibration (INTCAL09) (Reimer et al., 2009). These "true $^{14}C_{atm}$" ages were then subtracted to the conventional ^{14}C age of the corals to obtain the ventilation ages of the water in which the corals grew.

By comparison the "backtrack" method, the past atmosphere values are used as the reference point and are then corrected for surface reservoir (Adkins and Boyle, 1997). The $^{14}C/^{12}C$ ratio of the seawater that had equilibrated with the past atmosphere $\Delta^{14}C_{SW\text{-}Atm}$ is therefore retrieved from the atmospheric radiocarbon calibration (INTCAL09) (Reimer et al., 2009). Then the ventilation ages T(yr) can be calculated using $\Delta^{14}C_{SW\text{-}Atm}$ and $\Delta^{14}C_{SW}$ determined before (Mangini et al., 1998). This method implies that the mixing factor of two water masses for the area-depth considered is known. In this study only the surface NAC is assumed to bathe corals from Mingulay. Therefore, the equation to estimate the reservoir age of the study area is as following:

$$R(yr) = -\frac{1}{\lambda_L} \times \ln\left[\frac{\Delta^{14}C_{SW} + 1000}{\Delta^{14}C_{SW-Atm} + 1000}\right]$$

A2.4 δΔ^{14}C" index

The $\Delta^{14}C$ residual simulates the cosmic radiation as well as the relative $\Delta^{14}C_{atm}$ taken up throughout deep-water formation. The cosmogenic radionuclide ^{10}Be however is commonly seen as a solar output proxy (Steinhilber et al., 2009). To estimate the relative proportion of deep-water formation changes the $\Delta^{14}C$ residual dataset (Reimer et al., 2004) was normalized and subtracted to ΔTSI based on the cosmogenic ^{10}Be measured in ice cores (Steinhilber et al., 2009). A slight age offset of about 70 years between the two data set was however noticeable. Thus we corrected the $\Delta^{14}C$ residual by a factor 0.07 before to subtract the two normalized data set.

Globally, the THC seems to have been stronger from 9 to 4.2 kyr BP (Figure A2 - 1). In the North hemisphere, this period is characterized by relatively high but decreasing summer insolation (Berger, 1978; Wanner et al., 2011) favoring a more intense THC. In more detail, significant shift in the THC regime are recorded in 8 – 8.5, 4.7 – 5.3, around 3 and 4 and over the last 1.5 kyr BP (Figure A2 - 1). Those shifts of oceanic circulation could be associated with the global and abrupt climate changes (Mayewski et al., 2004; Wanner et al., 2011).

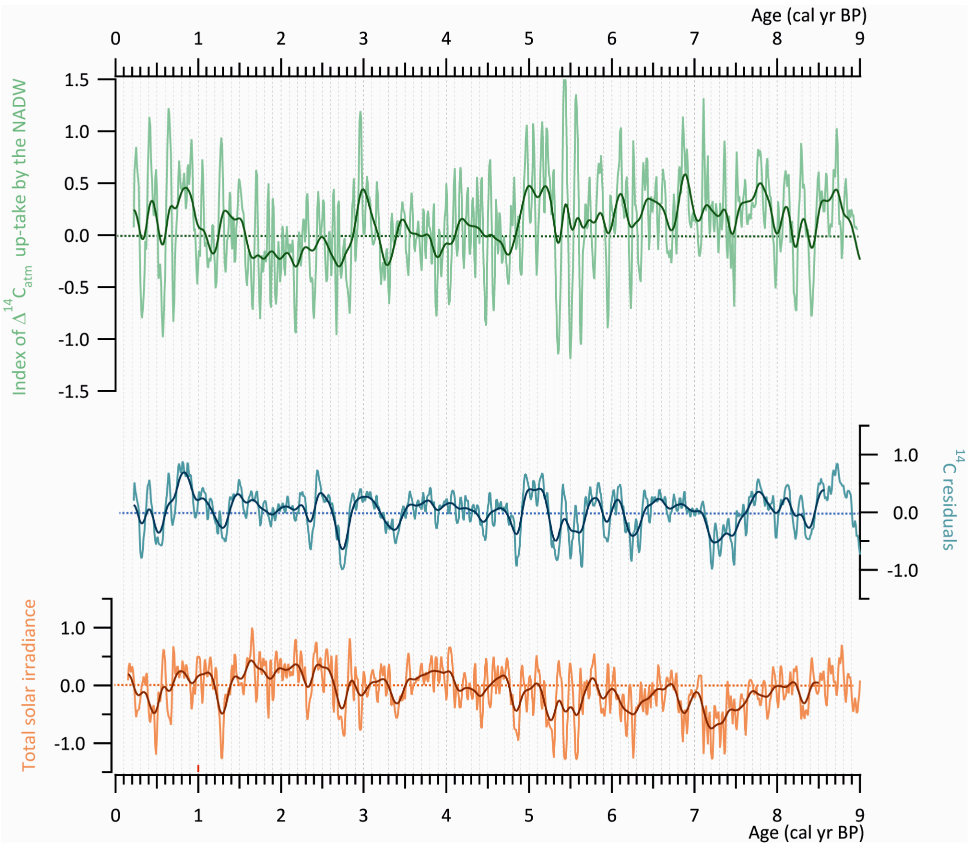

Figure A2 - 1: From top to Bottom, Index of $\Delta^{14}C_{atm}$ up-take by the NADW, Normalized $\Delta^{14}C_{residual}$ and the total solar irradiance based an ice-core ^{10}Be.

Appendix 3: Elemental profiles' reproducibility and ultra-structures correspondence of *Lophelia pertusa*

A3.1 Abstract

Coral-water corals have great potential for high-resolution ocean chemistry reconstructions. However, limited understanding of corals processes of bio-mineralization makes their use for palaeo-environmental reconstructions challenging. Coral has two main types of microstructure: (1) the early mineralization zones (EMZ) surrounded by (2) the sclerodermites. (1) and (2) are assumed to result from two distinct processes of calcification (Cuif and Dauphin, 2005; Cuif et al., 1998; Cuif et al., 2003; Lazier et al., 1999; Ogilvie, 1896). "Grey and white" bands within the sclerodermites were related to band of growth based on the analogy with the tropical corals, this is however debated and some authors refer to "EMZ-like" bands as they exhibit isotopic and trace element values similar to the EMZ. In this study we aimed to document 1) the reproducibility of trace/minor element ratios variability within the coral skeleton and 2) to make accurate correspondence between coral's ultra-structures and trace/minor ratios composition.

A3.2 Introduction

Finding novel tools allowing accurate and high time-scale resolution palaeo-environmental reconstructions is becoming of prime interest to improve our understanding of natural climate variability.

Cold-water coral's aragonite is one of the most promising archive to reconstruct past environmental changes (Freiwald et al., 2005; Mikkelsen et al., 1982; Mortensen and Rapp, 1998; Spiro et al., 2000; Weber, 1973; Weber and Woodhead, 1970). First, their are widespread all over the world ocean and over a wide range of depth (Roberts et al., 2009b; Rogers, 1999). In addition, as their tropical counterpart, now commonly use for palaeo-environmental reconstructions, cold-water coral skeleton can be precisely dated by both U-series and radiocarbon techniques (Adkins et al., 1998; Cheng et al., 2000a; Frank et al., 2005; Frank et al., 2004; Frank et al., 2009; Mikkelsen et al., 1982; Schröder-Ritzrau et al., 2005). Further studies have illustrated that stable isotopes ($\delta^{18}O$ and $\delta^{13}C$) and trace elements (Mg/Ca, Sr/Ca Li/Mg, P/Ca…) analyses can potentially provide palaeo-environmental information such as temperature and productivity (Freiwald et al., 2005; Mikkelsen et al., 1982; Montagna et al., 2008; Mortensen and Rapp, 1998; Spiro et al., 2000; Weber, 1973; Weber and Woodhead, 1970).

However, coral processes of bio-mineralization and the incorporation of trace metals in its skeleton are still poorly understood. So far most geochemical models agree on bio-mineralization processes occurring in an extracytoplasmic calcifying fluid (ECF) located in between the calicoblastics cell from the ectoderm of the polyp and the corallium. However, models based on trace elements and isotopes signature in coral aragonite diverge in the mechanisms of bio-mineralization. Some assume that changes in the ion transport are induced by pH changes in the ECF (Adkins et al., 2003; Rollion-Bard et al., 2003), other referred to Rayleigh fractionation in a closed ECF (Cohen et al., 2006; Gaetani and Cohen, 2006; Gagnon et al., 2012). A better understanding of the physiological parameters controlling coral skeleton chemistry is therefore needed to see whether palaeo-environmental patterns can be measured within coral skeleton.

Corals have two main types of microstructure: (1) the "centres of calcifications" (CC) or early mineralization zones (EMZ) surrounded by (2) fibers named the sclerodermites which are assumed to result from two distinct processes of calcification (Cuif and Dauphin, 2005; Cuif et al., 1998; Cuif et al., 2003; Lazier et al., 1999; Ogilvie, 1896). There are "grey and white" bands within the sclerodermites of cold-water corals. Recently these bands have been related to growth band based on analogy with the tropical corals (Cohen et al., 2006; Gaetani et al., 2011), but this hypothesis is debated and some other refer to "CC-like" bands as their exhibit isotopic (B) and trace element values similar to the EMZ (Blamart et al., 2002; Blamart et al., 2007; Blamart et al., 2005; Rollion-Bard et al., 2010).

One of the possible uncertainties in understanding biomineralisation processes and trace metal incorporation in cold-water corals is lack of high resolution (<10 μm) trace metals analyses across different structural components of coral skeleton. This type of analyses can potentially provide unique information for understanding biomineralisation of the cold-water corals and consequently their use as proxy for environmental studies. Our study proposes to document trace elements variability and reproducibility within *Lophelia perstua* skeleton and to make accurate correspondence between coral's microstructures and trace/minor ratios composition.

Trace elements variability within coral skeleton could be affected by several factors such as: temperature, salinity, vital effects, growth rate, productivity… Our study proposes to see which part of this variability could be explained by the ultra-structures.

A3.2 Material and Methods

A3.2.1 Samples description and preparation

The coral colony (sample 1492) used for this study was collected alive at the Mingulay Reef Area 1 (56°49N, 7°23W, and 127m) in July 2009 during the D340 cruise on board of the *RV Discovery*.

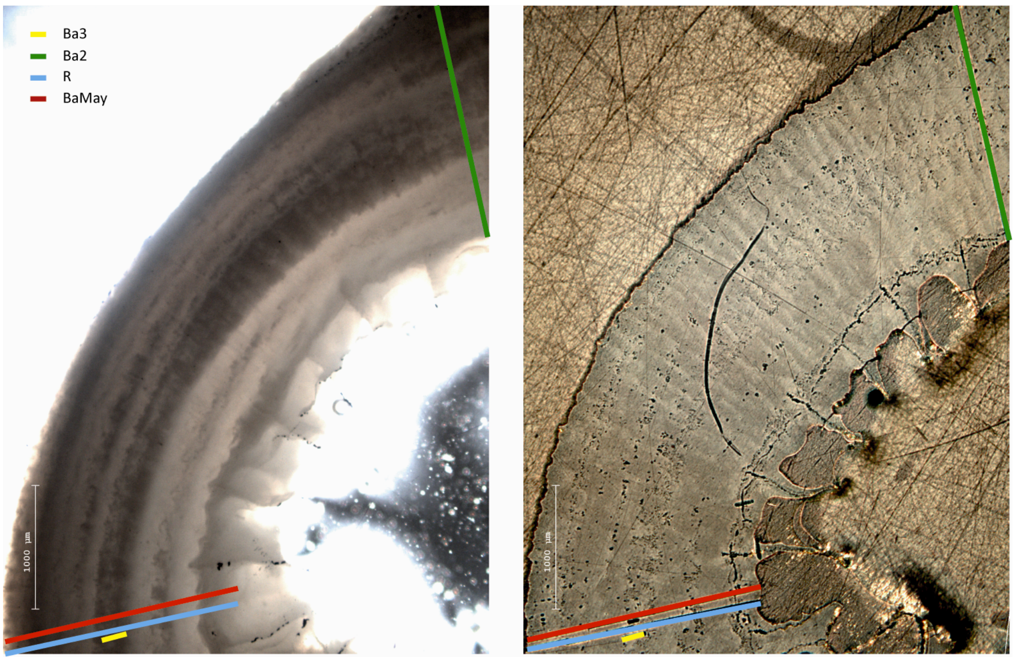

Figure A3 - 1: Ion microprobe tracks (Ba3 in yellow, Ba2 in green, R in blue and BaMay in red) on 1 calyx of the specimens of *L. pertusa*. Four radial ion microprobe profiles with a 10 µm step and aperture were run. Two ion microprobe profiles were also performed with a 1 µm step et aperture in the same calyx.

A calyx cut perpendicular to the coral growth axis and presenting a wide wall and "dark and white" banding pattern was selected to conduct this study. The calyx section selected was then mounted in epoxy and polished down to 0.3 μm with aluminium oxide powder. Prior to analyses the sample was ultrasonically cleaned in a bath of MilliQ water and dried in an oven at 40° before to be gold coated to avoid potential contamination. Once the analytical work was performed the stub holding the sample was cut to 1mm thick and photographed on reflected and polarised light to reveal the banding pattern (Figure A3 – 1).

A3.2.2 Microprobe Analysis

The profiles were conducted in the School of GeoSciences at the University of Edinburgh using the camera ims-4f Secondary Ion Mass Spectrometer (SIMS). The first set of profiles was defined using a 25 μm maximum image field and a 10 nA primary beam of $^{16}O^-$ accelerated at 15kV. Low energy secondary ions with a 40eV energy window were extracted. The field aperture n°2 reducing the analysed area to ~ 10 μm and a step scan of 10 μm was chosen. Each analysis point was recorded for 56 seconds including ^{7}Li (counting time 5 s), ^{11}B (5 s), ^{26}Mg (4 s), ^{27}Al (1 s), ^{48}Ca (3 s), ^{55}Mn (3 s) and ^{87}Sr (3 s) plus a 20 seconds delay between each spot. Cycles where $^{1.38}Ba$ (5 s) was also recorded the total analyses time per point was 63 seconds. The second set of analyse was obtained with a low beam current of 1 nA of $^{16}O^-$ of 15kV and low energy ions with a 40eV window were extracted. The field aperture n°1 restricting the analytical area to 2 – 3 μm and a step scan of 1 μm was used. Each cycle of analyses was 95 s including ^{7}Li (counting time 25 s), ^{11}B (35 s), ^{26}Mg (24 s), ^{27}Al (2 s), ^{48}Ca (4 s), ^{55}Mn (2 s) and ^{88}Sr (4 s). A delay of only 2 seconds was used between points as each point analytical value overlapped.

The accuracy of the SIMS measurement was estimated from the uncertainty on the composition of the following standards OKA, M93coral and HAxBY. Before each daily session East-West and North-South profiles were performed in the same analytical conditions as described above for the sample of interest in this study.

A3.4 Results

A3.4.1 Early Mineralization Zone

The high-resolution profile (1 µm step and spot) performed perpendicular to the EMZ confirms the singularity of those microstructures regarding to sclerodermites (Figure A3 - 2). The species considered in this study, *Lophelia pertusa,* exhibits thin EMZ zones, centred around 80 µm (Figure A3 - 1), which do no exceed 10 µm wide and are surrounded by a white bands of sclerodermites. The EMZ are characterised by singular TE/Ca values. The Mg/Ca ratio present values higher by a factor 2 than the surrounding sclerodermites reaching 8 mmol/mol. The opposite is observe for the Li/Ca ratio, where the EMZ presents values centred at 10 µmol/mol, which it two times the values recorded in the sclerodermites. The Sr/Ca and B/Ca ratio in the EMZ do not show any singularity by comparison to the other micro-structures with values always centred at 9.5 mmol/mol and 0.55 mmol/mol, respectively.

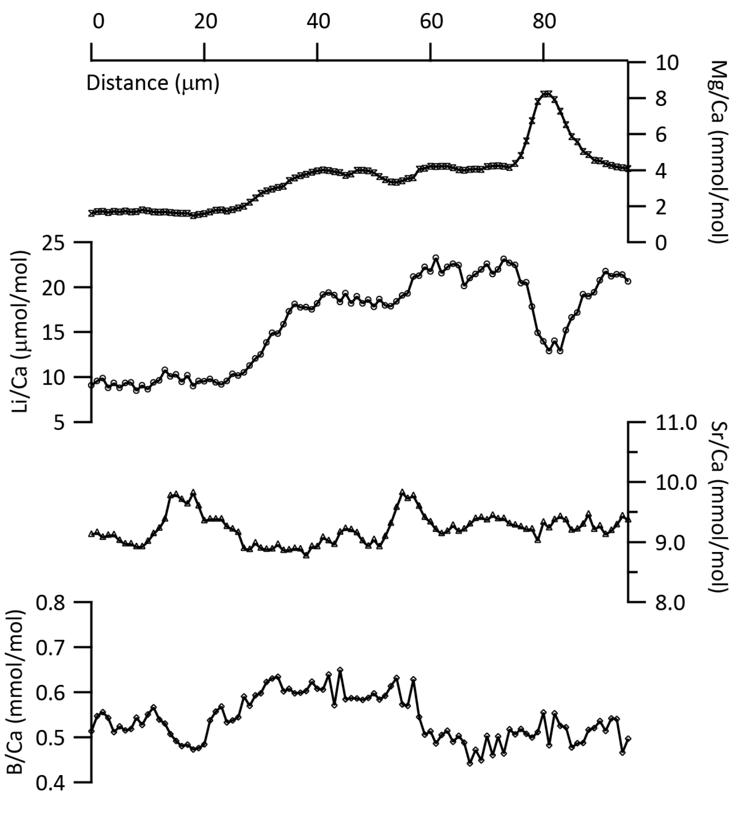

Figure A3 - 1: Profiles of Mg/Ca (panel a), Li/Ca (b) Sr/Ca (c) and B/Ca (d) with 1 µm step profiles crossing the EMZ at 80µm.

A3.4.2 Sclerodermites

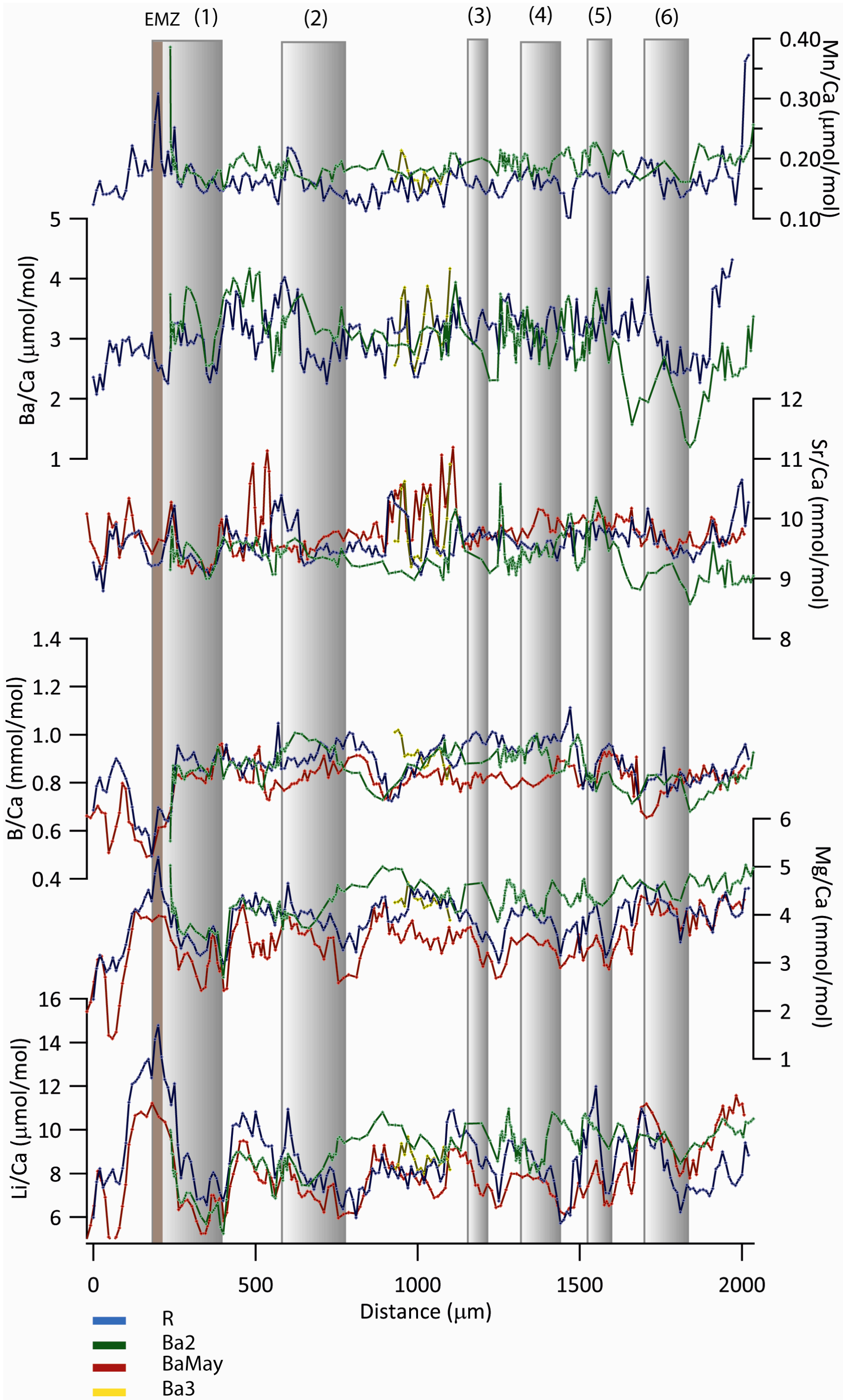

Figure 8 - 2: Four profiles (Ba3 in yellow, Ba2 in green, R in blue and BaMay in red) performed perpendicular to the growth axis. The profiles were correlated to each other according to the grey/white bands present within the aragonitic fibres zone. Grey bands represent the cc-like bands. For the profile BaMay, the manganese and barium were not measured.

In order to compare the elemental Mn, Ba, Sr, B, Mg and Li (relative to Ca) ratios obtained from the 4 SIMS profiles accurately we derived a similar distance scale for all profiles using the Analyseries software. Our strategy was to follow the banging patterns of the sclerodermites to test the reproducibility of the element variability within coral skeleton (Figure A3 - 3).

Within the sclerodermites large variation associated with the skeletal features are observed. The SIMS data shows that the Li/Ca, Mg/Ca, B/Ca, Sr/Ca, Ba/Ca and Mn/Ca ratios within coral microstructures are of 6 – 12 µmol/mol, 2.5 – 5 mmol/mol, 0.7 – 1 µmol/mol, 9 – 11 mmol/mol, 2 – 5 µmol/mol, 0.1 – 0.25 µmol/mol, respectively, which is coherent with the literature (Meibom et al., 2008; Montagna et al., 2008; Rollion-Bard et al., 2009). For the Li/Ca, Mg/Ca, B/Ca ratios the 4 profiles exhibit relatively similar patterns and relatively similar ranges of value. As observed in previous study the "grey bands" present often relatively high values comparing to the band zones within the sclerodermites but to necessary the highest values. The Sr/Ca ratios show a relatively good reproducibility between the different profiles. However, higher values not corresponding to "white" bands are observed at 50 and 1000 µm, from the composite figure. Finally, the Ba/Ca and Mn/Ca ratios show values that are relatively reproducible in between the profiles but random variability.

A3.5 Discussion

A3.5.1 Sr/Ca-Mg/Ca

Mg/Ca and Sr/Ca ratio in *L. pertusa* vary from 2.5 to 5 mmol/mol and from 9 to 11 mmol/mol, respectively. Mg/Ca and Sr/Ca measured on Micromilled samples of *Desmophyllum dianthus* are respectively of ~10.6 mmol/mol and above 3 mmol/mol within the EMZ (Gagnon et al., 2007). From the same study the Sr/Ca and Mg/Ca ratios within the aragonitic fibres are of 10.2 – 11 mmol/mol and 1.5 – 3 mmol/mol. The variability of the Sr/Ca seems less affected by the micro-structures than the Mg/Ca ratio which exhibits values significantly lower within the aragonitic fibers than the EMZ (Gagnon et al., 2007). Within the aragonitic fibers the Mg/Ca ratio increase when the Sr/Ca ratio drop from this observation it has been suggested that a Rayleigh fractionation occurred during the precipitation of these microstrutures (Gagnon et al., 2007).

NanoSIMS analysis performed on the cold water coral species *Caryophyllia ambosia*, showed that the Mg/Ca ratio within *Caryophyllia ambosia* aragonitic fibres waves between 1 and 1.5 mmol/mol and increase within the EMZ with values around 2 mmol/mol (Meibom et al., 2008). For the same species the Sr/Ca ratio fluctuates between 8.5 and 11.5 mmol/mol and does not show any specific trend within the EMZ. Both ratios or not correlated for *Caryophyllia ambosia* and do not exhibit similar patterns (Meibom et al., 2008).

A comparable study performed with SIMS analysis (~100 µm resolution) on the cold-water coral species *Lophelia pertusa* shows Sr/Ca and Mg/Ca variability within coral skeleton of 9.8 – 10.8 mmol/mol and 2.6 – 4.4 mmol/mol respectively (Cohen et al., 2006). Those values are slightly lower but remain coherent with data acquired for the same species from laser ablation (Montagna et al., 2008). In Cohen et al., study however, both ratio are in apparent inversely correlated with lower Sr/Ca ratio and higher Mg/Ca ratio within the “white” bands (Cohen et al., 2006; Gaetani and Cohen, 2006; Gaetani et al., 2011). The Sr/Ca ratio within *Lophelia pertusa* skeleton is according to the authors temperature dependant with a sensitivity of -0.18 mmol/mol/°C (Cohen et al., 2006). For this same species a Rayleigh fractionation is observed (Gaetani et al., 2011).

Although we observe a similar range of values for both ratios Sr/Ca and Mg/Ca that previous studies based on *Lophelia pertusa* analyses (Cohen et al., 2006; Gaetani and Cohen, 2006; Gaetani et al., 2011; Montagna et al., 2008), our study do not confirm a Rayleigh distribution between the two ratios. Indeed, both profile do not present the same trend at all and no convincing correlation in between the two ratios is appreciable for our data (Figure A3 - 3 A). The calibration of temperature made from the Sr/Ca ratio apply to our data would give us temperatures of about 18±10°C, which is about two times what would be expected in our study site. Contrarily to Cohen and Gaetani, (2006), in our study the EMZ do not present distinctive Sr/Ca ratios comparing to the aragonitic fibres. This is However in agreement with other studies performed on *Lophelia sp.* but also on other species

(Gagnon et al., 2007; Montagna et al., 2008). The distinct values and distribution of the elemental ratios considered here suggest however, distinct geochemical and thus fractionation between the different coral species as suggested before (Sinclair et al., 2006).

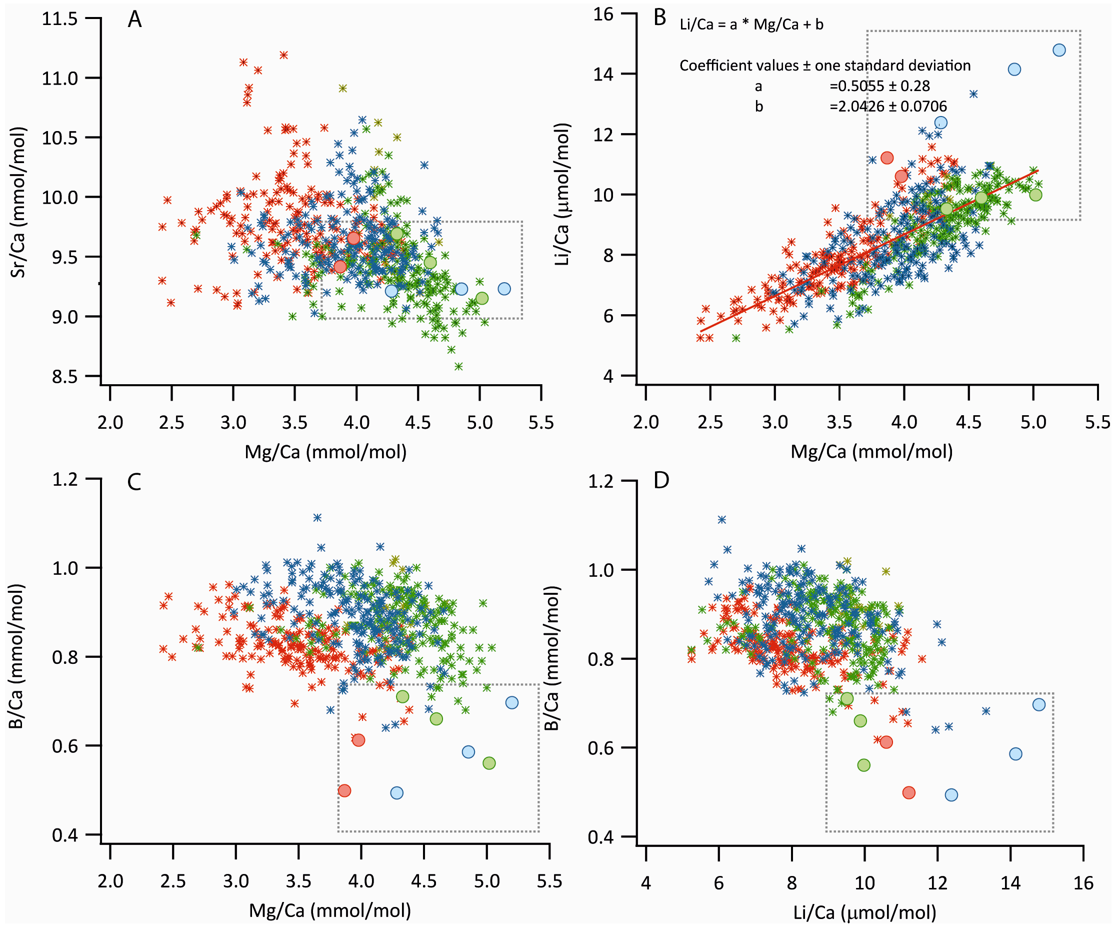

Figure 8 - 3: Sr/Ca vs Mg/Ca (A), Li/Ca vs Mg/Ca (B), B/Ca vs Mg/Ca (C) and B/Ca vs Li/Ca (D) correlation for each profile. The yellow, green, blue and red asterisks represent the data points obtained from the profiles Ba3, Ba2, R and BaMay respectively. The circles represent the data point obtained with the EMZ.

A3.5.2 B/Ca

It has been hypothesized that changes in the ions transport induced by pH changes in the ECF would be a possible mechanisms of bio-mineralization (Adkins et al., 2003; Rollion-Bard et al., 2003). The two dominant aqueous species of boron in seawater are the boric acid $B(OH)_3$ and the borate ion $B(OH)^-_4$. The relative proportion of these two species in seawater is depending on the pH (Hemming and Hanson, 1992). Thus B/Ca ratio could potentially indicate changes in pH affecting the relative incorporation of the other trace elements. However, from our records B/Ca ratios behave very differently regarding to the other ratios. Thus it is difficult to make any conclusions from our records but would be in agreement with previous findings based on the intercomparison better Boron, Carbon and Oxygen isotopes (Blamart et al., 2007).

A3.5.3 Mg/Ca-Li/Ca

The Li/Ca ratio measured along the aragonitic fibers of *Lophelia pertusa* skeleton varies between 6 to 16 µmol/mol with the highest values within the EMZ and the "white" bands with is coherent with previous studies (Montagna et al., 2008; Rollion-Bard et al., 2009). For *Desmophyllum cristagalli* however, the values of the Li/Ca ratios are slightly lower and waving between 4.9 and 6.6 µmol/mol (Rollion-Bard et al., 2009). Therefore, here again the distribution of the ratio seems to be species dependent.

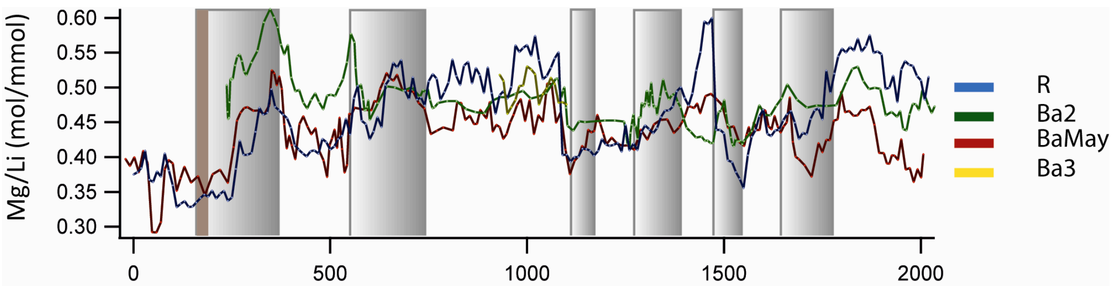

Figure 8 - 4: Mg/Ca profiles

Our study shows that the Li/Ca and Mg/Ca ratios present similar trend, and are well correlated (Figure A3 – 3 and Figure A3 - 4). The correlation between the two ratios suggests that a common factor controlled the concentration of these two elements during the calcification of the aragonitic fibres. Thus, from similar observations for *Lophelia pertusa* but also other species, several authors have proposed to reconstruct temperatures from the Li/Mg or Mg/Li ratios (Case et al., 2010; Montagna et al., 2008). Montagna et al. (2008) calibration of temperature was established from Li/Mg ratios measured in *Lophelia pertusa* and *Cladocora caespitose* (Montagna et al., 2008). If we applied this calibration of temperature to our data we obtain an estimated temperature of about 22±22 °C, which is more than two times what would be expected in our study site. One possible explanation would be that despite a temperature control of the lithium and magnesium incorporation in cold-water coral skeleton, the high fluctuation of the ratio within the microstructures induced by vital effects has a non-negligible impact and needs to be better constrained the obtain an accurate temperature signal.

The second study is based on several species Mg/Li ratios (Case et al., 2010). Using the relationship derived by this study the temperature estimated from our data would be of 30±15°C. The difference of temperature between the geochemical thermometer and the in-situ temperatures could be explain by the fact that this calibration of temperature is based on several families of cold-water corals mostly *Desmophyllum sp*. However, this species of coral present lower Mg/Ca and Li/Ca ratio than *Lophelia pertusa* thus it could be hypothesised that there species-specific effect and that an independent relationship need to be derived for *L. pertusa*.

A3.5.4 Mn/Ca-Ba/Ca

It has been shown that Ba/Ca, P/Ca and Mn/Ca are positively correlated in *Desmophyllum dianthus* skeleton (Montagna et al., 2005). The variability of these ratio within *D. dianthus* skeleton could be explain by either productivity changes or by growth rates variability (Montagna et al., 2005). Our results do not show any obvious correlation thus any conclusions can be made from our data.